TECH LIBRARY KAFB, NM
0061909

NASA CONTRACTOR REPORT

NASA CR-18
C. 1

NASA CR-1886

LOAN COPY: RETURN TO
AFWL (DOUL)
KIRTLAND AFB, N. M.

VAPOR PHASE GROWTH SYSTEM AND ITS USE IN THE PREPARATION OF SEVERAL III-V COMPOUND SEMICONDUCTORS

by R. E. Enstrom, E. A. Miller, and A. G. Sigai

Prepared by
RCA LABORATORIES
Princeton, N.J. 08540
for

NATIONAL AERONAUTICS AND SPACE ADMINISTRATION • WASHINGTON, D. C. • DECEMBER 1971

TECH LIBRARY KAFB, NM

0061009

1. Report No.	2. Government Accession No.	3. Recipient's Catalog No.
NASA CR-1886		

4. Title and Subtitle	5. Report Date
Vapor Phase Growth System and Its Use in the Preparation of Several III-V Compound Semiconductors	December 1971
	6. Performing Organization Code
7. Author(s)	8. Performing Organization Report No.
R. E. Enstrom, E. A. Miller, and A. G. Sigai	
9. Performing Organization Name and Address	10. Work Unit No.
RCA Laboratories Princeton, New Jersey 08540	11. Contract or Grant No. NAS 12-538
	13. Type of Report and Period Covered Final Report 15 March 1967 to 14 December 1970
12. Sponsoring Agency Name and Address	14. Sponsoring Agency Code
National Aeronautics and Space Administration Washington, D.C. 20546	

15. Supplementary Notes

16. Abstract

During the latest contract period, the vapor growth and characterization of AlAs, $Al_{1-x}In_xP$, GaN, $In_{1-x}Ga_xP$, and $GaAs_{1-x}Sb_x$ have been emphasized and excellent results have been realized. The dominant electrically active impurity in undoped AlAs layers is Si, and by appropriate modifications of the growth apparatus, the net donor concentration has been reduced from $10^{18}cm^{-3}$ to $10^{16}cm^{-3}$. As a result, room-temperature mobility values as high as 294 cm^2/V-sec have been attained, and this represents the highest value ever reported. Further, by diffusing Zn into these improved layers, abrupt p-n junction diodes have been prepared for the first time, and they emit yellow bandgap light. Next, $Al_{1-x}In_xP$ alloys containing up to 14% AlP were prepared by closed-tube chemical transport, thereby demonstrating that vapor growth of these alloys is feasible. The donor concentration in GaN has been reduced from 3×10^{19} to $1 \times 10^{18}cm^{-3}$, which is the lowest value obtained so far in as-grown material, by increasing the NH_3 flowrate and the thermal gradient in the deposition zone. Photoluminescence experiments on GaN have demonstrated that radiative recombination is very efficient in this material, indicating great potential for UV injection lasers and electroluminescent diodes operating over a wide spectral range, including the visible spectrum. Efforts to achieve p-type conductivity in GaN have been pursued. Vapor-grown $In_{1-x}Ga_xP$ alloys have been prepared with greatly improved homogeneity, compositional control, and structural perfection, necessary for the fabrication of high-brightness electroluminescent diodes. New insight was gained into the conditions necessary for the reproducible preparation of alloys containing Sb. As a result, $GaAs_{1-x}Sb_x$ alloys can now be routinely prepared over the entire compositional range using newly developed procedures. High-conductivity p-type layers with good surfaces have been achieved, and these materials are of interest for infrared-sensitive photocathodes. As a result of these advances, and those realized during the first two years of this contract, virtually all of the objectives of developing a compatible vapor-phase system for the preparation of several III-V compounds have been attained. The system developed, to date, has the capability of preparing an outstanding number of materials as single-crystalline layers, doped either n- or p-type, and in the form of multilayer structures, including p-n junctions. Included in these materials are GaAs, GaP, GaSb, GaN, InAs, InP, AlAs, AlP, AlN, $GaAs_{1-x}P_x$, $GaAs_{1-x}Sb_x$, $Ga_{1-x}In_xAs$, $In_{1-x}Ga_xP$, $InAs_{1-x}P_x$, and $Ga_{1-x}Al_xAs$. Further, these materials have found application in a large number of devices, many of which exhibit exceptional characteristics. These include varactor diodes, transferred electron oscillators, electroluminescent diodes, injection lasers, high-temperature rectifiers and transistors, electro-optic modulators, secondary-emission dynodes, and photocathodes.

1. Vapor phase
2. Alloys -- Testing

17. Key Words (Selected by Author(s))		18. Distribution Statement
III-V compounds	$GaAs_{1-x}Sb$	
Vapor-growth	GaN	
AlAs	$In_{1-x}Ga_xP$	
$Al_{1-x}In_xP$	$Ga_{1-x}In_xAs$	

19. Security Classif. (of this report)	20. Security Classif. (of this page)	21. No. of Pages	22. Price*
Unclassified	Unclassified	112	$3.00

*For sale by the National Technical Information Service, Springfield, Virginia 22151

11 Feb 72

VAPOR PHASE GROWTH SYSTEM AND ITS USE IN THE PREPARATION OF SEVERAL III-V COMPOUND SEMICONDUCTORS

by

R. E. Enstrom, E. A. Miller, and A. G. Sigai

RCA Laboratories
Princeton, New Jersey

SUMMARY

During the latest contract period, the vapor growth and characterization of AlAs, $Al_{1-x}In_xP$, GaN, $In_{1-x}Ga_xP$, and $GaAs_{1-x}Sb_x$ have been emphasized and excellent results have been realized. The dominant electrically active impurity in undoped AlAs layers is Si, and by appropriate modifications of the growth apparatus, the net donor concentration has been reduced from $10^{18}cm^{-3}$ to $10^{16}cm^{-3}$. As a result, room-temperature mobility values as high as 294 cm^2/V-sec have been attained, and this represents the highest value ever reported. Further, by diffusing Zn into these improved layers, abrupt p-n junction diodes have been prepared for the first time, and they emit yellow bandgap light. Next, $Al_{1-x}In_xP$ alloys containing up to 14% AlP were prepared by closed-tube chemical transport, thereby demonstrating that vapor growth of these alloys is feasible. The donor concentration in GaN has been reduced from 3×10^{19} to $1 \times 10^{18}cm^{-3}$, which is the lowest value obtained so far in as-grown material, by increasing the NH_3 flowrate and the thermal gradient in the deposition zone. Photoluminescence experiments on GaN have demonstrated that radiative recombination is very efficient in this material, indicating great potential for UV injection lasers and electroluminescent diodes operating over a wide spectral range, including the visible spectrum. Efforts to achieve p-type conductivity in GaN have been pursued. Vapor-grown $In_{1-x}Ga_xP$ alloys have been prepared with greatly improved homogeneity, compositional control, and structural perfection, necessary for the fabrication of high-brightness electroluminescent diodes. New insight was gained into the conditions necessary for the reproducible preparation of alloys containing Sb. As a result, $GaAs_{1-x}Sb_x$ alloys can now be routinely prepared over the entire compositional range using newly developed procedures. High-conductivity p-type layers with good surfaces have been achieved, and these materials are of interest for infrared-sensitive photocathodes.

As a result of these advances, and those realized during the first two years of this contract, virtually all of the objectives of developing a compatible vapor-phase system for the preparation of several III-V compounds have been attained. The system developed, to date, has the capability of preparing an outstanding number of materials as single-crystalline layers, doped either n- or p-type, and in the form of multilayer structures, including p-n junctions. Included in these materials are GaAs, GaP, GaSb, GaN, InAs, InP, AlAs, AlP, AlN, $GaAs_{1-x}P_x$, $GaAs_{1-x}Sb_x$, $Ga_{1-x}In_xAs$, $In_{1-x}Ga_xP$, $InAs_{1-x}P_x$, and $Ga_{1-x}Al_xAs$.

Further, these materials have found application in a large number of devices, many of which exhibit exceptional characteristics. These include varactor diodes, transferred electron oscillators, electroluminescent diodes, injection lasers, high-temperature rectifiers and transistors, electro-optic modulators, secondary-emission dynodes, and photocathodes.

TABLE OF CONTENTS

Section		Page
I.	INTRODUCTION	1
II.	TECHNICAL DISCUSSION	2
	A. Growth of GaN	2
	B. Growth of $In_{1-x}Ga_xP$ Alloys	5
	C. Growth of AlAs	11
	D. Growth of $Al_{1-x}In_xP$	16
	1. Sealed-Tube Vapor Growth of $Al_{1-x}In_xP$	17
	2. Open-Tube Vapor Growth of $Al_{1-x}In_xP$	18
	E. Growth of $GaAs_{1-x}Sb_x$	20
	F. Growth of $InAs_{1-x}P_x$ Alloys	21
	G. Construction of Vapor-Growth Apparatus	21
III.	CONCLUSIONS AND RECOMMENDATIONS	22
IV.	NEW TECHNOLOGY APPENDIX	23
APPENDIXES		
A.	THE VAPOR PHASE GROWTH OF SEVERAL III-V COMPOUND SEMICONDUCTORS	27
B.	THE PREPARATION AND PROPERTIES OF VAPOR DEPOSITED SINGLE-CRYSTALLINE GaN	35
C.	THE PREPARATION AND PROPERTIES OF VAPOR GROWN $In_{1-x}Ga_xP$	39
D.	VAPOR GROWTH OF $Ga_{1-x}In_xAs$ ALLOYS FOR INFRARED PHOTOCATHODE APPLICATIONS	51
E.	VAPOR GROWTH AND PROPERTIES OF AlAs	62
F.	PHOTO- AND CATHODOLUMINESCENCE IN VAPOR GROWN AlAs	70
G.	THERMAL EXPANSION OF AlAs	74
H.	THE PREPARATION OF VISIBLE-LIGHT-EMITTING P-N JUNCTIONS IN AlAs	78
I.	VAPOR PHASE GROWTH OF EPITAXIAL $GaAs_{1-x}Sb_x$ ALLOYS USING ARSINE AND STIBINE	83
J.	THE PREPARATION AND PROPERTIES OF VAPOR DEPOSITED EPITAXIAL $InAs_{1-x}P_x$ USING ARSINE AND PHOSPHINE	89
REFERENCES		96

LIST OF ILLUSTRATIONS

Figure		Page
1.	Schematic diagram of apparatus used for vapor growth of $In_{1-x}Ga_xP$ alloys.	8
2.	Composition of the $In_{1-x}Ga_xP$ alloy as a function of the ratio of the HCl flow rates to the In and Ga metal sources	8
3.	Energy gap as a function of alloy composition for $In_{1-x}Ga_xP$. The solid lines are from Hilsum et al. (Ref. 6) and Rodot et al. (Ref. 7). The broken curves are from Lorenz and Onton (Ref. 4) and agree with Nuese et al. (Ref. 5).	10
4.	Carrier concentration as a function of temperature for vapor-grown AlAs.	14
5.	Projected variation of the direct and indirect conduction-band minima in the $Al_{1-x}In_xP$ alloy system.	17
6.	Schematic diagram of apparatus used for growth of III-V compounds and alloys	29
7.	Schematic diagram of growth system used for vapor-phase deposition of $In_{1-x}Ga_xP$	40
8.	$In_{1-x}Ga_xP$ alloy composition versus deposition temperature. All other growth parameters were held constant.	41
9.	$In_{1-x}Ga_xP$ alloy composition versus the fraction of the total HCl flow over the Ga source. Composition variations produced by changing the phosphine flow rate and by eliminating the use of a mixing bulb (for diluting the HCl) are also shown	42
10.	Energy gap at 300°K versus $In_{1-x}Ga_xP$ alloy composition. Direct-indirect transition occurs at 2.20 eV and 70% GaP	44
11.	Photovoltage response of an $In_{.60}Ga_{.40}P$ p-n junction at T = 77°, 200°, and 300°K	46
12.	Room-temperature emission spectra of $In_{1-x}Ga_xP$ electroluminescent diodes with x = 0.40 and x = 0.88. Spectra are not corrected for Si photomultiplier response. $J \approx 50$ A/cm^2.	48
13.	Near-bandgap and impurity peaks in $In_{1-x}Ga_xP$ electroluminescent diodes, $x \geq 0.4$. T = 300°K	48

LIST OF ILLUSTRATIONS (CONT'D)

Figure		Page
14.	Electroluminescent emission spectrum of $In_{.35}Ga_{.65}P$ Zn-diffused p-n junction at room temperature. Spectrum is not corrected for S1 photomultiplier response. $J \approx 10$ A/cm^2.	
15.	Schematic representation of apparatus for the growth of $Ga_{1-x}In_xAs$ alloys	52
16.	Composition of $Ga_{1-x}In_xAs$ alloy as a function of the HCl flow ratio to the In and Ga sources.	54
17.	Surface of $Ga_{1-x}In_xAs$ alloy layer showing checker-board pattern associated with grading dislocations. 50 X magnification . . .	55
18.	Transmission electron micrograph of the graded region of a $Ga_{.86}In_{.14}As$ alloy doped with zinc acceptor impurities to about 1×10^{19}cm^{-3}. Grading dislocations, but no precipitates are available	55
19.	Transmission electron micrograph of the constant composition region of a $Ga_{.86}In_{.14}As$ alloy doped with zinc acceptor impurities to about 1×10^{19}cm^{-3}. Inclined dislocations, but no stacking faults, grading dislocations or precipitates are observed.	56
20.	Micrograph of the (110) cleaved face of a Zn-doped $Ga_{.85}In_{.15}As$ alloy graded at the rate of about 0.3% InAs/μm. Etched with the A-B dislocation etchant to reveal the microstructure. 500 X magnification	57
21.	The energy gap for undoped $Ga_{1-x}In_xAs$ alloys as a function of composition	59
22.	Aluminum arsenide vapor growth system	63
23.	Standard free energy changes for aluminum reactions	67
24.	Standard free energy changes for formation of AlAs in vapor growth system	67
25.	Photoluminescence at 7°K of a sample (#37) with a free electron concentration at room temperature of $\sim 10^{17}$cm^{-3}. The mobility of this sample was not determined, but similar samples have 300°K mobilities of $\sim$ 300 cm^2/V-sec. The bandgap energy is 2.238 eV at 2°K and decreases only slightly to 2.233 eV at 77°K (Ref. 111). Thus the bandgap is $\sim$ 2.237 eV at 7°K	71

Figure		Page
26.	Cathodoluminescence of the same sample shown in Figure 25 at two different electron beam excitation levels: (a) 5 A/cm^2 and (b) 1 A/cm^2. Note the change in wavelength scale.	72
27.	Lattice parameter of AlAs vs. temperature.	77
28.	I-V characteristics for Zn-diffused AlAs p-n junction at 300°K. I = 100 μA/div, V = 2 V/div. Note that the origin has been displaced horizontally three divisions from the center of the grid	79
29.	Electroluminescent spectra at 3000°K for AlAs p-n junction. J = 10 A/cm^2. Spectra have been corrected for S-1 photomultiplier response. Note that the weaker 2.146 eV peak has been amplified by a factor of 50.	81
30.	Schematic representation of vapor deposition apparatus	84
31.	Schematic representation of stibine storage and sampling apparatus.	85
32.	Schematic representation of vapor deposition apparatus	90
33.	The dependence of the alloy composition on the concentration of PH_3 in the AsH_3-PH_3 gas mixture	91
34.	The dependence of the lattice constant on alloy composition in the system $InAs_{1-x}P_x$. The dependence observed by Folberth (Ref. 137) and Koster and Ulrich (Ref. 144) is also included: ---Folberth; ___ _ ___Koster and Ulrich; _____this Appendix. .	92
35.	The dependence of the electron mobility on alloy composition in the system $InAs_{1-x}P_x$ at room temperature. The experimental results of Weiss (Ref. 138) and a theoretical analysis of Ehrenreich (Ref. 145) are also included. _ _ _Weiss; _____Ehrenreich.	93
36.	The dependence of the electron mobility on alloy composition in the system $InAs_{1-x}P_x$ at 77°K	94

LIST OF TABLES

Table		Page
I.	Effect of NH_3 Flowrate on Carrier Concentration in GaN	3
II.	Electrical Properties of GaN Prepared with Various Potential Acceptor Impurity Additions.	4
III.	Conditions Used for Vapor Growth of $In_{1-x}Ga_xP$ Alloys	6
IV.	Summary of Experimental Results in Vapor Growth of $In_{1-x}Ga_xP$ Alloys	9
V.	Temperature Dependence of the Electrical Properties of Vapor-Grown AlAs	13
VI.	Experimental Conditions for the Vapor Transport of $Al_{1-x}In_xP$ Alloys	18
VII.	Experimental Conditions Used for Open-Tube Vapor Growth of $Al_{1-x}In_xP$ Alloys	19
VIII.	Weight of Antimony Transported in 30 Minutes With and Without an HCl Flow, at Several Temperatures	21
IX.	Characteristics of Transferred Electron Oscillators and Amplifiers Prepared by Vapor-Phase Growth.	34
X.	Room-Temperature Hall Mobilities and Carrier Concentrations for $In_{1-x}Ga_xP$.	43
XI.	Electrical Properties of Vapor Grown $Ga_{1-x}In_xAs$ Alloys	57
XII.	Impurity Analysis.	65
XIII.	Electrical Properties and Chemical Analyses of Vapor Grown AlAs Removed from GaAs Substrates	66
XIV.	AlAs Lattice Parameter	75
XV.	Electrical Properties of P-Type $GaAs_{1-x}Sb_x$ Alloys.	87
XVI.	Electrical Properties of N-Type $GaAs_{1-x}Sb_x$ Alloys.	88

I. INTRODUCTION

During the first year of this contract, the primary objective was to develop a compatible vapor phase growth system for the preparation of GaAs, GaP, GaSb, InAs, InP, InSb, and selected alloys of these compounds. Further, the system was to have the capability of providing both n- and p-type doping and the preparation of multilayer structures. To accomplish these objectives, the RCA method of vapor growth, used previously with great success for the preparation of GaAs and $GaAs_{1-x}P_x$ alloys, was further developed to permit the preparation of compounds containing In and Sb.

In this way, all of the above compounds, except InSb, were prepared as single crystals. In addition, alloys of $GaAs_{1-x}P_x$, $InAs_{1-x}P_x$, $GaAs_{1-x}Sb_x$, $Ga_{1-x}In_xAs$, and $In_{1-x}Ga_xP$ were also grown as pure, single-crystalline epitaxial layers. Also, p- and n-type doping and the preparation of multilayer structures in selected materials were achieved, which demonstrated the ability of this vapor phase system to fulfill the objectives of the program.

In order to extend the utility of this vapor growth system, work during the second year focused on the preparation of III-V compounds containing Al and nitrogen by the addition of Al and NH_3 sources. Also, the antimonide work was completed, and the growth and characterization of $In_{1-x}Ga_xP$ alloys was continued because of its potential for visible electroluminescence. Again the system demonstrated its ability to meet the program objectives, even though several of these goals were exceptionally difficult to attain because of problems related to the instability of SbH_3 at room temperature and the corrosiveness of the aluminum chlorides.

The work during the next nine-month period emphasized the preparation of those materials which showed promise during previous periods, and without exception, significant improvements in material quality were made. This included the growth of AlAs, GaN, GaSb, and $In_{1-x}Ga_xP$ alloys. In addition, the vapor growth of AlN, AlP, and $In_{1-x}Ga_xN$ was investigated.

The work during the last nine-month period included improving the purity and crystalline perfection of vapor grown AlAs, initiating the growth of $Al_{1-x}In_xP$ alloys, preparing $In_{1-x}Ga_xP$ alloys with greatly improved crystalline perfection and with good control of the alloy composition, preparing GaN single-crystalline layers with improved electrical properties and a significantly lower donor concentration, and finally preparing $GaAs_{1-x}Sb_x$ alloy by an improved method of growth. The growth of such a wide variety of III-V compounds further demonstrates the versatility and utility of this vapor growth system. The details of this work are included in the following sections and in the 10 published papers given in the Appendixes. In particular, Appendix A summarizes the compounds and alloys prepared by this vapor growth method and the numerous device applications. Without exception, the devices prepared from these materials have had outstanding properties.

II. TECHNICAL DISCUSSION

A. Growth of GaN

GaN is a material with great potential for use as electroluminescent devices over the entire visible spectrum because of its large bandgap. Indeed, photoluminescence measurements indicate that external quantum efficiencies as high as 5% can be attained, thus confirming the suitability of our vapor grown GaN for efficient light-emitting devices. For the preparation of electroluminescent devices, such as light-emitting diodes and injection lasers, p-n junctions must be fabricated; this involves incorporating enough acceptor impurities into the normally n-type GaN so that conducting p-type material results.

The details of the preparation and properties of vapor-grown GaN are given in Appendix B. This work showed that high-quality single-crystalline GaN layers on sapphire could be achieved, but that the as-grown donor concentration is in the range of $10^{19}cm^{-3}$. This high donor concentration has been attributed to the presence of nitrogen vacancies in the as-grown material.

Attempts to achieve p-type material by post-growth annealing or by doping with acceptor impurities during growth have been unsuccessful or have yielded inhomogeneous material. The very high as-grown free electron concentration makes meaningful doping experiments difficult to perform since very high concentrations of the dopant must be soluble in GaN to overcome the electron density. Therefore, a systematic study of the growth parameters was undertaken to see if a reduction in the as-grown donor concentration could be achieved.

The system variables studied included HCl flow rate, NH_3 flow rate, deposition temperature, and changing the carrier gas from hydrogen to helium. Of these variables only the deposition temperature and the NH_3 flow rate had noticeable effects upon the electrical properties of the grown layers. Increasing the ammonia flow rate from 1500 to 7500 cc/min reduced the carrier concentration from 3×10^{19} to 3×10^{18} with the mobility increasing about 10% to 150 cm^2/V-sec at the lower carrier concentration as shown in Table I. Raising the growth temperature in 50° steps from 950° to 1100°C caused a monotonic increase in the free carrier concentration from 3×10^{18} to 2×10^{19} over the temperature interval and a severe degradation of the carrier mobility from 150 cm^2/V-sec to 10 cm^2/V-sec at the highest temperature. Increasing or decreasing the HCl flow rate from the standard value did not reduce the carrier concentration; in fact, it caused a slight increase in the free carriers. By increasing the thermal gradient in the deposition zone we achieved a further slight reduction in the carrier concentration to $1\text{-}2 \times 10^{18}cm^{-3}$, and this is the lowest value obtained so far in as-grown material. For this carrier concentration the mobility was found to be 125 cm^2/V-sec.

Table I

EFFECT OF NH_3 FLOWRATE ON CARRIER CONCENTRATION IN GaN

Approximate Flowrate (cm^3/min)	Free Electron Concentration (cm^{-3})	Mobility (cm^2/V-sec)
1500	3×10^{19}	140
3000	7.3×10^{18}	143
4500	5.2×10^{18}	125
$\sim$ 7500	3.6×10^{18}	150

Having achieved better than a one order of magnitude reduction in the free donor concentration, a series of doping experiments were carried out using Zn, Ge, Si, Mg, Be, and C as dopants. The electrical properties of these layers are given in Table II. None of these experiments yielded p-type material nor was there any significant reduction of the free donor concentration as might be expected if compensation had occurred. The Zn and Be samples initially appeared to be high resistivity when using pressed In contacts, as had been done previously. However, alloying the contacts at approximately 200°C revealed that the sample resistivity was not significantly higher than for other samples. Thus the previous observations of high resistivity using Zn and Mg are probably in error, because of a high contact resistance when the Hall measurements were made. In any event, the lowest donor concentration was achieved with a Zn-doped sample as may be seen in Table II. In addition, p-type conductivity using Ge impurities or partial compensation with carbon as previously reported could not be reproduced in these later experiments.

Samples lightly doped with Si, another potential acceptor impurity, resulted in carrier concentrations of 4×10^{18} with a significantly higher mobility, 185 cm^2/V-sec, than is generally observed for undoped layers. But, increased Si concentrations raised the donor concentration and lowered the mobility, thus suggesting that Si acts as a donor in GaN rather than as an acceptor impurity as had been inferred previously from an observed reduction of the donor concentration to $3 \times 10^{16} cm^{-3}$.

At this time, reliable p-type doping of GaN has not been obtained. However, it has been possible to lower the donor concentration of the as-grown material by over one order of magnitude. Further work must be done to establish if a tractible solution to the doping problem is possible.

In addition, the effects of substrate preparation treatments and orientation were examined. Etching the surface of the sapphire wafer in hot phosphoric acid, to remove work-damaged material introduced during the polishing steps, followed by a Caro's acid clean-up rinse has yielded smoother growths

Table II

ELECTRICAL PROPERTIES OF GaN PREPARED WITH VARIOUS POTENTIAL ACCEPTOR IMPURITY ADDITIONS

Dopant	Donor Concentration (cm^{-3})	300°K Mobility (cm^2/V-sec)
Be	1.1×10^{18}	150
Mg	3.5×10^{18}	113
Zn	9×10^{17}	70
C	7×10^{18}	123
Si	3.8×10^{18}	125
	4.2×10^{18}	185
	4.5×10^{18}	172
	1.0×10^{19}	143
	1.9×10^{19}	135
	2.0×10^{19}	135
Ge	7.5×10^{18}	10*
	4.3×10^{19}	111
	4.4×10^{19}	140
	5.0×10^{19}	136
	5.4×10^{19}	129
Be+Ge	9.4×10^{18}	23
Undoped†	1.1×10^{18}	192

* High-temperature growth.

† Minimum donor concentration and maximum mobility of 23 undoped samples tested.

but did not affect the electrical properties of the epitaxial GaN layer. Next, it was found that while samples grown on <0001> orientation have a <0001> orientation and are of high crystalline quality, those grown on $<1\bar{1}02>$ oriented sapphire substrates have a $<11\bar{2}0>$ orientation and are of poorer crystalline quality, as evidenced by reflection electron diffraction and Laue patterns. On the other hand, $<11\bar{2}0>$ oriented samples are perfectly clear and have shiny, mirror surfaces, while <0001> oriented samples always have poor surfaces as grown and so appear cloudy unless polished. Thus, surface appearance is not an indication of crystalline quality. No consistent differences between the electrical properties of samples of both orientations have been found.

Evidently the lattice parameter and thermal-expansion mismatch is poorer between <11$\bar{2}$0>-GaN and <1$\bar{1}$02>-sapphire than between the <0001>-orientations, because many of the <11$\bar{2}$0>-GaN layers were found to peel off the substrates.

The photo- and cathodoluminescent properties of undoped, large-area single-crystalline layers of GaN have been investigated and determined for the first time (Ref. 1). It has been found that the vapor-grown GaN layers are very efficient sources of UV (0.36 μm) radiation. The most frequent emission peaks obtained by cathodoluminescence employing a 20 KeV electron beam in undoped crystals as well as crystals doped with Si, Ge, Sn, Mg, or Zn were found at 3.7, 3.5, 3.4, 3.27, 3.19, 2.88, 2.5, 2.2, 1.7, and 1.3 eV. No strong systematic correlation was found between peak position and doping except that Si-, Ge-, and Sn-doped layers always contributed a peak at 3.4 eV.

Photoluminescence measurements performed with a UV laser emitting at 3250 Å showed a near-bandgap peak emission at 3.48 eV (at low temperatures) and some samples showed another broad doublet peak at 3.37 eV. The intensity of the 3.48 eV near-gap peak remains approximately constant up to about 50°K and then decreases with increasing temperature, which indicates that competing non-radiative recombination processes are occurring. The photoluminescence intensity at 77°K is a linear function of the excitation over three orders of magnitude, from which an external quantum efficiency of 5% is calculated. In view of its electrical and optical properties, GaN appears to be a potentially efficient material for electroluminescent devices.

B. Growth of $In_{1-x}Ga_xP$ Alloys

Theoretical and experimental evidence (Refs. 2-5), see also Appendix C, has recently supported the contention set forth earlier in this contract that $In_{1-x}Ga_xP$ alloys should have tremendous potential for electroluminescent applications. However, earlier attempts to prepare highly efficient e-ℓ diodes by the vapor-phase growth technique resulted in low efficiencies, typically 10^{-6} at 300°K (Ref. 5). These low efficiencies have been thought to be due to the low crystalline perfection of the vapor grown layers as evidenced by:

(1) Relatively matte crystal-growth surfaces, as compared to those of vapor-grown GaAs or $GaAs_{1-x}P_x$.

(2) Frequent warping of the layers, probably resulting from lattice and thermal mismatch between the $In_{1-x}Ga_xP$ layer and the GaAs substrate.

(3) Abnormally high dislocation and stacking-fault densities, as determined from transmission electron microscopy.

(4) Anomalously high Zn-diffusion rates, consistent with diffusion in semiconductors with large defect concentrations.

Accordingly, a re-investigation of this alloy system has been undertaken to develop vapor growth techniques which prepare this material reproducibly with controlled composition, homogeneity, purity, and crystalline perfection required for optimum electroluminescent performance.

The apparatus used to grow epitaxial $In_{1-x}Ga_xP$ shown in Figure 1 is essentially the same as has been used earlier for the growth of $In_{1-x}Ga_xP$ and $Ga_{1-x}In_xAs$. The principal feature of this system is the use of separate quartz tubes for the metal sources. This allows independent control of the temperatures, temperature profiles, and the HCl concentrations over each metal source. The layers were deposited on chemically cleaned GaAs substrates oriented 3° off <100>. The growth conditions initially used, given in Table III, required the use of a dilution bulb for the HCl to the Ga in order to reduce the HCl concentration. Some of the first experiments, given in Table IV, yielded single-crystal layers which were very graded (up to 12 mole %).

Table III

CONDITIONS USED FOR VAPOR GROWTH OF $In_{1-x}Ga_xP$ ALLOYS

GAS	Flowmeter	Setting	Approx. Flow (cc/min)
GALLIUM:			
HCl to bulb	1/16(0-8)	3.0	3
H_2 to bulb	1/8(0-16)	4.0	300
Dilute HCl	1/16(0-8)	4.5	32
INDIUM:			
HCl	1/16(0-8)	3.5	8
H_2 Carrier	1/8(0-16)	4.0	300
PHOSPHINE:			
10% PH_3 in H_2	1/16(0-20)	11.0	290
H_2 Carrier	1/8(0-16)	4.0	300

FURNACE	TEMPERATURE (°C)
Gallium Zone	850
Indium Zone	980
Mixing Zone	1000
Deposition Zone	775
Sidearm Furnace	600

Calculations of the dependence of alloy composition on deposition temperature revealed that the small variations in deposition temperature (<5°C) were negligible. However, calculations of the expected variation in composition with observed variations in the HCl flows to the Ga and In demonstrated that the alloy gradations were primarily due to poor control of the HCl to the Ga. This results from the inability to accurately control the three flowmeters needed for the dilution of the HCl to the Ga. For this reason all subsequent runs (Table IV, 12·7·70 on) were grown without a dilution bulb, using HCl and a H_2 carrier gas directly into the metal sources. Also, calibrated flowmeters were used to get more precise estimates of the correlation between composition and HCl_{In}/HCl_{Ga}. A series of experiments presented in Table IV were carried out to determine this dependence of composition on HCl_{In}/HCl_{Ga}. The results are plotted in Figure 2. It can be seen that there is approximately a linear relationship between the composition of the deposited layer and the HCl metal ratio, indicating that under the existing growth conditions the composition is controlled solely by the HCl flow to each metal source. It should be noted that for compositions of around 40 mole % InP, the HCl_{In}/HCl_{Ga} ratio is approximately 50:1. Therefore, the homogeneity of the layer as well as the specific composition will depend primarily on the extent to which very precise control of HCl to the Ga can be maintained. The reason for such large HCl ratios is not clear at this time but similar findings have been observed for the $Ga_{1-x}In_xAs$ system (Ref. 8, also Appendix D) and is probably related to the free energy changes for the deposition of InP and GaP or to differences in the relative rates of reaction of InCl and GaCl with the Group-V species present during the deposition process. No direct correlation appears to be present at this time between growth rate and alloy composition; the growth rate remains between 20 and 30 μm/hr.

One decisive feature of the use of higher HCl flows to the metal sources is a notable improvement in crystalline quality as evidenced by a marked improvement in surface appearance. Whereas the surfaces of the samples grown using the lower flows appeared to be matte, the more recent samples using the higher flows are smooth and highly reflective. Similar improvements in crystallinity have been observed (Ref. 9) in the Ga(As,P) system and a correlation between the crystalline quality, the Ga/As+P ratio, and the photoluminescence was observed (Ref. 9). It should be noted that a similar correlation between the crystalline quality and Al/As ratio was observed in the vapor growth of AlAs*. Although the results are preliminary, initial experiments indicate this dependence in the $In_{1-x}Ga_xP$ system also.

Several attempts were made to reproducibly grow layers of the same composition in the direct bandgap region (>30 mole % InP). As can be seen in Table IV, the compositions are indeed reproducible to within 2 mole %. It should be noted, however, that to achieve this reproducibility, constant monitoring of the HCl flow rate to the Ga is required.

---

*A. G. Sigai, RCA Laboratories, private communication.

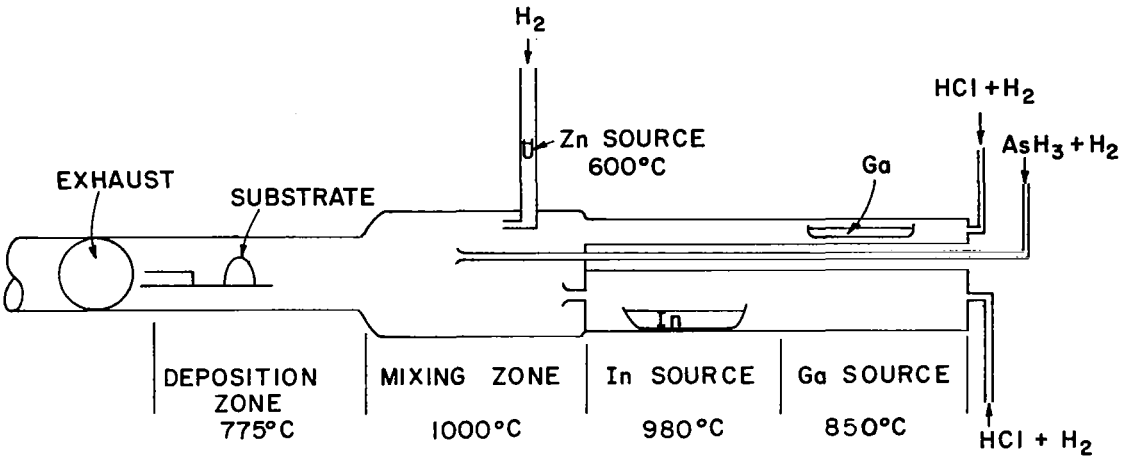

Figure 1. Schematic diagram of apparatus used for vapor growth of $In_{1-x}Ga_xP$ alloys.

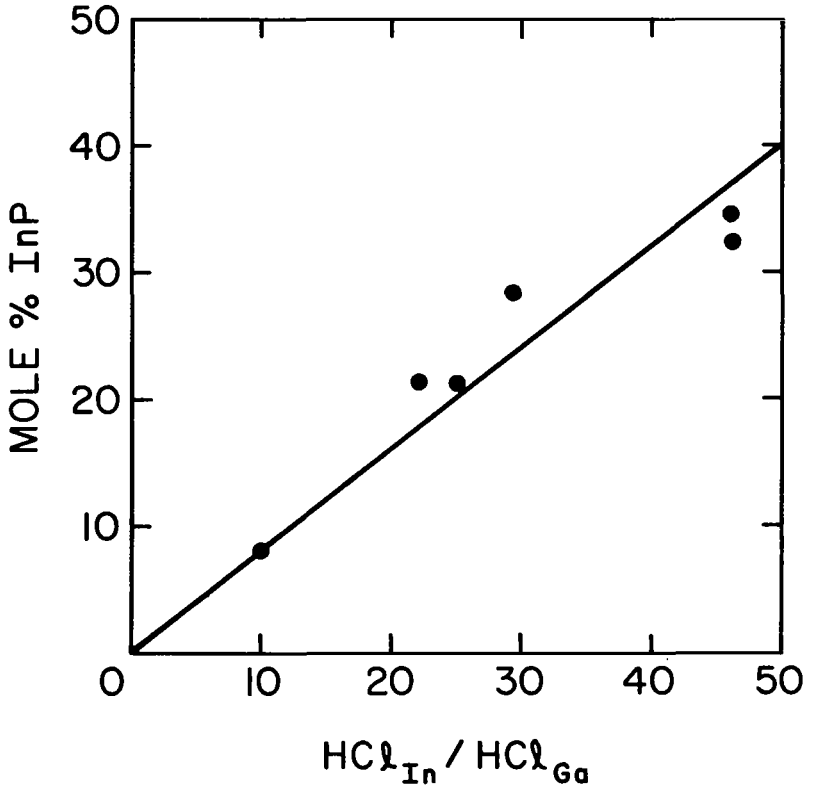

Figure 2. Composition of the $In_{1-x}Ga_xP$ alloy as a function of the ratio of the HCl flow rates to the In and Ga metal sources.

Table IV

Summary of Experimental Results in Vapor Growth of $In_{1-x}Ga_xP$ Alloys

RUN		HCl_{Ga} (cc/min)	HCl_{In} (cc/min)	HCl_{In}/HCl_{Ga}	Growth Rate (μm/hr)	Composition (Mole % InP)	Electrical Properties[2] η ($\frac{carriers}{cc}$)	Electrical Properties[2] μ(cm^2/V-sec)	Photoluminescence	E_G(eV)	$\frac{I\ Bandgap}{I\ Impurity}$
10·29·70	Dilution Bulb	0.32	8	24.2[(1)]	17.4	19 (major) graded to 30			Broad impurity Band, λ max. 7600 Å		
10·30·70	Dilution Bulb	0.32	8	24.2[(1)]	14.0	24	2.0×10^{17}	3,050[(3)]	Broad impurity Band, λ max. 7600 Å		
11·5·70	Dilution Bulb	0.32	8	24.2[(1)]	12.5	9.4 graded to 14.9	2.7×10^{19}	51.2[(3)]			
12·7·70	No Dilution Bulb	3.40	75.5	22.2	30.9	21.6					
12·8·70A	No Dilution Bulb	3.40	101.5	29.8	26.8	28.4	7×10^{17}		Broad impurity Band, λ max. 8000 Å		
12·8·70B	No Dilution Bulb	3.40	33.5	9.85	21.5	7.8	8×10^{17}		Broad impurity Band, λ max. 8000 Å		
12·9·70	No Dilution Bulb	3.40	85.0	25.0	25.7	20.9			Broad impurity Band, λ max. 7700 Å		
12·10·70: Cr	No Dilution Bulb	2.2	101.5	46.2	24.4	32.2	7×10^{17}		Sharp peak (5940 Å), Broad impurity band, λ max. 8000 Å	2.09	2.0
12·10·70: Te	No Dilution Bulb	2.2	101.5	46.2	20.0	34.2			Sharp peak (6035 Å), Broad impurity band, λ max. 8300 Å	2.06	7.8
12·14·70: Te	No Dilution Bulb	2.2	101.5	46.2	19.2	34.3			Sharp peak (6025 Å), Broad impurity band, λ max. 8200 Å	2.06	1.0

(1) HCl_{In}/HCl_{Ga} flows using dilution bulb are only estimates, since calibrated flowmeters were not used.

(2) Carrier concentrations listed with mobilities were obtained from Hall measurements; all others were determined from reverse bias breakdown voltage.

(3) Hall measurements were made while layer was on the Cr-doped substrate.

Photoluminescence of the layers revealed that for alloys with an indirect-bandgap region structure (>30 mole % InP) the spectra are dominated by a broad impurity peak and absence of a near-bandgap peak as expected for the GaP-like indirect recombination processes in these alloys. Although the impurity band is still present for compositions with a direct energy-gap structure (>30 mole % InP), a strong near-bandgap peak is also observed which is highly desirable. In fact, in two cases(12·10·70:Cr and 12·10·70:Te) the ratio of the near-bandgap to impurity intensity is as large as 7.8 to 1. This is the first time that strong near-bandgap photoluminescence peaks have been observed for vapor-grown $In_{1-x}Ga_xP$ alloy and is indicative of the more efficient band-gap recombination process which accompanies the recent improvements in surface appearance and crystalline quality. Strong near-bandgap recombination processes are essential for high-brightness e-ℓ diodes and for injection lasers of $In_{1-x}Ga_xP$.

Since significant variations in energy gap with composition are present (see Figure 3), the photoluminescence data from runs 12·10·70:Cr and 12·10·70:Te were evaluated and plotted in Figure 3. As can be seen, the present data closely follows the energy-gap versus composition relationship of Lorenz, et al. (Ref. 4) and Nuese, et al. (Ref. 5).

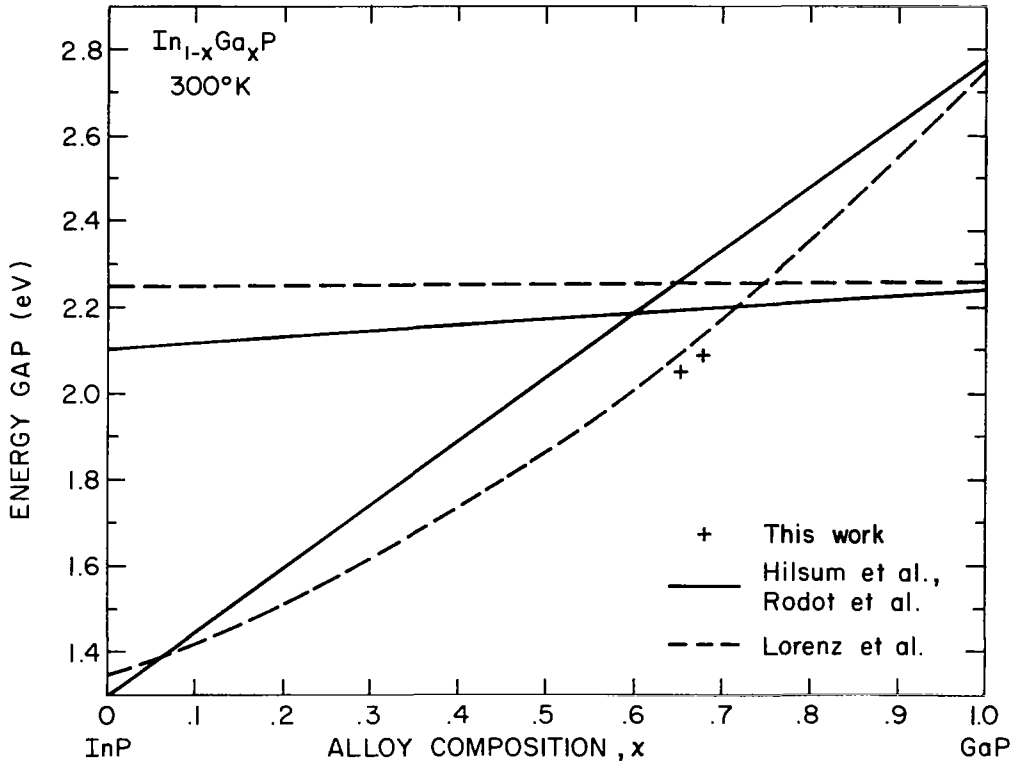

Figure 3. Energy gap as a function of alloy composition for $In_{1-x}Ga_xP$. The solid lines are from Hilsum et al. (Ref. 6) and Rodot et al. (Ref. 7). The broken curves are from Lorenz and Onton (Ref. 4) and agree with Nuese et al. (Ref. 5).

Carrier concentrations measured by reverse-bias breakdown voltages indicate about 7 x $10^{17}cm^{-3}$ on samples grown in the direct bandgap region. Mass spectrometric analysis of several layers showed that Si is the largest impurity and is present in amounts which closely correlate with the observed number of carriers, thus indicating that Si is the predominant electrical impurity.

C. Growth of AlAs

AlAs is of interest for semiconducting applications, such as high-temperature or optical devices, because of its large bandgap (2.17 eV). In addition, AlAs had not been well characterized previously, and therefore part of our efforts have been devoted to this task. The high reactivity of the aluminum chloride initially created problems in the preparation of high-purity material, but these were subsequently satisfactorily solved and resulted in AlAs with the lowest donor concentration and highest mobility yet reported. Useful devices require that p-n junctions be formed in the AlAs layers. Accordingly, doping of AlAs with acceptor impurities was investigated. This investigation resulted in the fabrication for the first time of p-n junctions in AlAs which were found to emit yellow bandgap light at 2.146 eV at room temperature. Further, the AlAs layers and devices were found to be more stable in air than previously had been thought, probably because of their greater purity and improved crystalline perfection. Thus much has been learned about the preparation of this material and its properties, as well as the general techniques required for the handling of the gaseous corrosive aluminum chlorides that will be applicable for the growth of other aluminum-containing III-V compounds.

The vapor growth of AlAs and its properties are described in Appendix E. In addition, other experiments have been conducted in an attempt to further increase the purity and to achieve improved epitaxial layers. These included the modifications of the vapor-growth system to reduce the Si contamination, since this was shown in Appendix E to be the major impurity, as follows:

(1) The BN plug at the end of the alumina tube which appeared to react with the Al chloride was replaced with an alumina plug.

(2) The use of silicone grease to seal ground glass joints was discontinued in favor of Si-free halocarbon grease.

(3) A high-purity (99.95%) tungsten foil liner was used in the deposition region to reduce reaction between the Al compounds and the quartz wall.

(4) A uniform growth tube temperature (1050°C) was used rather than a temperature gradient between the Al metal source and the deposition zones.

(5) The Zn arm nozzle was modified so that the H_2 carrier gas is injected perpendicular rather than parallel to the main gas flow within the growth tube (to promote mixing).

(6) Gaseous HCl cleaning of the carbon substrate holder was initiated.

(7) The alumina tube was cleaned with an $HF-HNO_3$ acid solution to leach out SiO_2 and metal impurities in the alumina.

These new growth conditions resulted in mirror-smooth deposits of AlAs which are the best obtained so far and which are nearly comparable in appearance to vapor grown GaAs layers. Emission spectrographic analyses demonstrate that Si and other impurities have been reduced by a factor of 20. As a result, donor concentrations as low as $4 \times 10^{17} cm^{-3}$ were achieved. To achieve even lower carrier concentrations, even more subtle sources of contamination had to be eliminated. Accordingly the system was further modified by substituting high-purity carbon for the lower-purity alumina parts as follows:

(1) The replacement of the relatively impure (99.9%) alumina liner and alumina plug with high-purity graphite parts which had been chemically cleaned and vacuum RF fired prior to use.

(2) The replacement of the alumina boats used to contain the aluminum with those of high-purity vitreous carbon.

(3) Coating all parts in the aluminum, reaction, and deposition zones as well as the trubore quartz rod in the vicinity of the deposition zone with a coherent film of carbon by pyrolytic cracking of acetone.

(4) The replacement of the carbon substrate holder with one of higher purity which had been chemically cleaned and vacuum RF fired prior to use.

(5) The use of a higher-purity source of aluminum, containing < 5 ppm total metal impurities (confirmed by mass spectrographic analysis).

The excellent surface quality and abrupt AlAs/GaAs interface achieved suggest that the material grown is of superior metallurgical quality compared to layers grown earlier in the contract.

Although the material presently obtained appears to be of superior quality, electrical measurements on one of the layers removed from the substrate gave a carrier concentration of 1×10^{17} carriers/cm^3 with a mobility of 294 cm^2/V-sec at room temperature. While this represents the lowest carrier concentration and highest mobility yet obtained for this material, emission spectrographic analysis of this layer, as well as others grown subsequently, indicate that the Si content is still between 1 and 10 ppm which is surprising in light of the precautions taken to reduce the Si contamination. Examination of the growth tube after the series of runs, however, revealed that substantial reaction had occurred between the aluminum or gaseous aluminum chlorides and the carbon growth components. In view of the difficulties in achieving higher-purity vapor grown AlAs with only marginal increases in the electrical properties, no further modifications were made.

Earlier work on III-V compounds grown in quartz systems have shown that Si is typically the predominant, residual, electrically-active impurity. Mass spectrographic and emission spectrographic analyses of samples grown in this work have shown a close correlation between the carrier concentration and the total Si content. The abundance of Si in vapor-grown AlAs has been observed by others (Refs. 10,11) and is to be expected based on the corrosive nature of the aluminum chloride with quartz at the high-growth temperature. Based on the assumption that Si is the predominant electrically active impurity, the donor ionization energy can be determined by measuring the temperature dependence of the carrier concentration. To insure that a true equilibrium temperature was achieved, the entire sample was immersed in various low-temperature refrigerants. The temperature was independently monitored by an iron-constantan thermocouple. To confirm that the electrical properties did not change after each immersion because of the condensation of water vapor on the sample, the room-temperature electrical properties were remeasured after each low-temperature measurement and found to be unchanged. The stability of the electrical properties even in the presence of water vapor further supports the contention that the bulk properties of vapor grown AlAs are not perturbed and that previously observed degradation occurs only on the surface.

The electrical properties of the sample measured are presented in Table V.

Table V

TEMPERATURE DEPENDENCE OF THE ELECTRICAL PROPERTIES OF VAPOR GROWN AlAs

T °K	n carriers/cm^3	cm^2/V-sec	ρ ohms-cm
77	2.19×10^{16}	180	1.58
113	9.24×10^{16}	237	2.86×10^{-1}
146	1.78×10^{17}	294	1.19×10^{-1}
191	3.09×10^{17}	236	8.55×10^{-2}
298	5.78×10^{17}	154	7.45×10^{-2}

Since carrier concentrations as low as $2 \times 10^{16}/cm^3$ were achieved, the electrical properties of AlAs probably are not dominated by native point defects as has been suggested for GaN (Ref. 12) but rather reflect the background impurity content. The log of the carrier concentration is plotted as a function of 1/T in Figure 4. The linearity of this plot suggests that only one electrically active impurity is dominant. Assuming that impurities observed by mass spectrometric analysis behave in AlAs as in other III-V compounds, there are almost as many potential acceptors ($\sim$ 40 ppm Fe = 2×10^{18} atoms/cm^3, $\sim$ 40 ppm Zn = 2×10^{18} atoms/cm^3) as donors ($\sim$ 100 ppm Si = 5×10^{18} atoms/cm^3).

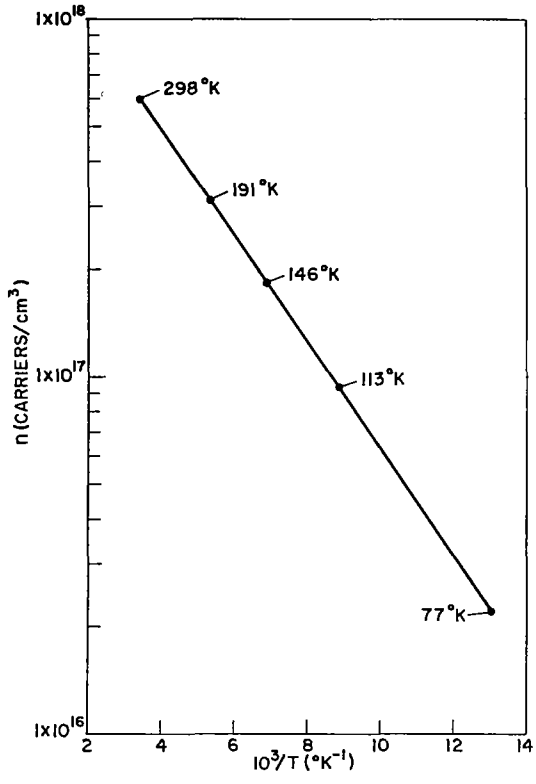

Figure 4. Carrier concentration as a function of temperature for vapor grown AlAs.

Based on this observation the sample is considered to be partially compensated. The decrease in the electron mobility at low temperatures is dominated by ionized impurity scattering which would be consistent for a partially compensated sample. For a partially compensated ($n_0 < N_A < N_D$) sample, the slope of log n versus 1/T can be equated to E_D/K and in this case the donor ionization energy is found to be 0.029 eV. This value is in reasonable agreement with Whitaker's value (Ref. 10) of 0.018 eV derived from Hall-effect measurements on vapor-grown material, but is significantly different from the value of 0.073 eV recently derived independently from photoluminescence and cathodoluminescence measurements by Kressel, et al. (Ref. 13 and Appendix F).

For thick as-grown AlAs layers deposited on undoped GaAs substrates, the wafer is typically badly bowed toward the GaAs substrate, indicative of strain in the layer. From a comparison of the x-ray line widths of the epitaxial layers, the strain in the AlAs layer deposited on undoped GaAs is estimated to be more than five times greater than an undoped GaAs layer deposited on an undoped GaAs substrate. This is not to be expected because of the similarity of the lattice constants and thermal expansion coefficients of AlAs and GaAs (see Appendix G) which would yield a minimum amount of strain.

In order to elucidate the origin of the strain, several samples were examined by transmission electron microscopy (TEM). The initial findings revealed that the magnitudes of the dislocation and stacking-fault densities of the AlAs layer are significantly different from what is to be expected for an AlAs layer deposited on a GaAs substrate. Based on lattice parameter differences (for GaAs, $a_o = 5.6533$ Å; for AlAs, $a_o = 5.6610$ Å at room temperature), approximately 2×10^5 dislocations/cm^2 would be expected. However, 5×10^6 dislocations/cm^2 are observed. Furthermore, a stacking-fault density = 0 is expected in the AlAs because of complete removal of work damage of the substrate surface prior to growth and because both epitaxial layer and substrate are free of second-phase particles. But, in fact, stacking-fault densities of around 3×10^6/cm^2 are observed.

To further investigate the origin of these apparent anomalies, thick single-crystalline layers, up to 15 mils thick, were prepared on (100)-oriented GaAs substrates so that sections perpendicular to the growth interface could be prepared for optical and TEM studies. An interfacial layer about 1.5 μm thick was found and is easily distinguished from either AlAs or GaAs. During thinning of the sample by ion bombardment for TEM, the layer was found to be quite different from either the GaAs or AlAs. Practically all of the GaAs is removed from the heterojunction structure before the interfacial layer is sufficiently thin for transmission of the 100 KV electron beam. Although the identity of the interfacial layer is not clear at this time, it is unlikely that it is a (Ga,Al)As alloy since this is inconsistent with the defect densities reported above. We believe that the interfacial layer is an aluminum-oxygen containing compound, although firm conclusions cannot be made at this time. This is based on:

(1) The strong tendency of aluminum compounds to form oxides, particularly at high temperature.

(2) The observed high dislocation and stacking-fault densities suggestive of thermal or lattice mismatch.

(3) The difficulty of ion sputtering the intermediate layer indicating strong atomic bonding such as found in Al-O.

The optical-absorption spectrum of vapor grown AlAs was re-investigated to determine more precisely the optical-energy gap. Several single-crystal layers were removed from the substrate and chemically polished with a 1/2% bromine-methanol solution; the resulting samples were then highly transparent. The linear dependence of the square root of the absorption coefficient versus photon energy confirms that AlAs is indirect and yields an energy gap of 2.17 ± 0.02 eV, which is in excellent agreement with recently published values of 2.15 eV (Ref. 11) and 2.16 eV (Ref. 14). In addition to the main bandgap absorption, a weaker absorption at 1.3 μm has been observed by Yim (Ref. 11), and this peak has been suggested to be associated with deviations from stoichiometry (excess As atoms or Al vacancies). Since this peak was never observed in the samples grown previously in this work, efforts were made to verify the existence of this absorption peak. Therefore, several samples were

grown in a large excess-arsenic vapor concentration. Then the peak at 1.3 μm was found to be present. Furthermore, this peak could be eliminated by annealing the samples at 800°C for approximately 4 hours. These results suggest that deviations from stoichiometry may exist in AlAs but that the growth conditions can be suitably chosen to prevent such deviations. It should be noted that lower AsH_3 flowrates both eliminate the 1.3 μm peak and result in significantly better surfaces.

Attempts to dope AlAs p-type using a very high gas-phase Zn-acceptor impurity concentration have resulted in only 1-ppm Zn in the AlAs layer which is not sufficient to overcompensate the background n-type impurities to produce p-type material. This difficulty in doping is probably due to poor mixing of the Zn vapor with the other gaseous constituents and, therefore, the vertical doping arm was modified. Previously, the Zn vapor stream had converged with the main gas stream and it was suspected that Zn vapor may have tended to pass over the top of the wafer without doping the AlAs. Therefore, the vertical doping arm was modified to promote more homogeneous mixing of the Zn vapor stream with the main gas stream. However, this modification was not successful in producing p-type AlAs in any of the runs made. It is now thought that the inability to dope the AlAs during vapor growth may be related to either the very high (1000 Torr) vapor pressure of Zn at the 1000°C growth temperature thereby requiring higher Zn concentrations in the vapor phase than have been used, or to the rapid depletion of the Zn reservoir and subsequent out diffusion of Zn from the growing AlAs layer.

Zn diffusion has been used as an alternative method of fabricating p-n junctions in the AlAs layers. The higher purity and perfection of the recent AlAs layers have led to the formation of abrupt, planar p-n junctions, as determined by capacitance-voltage measurements, with significantly improved light emission. The diodes now emit yellow bandgap light rather than in the infrared as was observed initially and the details of this work are presented in Appendix H.

D. Growth of $Al_{1-x}In_xP$

For many applications, especially for electroluminescence and detection of visible radiation, large direct bandgaps are very desirable. It has been theoretically predicted by Archer (Ref. 15) that $Al_{1-x}In_xP$ should have the highest luminous efficiency for electroluminescence of any III-V alloy. In Figure 5 the (000) and (100) conduction-band minima for InP and AlP are shown. Here the variation of the direct and indirect energy gaps is extrapolated linearly across the alloy system. The crossover occurs at a composition of 39% AlP and at an energy of 2.23 eV (5400 Å), which corresponds to green light emission. Onton and Chicotka (Ref. 16) have prepared $Al_{1-x}In_xP$ alloys and have measured their cathodoluminescent efficiency. Their results confirm the linear variation of the energy gap with composition and suggest that this alloy possesses great potential for efficient electroluminescence.

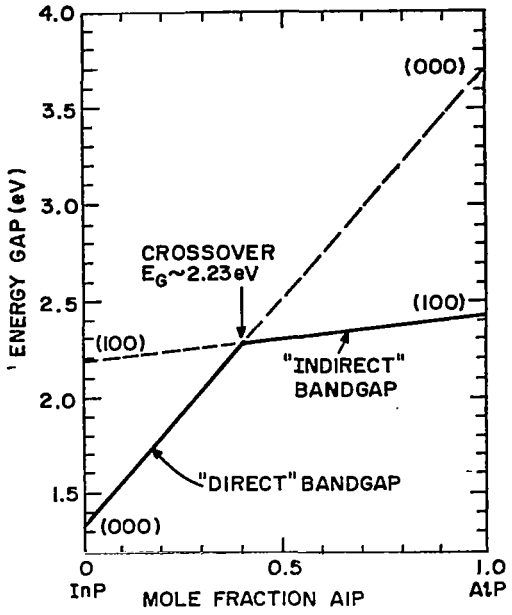

Figure 5. Projected variation of the direct and indirect conduction-band minima in the $Al_{1-x}In_xP$ alloy system.

1. Sealed-Tube Vapor Growth of $Al_{1-x}In_xP$. - It is known that single crystals of both InP and AlP can be prepared by a vapor-phase chemical transport using a halogen as the transporting agent. Therefore, it is of importance to examine this technique for crystal growth of the alloy. Table VI summarizes the experimental conditions for the transport experiments. Appropriate quantities of InP, AlP, and iodine were placed into a specially machined alumina capsule which was then inserted into a quartz ampoule. After evacuating the alumina capsule and quartz ampoule to a pressure of 10^{-4} Torr or less, the ampoule was sealed so as to provide an air-tight seal of the alumina capsule. The ampoule was slowly placed into a temperature gradient. Typically, the quartz ampoule cracked due to the large expansion of the alumina relative to that of the quartz. Nevertheless, sufficient pressure was applied to the alumina capsule to prevent any leakage of gases. From Table VI it can be seen that using a deposition temperature of 850°C yields a range of composition containing between 8.9 to 13.7 mole % AlP; the transport yield was found to be very low. By increasing the deposition temperature to 950°C, the amount of AlP in the deposited material is substantially increased. Also, the amount of transported material is significantly lower than obtained using deposition temperatures of 850°C. This is in keeping with the known thermal stabilities of the compounds involved in these reactions. The crystals produced by sealed-tube vapor growth are too small for adequate characterization of their properties, because of the low transport rate and the presence of many nucleation sites on

the surface of the alumina capsule. Nonetheless, the significant feature of these experiments is that $Al_{1-x}In_xP$ alloys can be prepared by chemical vapor-phase-growth techniques.

Table VI

EXPERIMENTAL CONDITIONS* FOR THE VAPOR TRANSPORT OF $Al_{1-x}In_xP$ ALLOYS

Temperature Gradient (°C)	a_o (Å)	Transported Composition** (Mole % AlP)	Comments
950 → 850	5.812-5.832	13.7-8.9	range of compositions very low yield
1050 → 950	5.576	70	very little transport
1050 → 950	5.468	96	very little transport

*For each of these experiments, the starting composition was 60 mole % AlP, the concentration of the iodine transport agent was 5 mg/cm^3, and the transport time was 7 days.

**The composition of the transported product was deduced from the measured lattice constant assuming that Vegard's law is followed in this system.

2. Open-Tube Vapor Growth of $Al_{1-x}In_xP$. - Because sealed-tube vapor-growth experiments have not led to large single crystals, future work should emphasize the open-tube vapor growth of $Al_{1-x}In_xP$ alloys. Several preliminary attempts to deposit the alloy are summarized in Table VII. The open-tube synthesis employs the alumina system previously described for the preparation of AlAs and an In-Al alloy as the metal source. To ensure that the metal alloy is equilibriated, the molten metals were typically heated at temperature for approximately one hour prior to starting growth. Using flow conditions which were previously used for vapor growth of AlAs, only AlP deposits resulted despite changes in the metal alloy composition from 68 to 95% In and lowering the deposition temperature from 830° to 740°C. InP was observed, however, in the exhaust traps. As a result of these experiments, future work should emphasize use of separate In and Al sources which permit complete control of the metal-chloride ratio, and adjustment of the growth conditions to promote alloy formation.

Due to the high reactivity of aluminum and its chlorides at the high temperatures (~ 1000°C) normally employed in this study, efforts were made to explore other vapor-phase methods of synthesizing aluminum - group V

Table VII

EXPERIMENTAL CONDITIONS USED FOR OPEN-TUBE VAPOR GROWTH OF $Al_{1-x}In_xP$ ALLOYS

SUBSTRATE: SAPPHIRE - (0001)

Gas	Flow Rate (cc/min)
HCl over In-Al metal alloy	14
Hydrogen carrier gas	2420
Phosphine (100%)	45
Hydrogen carrier gas	500

Run	Metal Alloy Composition (Mole % Al)	Metal Zone T (°C)	Center Zone T (°C)	Deposition Zone* T (°C)
9·9·70	32	1000	870	830
9·11·70	5	1000	850	800
9·15·70	5	1000	850	800
9·23·70	5	975	970	740

*All vapor grown layers are pure AlP.

compounds which employ lower growth temperatures. Based on results obtained by M. Yim of RCA Laboratories, solid $AlCl_3$ has been used to grow AlP layers on sapphire up to 100 μm thick at growth rates up to 25 μm/hr. A significant advantage of using the trichloride is that lower temperatures are required to vaporize the $AlCl_3$ ($T < 200°C$) thus decreasing contamination resulting from reactions with the quartz walls. Also, the deposition region is moved 3/4 in. from the point where the gases mix to 4 in. downstream. This is a desirable feature both for uniform doping of layers and for the preparation of homogeneous alloy compounds since it accommodates more complete mixing of the reactant gas.

E. Growth of $GaAs_{1-x}Sb_x$

The vapor growth of $GaAs_{1-x}Sb_x$ alloys using AsH_3 and SbH_3 is described in Appendix I. The alloy composition can be adjusted by varying the ratio of the SbH_3/AsH_3 gases and in this way alloys over the whole compositional range can be prepared. However, SbH_3 must be stored at 195°K to prevent decomposition and aliquot portions must be separately distilled for use during each growth period, which is inconvenient. To circumvent these problems, the use of a pure metallic Sb source in conjunction with HCl to transport it as the chloride to the growth zone was investigated. This method was used successfully to prepare the GaSb layers described in Interim Scientific Report No. 3, but attempts to prepare $GaAs_{1-x}Sb_x$ alloys were less successful due to difficulties in attaining the desired compositions reproducibly.

Our more recent work has sought to understand the reasons for this compositional problem, and significant progress has been made in the vapor growth of $GaAs_{1-x}Sb_x$ alloys using elemental Sb, Ga, and AsH_3. The results shown in Table VIII in which an attempt was made to control the vapor-phase concentration of Sb using HCl transport show, contrary to expectations, that the amount of Sb in the vapor phase and in the alloy layer does not depend on the HCl flow, but rather on the Sb furnace temperature and the H_2 flow rate. This indicates that the Sb vapor pressure is controlling its transport instead of the reaction with HCl. Furthermore, it has been found that the Sb is first depleted from the hotter end of the boat, so that the Sb vapor pressure drops from run to run, leading to lower Sb content in the samples grown in each subsequent run. In light of this, a new Sb boat was designed with an opening only at the colder end, which assured a constant Sb vapor pressure, and thus the problem was overcome.

Next, it was observed that unless the $GaAs_{1-x}Sb_x$ deposits are removed from the quartz deposition tube walls after each run by HCl cleaning, these deposits begin to compete with the substrate as a favored deposition site. Then, the growth rate and the Sb content of subsequent vapor-grown layers is reduced. In addition, it was found that more homogeneous $GaAs_{1-x}Sb_x$ alloy layers could be prepared by introducing the AsH_3 directly into the deposition tube rather than into the two-liter mixing bulb normally employed for the growth of III-V compounds utilizing the vapor hydride method. This arises from the long time needed for the AsH_3 concentration to reach a steady-state value in the bulb, which then causes grading of the alloy layers. Now, for the first time, homogeneous alloys across the entire composition range with very abrupt optical absorption curves at the bandgap wavelength can be reproducibly prepared.

Subsequently, doping of these alloys during growth with Zn acceptor impurities was investigated. A number of layers were produced in this way with doping levels in the mid-10^{18} to mid-10^{19} holes/cm^3 range thus demonstrating that high conductivity p-type layers can be prepared. It was found that Zn-doping at the high levels leads to poor surfaces (pits). However, the surface can be significantly improved by the use of a layer graded in composition from GaAs adjacent to the GaAs substrate to the final $GaAs_{1-x}Sb_x$ composition prior to the growth of the constant composition alloy layer.

Table VIII

WEIGHT OF ANTIMONY TRANSPORTED IN 30 MINUTES WITH, AND WITHOUT AN HCl FLOW, AT SEVERAL TEMPERATURES

Temp. (°C)	HCl Flow (ml/min)	H_2 Flow (l/min)	Wt. Loss (gm)
800	4.0	2.5	0.641
800	0	2.5	0.633
800	0	2.5	0.684
800	0	1.6	0.568
800	0	0.9	0.488
800	4.0	0.45	0.341
800	0	0.45	0.348
800	0	0.20	0.221
800	0	0.10	0.193
800	0	0	0.068
600	4.0	2.5	0.031
600	0	2.5	0.027
600	0	0.90	0.019
600	0	0.20	0.008

F. Growth of $InAs_{1-x}P_x$ Alloys

The vapor growth and properties of single-crystalline $InAs_{1-x}P_x$ alloys are described in Appendix J. These alloys exhibit electron mobilities equivalent to the highest yet reported for this system, and for InAs a mobility value of 120,000 cm^2/V-sec at 77°K was observed which is higher than previously reported. The alloys can be doped n- and p-type over a broad range, and the p-type alloys have great potential for use as negative-electron-affinity photocathodes sensitive in the near infrared. This application is of great interest currently because of the availability of efficient Nd:YAG lasers emitting at 1.06 μm.

G. Construction of Vapor Growth Apparatus

Construction and assembly of a vapor growth apparatus was completed, and the finished system was delivered to Langley Research Center in December 1970. The system was constructed using principles resulting from research on the growth of the wide variety of III-V compounds described in this report. The growth apparatus has the capability of preparing both the binary compounds and alloys containing multiple group III or group V elements. Instructions for the operation of the apparatus were previously furnished to the Contract Monitor.

III. CONCLUSIONS AND RECOMMENDATIONS

The system developed earlier in the contract period for the growth of III-V compounds containing Ga and In as group III elements has been successfully extended to the growth of Al-containing compounds, including AlAs, AlN, and AlP. In particular, single-crystalline AlAs layers have been prepared with the lowest carrier concentrations and highest mobilities yet observed for this compound. And, of equal importance, these layers have greatly enhanced chemical stability. In addition, later modifications and improvements in the growth procedures of GaN, $In_{1-x}Ga_xP$, and $GaAs_{1-x}Sb_x$ initiated earlier in the contract period have led to significant reductions in carrier concentration and improved crystalline perfection of these materials.

As a result of this program it is now possible to prepare high-quality single-crystalline layers of nine binary III-V compounds and representative compositions from six of their alloy series. Further, many of these compounds and alloys have been doped n- and p-type over broad ranges of conductivity and have been prepared in multi-layer structures. As a result, complete control of the composition and bandgap, the doping type and conductivity, and the growth sequence of these layers is now possible. This flexibility in turn has led to the preparation of a wide variety of important devices with outstanding properties. Thus, virtually all of the objectives of this contract have been successfully accomplished, benefiting many areas of III-V compound device applications.

Future work should be carried out to provide reproducible and controlled doping of GaN with acceptor impurities, and on the vapor growth of $Al_{1-x}In_xP$ alloys. The successful preparation of these materials, doped n- and p-type, should lead to the fabrication of electroluminescent devices useful in the spectral range from the visible through the UV and with high brightness, respectively, as well as to devices suitable for high-temperature applications. In addition, the vapor-growth and doping of $In_{1-x}Ga_xP$ alloys should be further explored because of its potential for operation at high brightness levels.

IV. NEW TECHNOLOGY APPENDIX

Numerous areas of new technology in the vapor growth of III-V compounds and their alloys have been developed. These have been of direct benefit to this NASA-sponsored program, but have also contributed importantly to the success of programs conducted for other Governmental agencies such as the Army and the Air Force. The items highlighted below cover the entire contract period.

A. Title: Control of $In_{1-x}Ga_xP$ Alloy Composition

Page Reference: 7

Comments: $In_{1-x}Ga_xP$ is a potential candidate for high-brightness electroluminescent diodes, but control of the composition has been a problem. It has been found that by adjusting the HCl_{In}/HCl_{Ga} ratio to the separate In and Ga metal sources that pre-selected alloy compositions can be prepared, and that complete control of the composition is possible. Other growth variables have been investigated, but none offer the control afforded by adjusting the HCl flow ratio.

B. Title: Visible Light Electroluminescent Diodes of $In_{1-x}Ga_xP$

Page Reference: 47-49

Comments: P-N junction electroluminescent diodes that emit orange light have been prepared both by vapor growth and by acceptor impurity diffusion in $In_{1-x}Ga_xP$ alloys.

C. Title: Mechanical-Chemical Polishing of <100> GaSb Substrates

Page Reference: 10 (Interim Scientific Report No. 1)

Comments: A mechanical-chemical polishing technique previously used with success on Si, Ge, GaAs, and CdS has been found to produce smooth damage-free (100) GaSb surfaces.

D. Title: Chemical Polishing of (100) and (110) InAs Surfaces

Page Reference: 90

Comments: No chemical etchants have yet been reported for polishing InAs. The etchant described is especially useful for providing smooth, damage-free, clean surfaces of InAs for epitaxial growth.

E. Title: Improved Procedure for the Growth of $Ga_{1-x}In_xAs$ Alloys

Page Reference: 51, 52-54

Comments: In previous vapor phase growth systems, the indium and gallium have either been mixed together, or have been maintained at the same temperature in the same furnace. Here, the indium and gallium sources are held at separate temperatures, and this allows superior control over the composition of the grown $In_{1-x}Ga_xAs$ alloys.

Note: Although the etchant described under D, and the growth system described under E are not new in themselves, their application to InAs and $Ga_{1-x}In_xAs$ alloys is new.

F. Title: Improved Cooled-Substrate-Holder

Page Reference: 11 (Quarterly Technical Report No. 3)

Comments: An improved cooled-substrate-holder which provides more uniform cooling of the substrate during vapor phase growth has been designed and constructed. More uniform cooling provides rapid uniform growth without compositional grading of the grown layers due to competition with the walls of the growth system.

G. Title: Vapor Phase Growth of III-V Antimonide Compounds and Alloys Using Stibine (SbH_3) Gas

Page Reference: 83-86

Comments: Procedures for storing and handling stibine and means to introduce it into the vapor phase growth system to grow antimonides are outlined.

H. Title: Vapor Growth of p-n Junctions in GaSb

Page Reference: 5 (Quarterly Technical Report No. 6)

Comments: A method is described for preparing p-n junctions in GaSb from the vapor phase, which necessitates using Te as the donor impurity and employing low growth temperatures.

I. Title: Low Temperature Growth of GaN

Page Reference: 5 (Quarterly Technical Report No. 4)

Comments: A method is described for preparing GaN at temperatures as low as 550°C. This has significant implications for the utility of this material, since it avoids problems relating to thermal decomposition.

J. Title: Growth of Single-Crystalline GaN

Page Reference: 35-36

Comments: A method of preparing single-crystalline GaN is described which involves the use of <0001>-oriented sapphire substrates and strict exclusion of oxygen contamination.

K. Title: Reduction of Donor Concentration in GaN

Page Reference: 2-3

Comments: GaN is a potential candidate for a full range of visible electroluminescent devices but the high donor concentration is an impediment to the routine attainment of high conductivity p-type layers and p-n junctions. It has been found that by increasing the flowrate of NH_3 into the growth tube from 1500 to 7500 cm^3/min, the donor concentration is reduced by an order of magnitude from $3 \times 10^{19} cm^{-3}$ to $3 \times 10^{18} cm^{-3}$. Accordingly, the possibility of achieving p-type conductivity reproducibly is enhanced.

L. Title: Ge-Acceptor Doping of Single-Crystal GaN

Page Reference: 38

Comments: The preparation of p-n junction structures in GaN requires that the high inherent n-type impurities be compensated before a conducting p-type sample can be achieved. Conducting p-type GaN has been prepared for the first time by doping with Ge-acceptor impurities.

M. Title: Vapor Growth of AlAs

Page Reference: 62-64

Comments: AlAs and $Ga_{1-x}Al_xAs$ alloys are potential candidates for visible electroluminescence diode materials, but growth problems had prevented the preparation of these materials as single-crystalline vapor-grown layers. Single-crystalline AlAs layers have now been prepared for the first time from the vapor phase by preventing attack of the deposition apparatus and by placing the aluminum-chloride outlet orifice within close proximity of the substrate.

N. Title: Reduction of Donor Concentration in AlAs

Page Reference: 11-13

Comments: AlAs is another potential candidate for visible electroluminescent devices. Up to now, the lowest donor concentrations achieved were about $5 \times 10^{17} cm^{-3}$. This has been reduced by a factor of 5 through the use of high-purity carbon parts, such as the protective liner, the substrate holder, and the boat for the Al metal source, and a pyrolytic carbon coating on all quartz parts exposed to the corrosive aluminum chloride vapors.

O. Title: AlAs p-n Junction Structures

Page Reference: 16, 78-82

Comments: The utility of AlAs for high-temperature applications, or for electroluminescence, would be greatly enhanced if stable p-n junctions could be fabricated in this material in a reproducible manner. Now, for the first time, it has been demonstrated that stable p-n junctions can be prepared in vapor-grown AlAs by diffusion of Zn-acceptor impurities.

P. Title: Vapor-Phase Transport of $Al_{1-x}In_xP$ Alloy

Page Reference: 17-19

Comments: $Al_{1-x}In_xP$ has been predicted to have one of the highest brightness values of any III-V compound electroluminescent device. Accordingly, the vapor-growth of this compound is important to its future use. Closed-tube vapor transport of InP and AlP starting compounds resulted in the formation of small crystals containing up to 14% AlP, thus demonstrating the feasibility of vapor-growth methods.

APPENDIX A

THE VAPOR PHASE GROWTH OF SEVERAL III-V COMPOUND SEMICONDUCTORS

J. J. TIETJEN, R. E. ENSTROM, AND D. RICHMAN

Abstract

A review is presented of the RCA vapor phase growth method which has been used for the synthesis of a broad spectrum of III-V compounds. This technique features the use of predominantly gases as the source chemicals which provide improved control of the chemical composition, homogeneity, crystalline perfection, and impurity concentrations and distributions of the epitaxial layers. As a result, a number of notable advances have been made with respect to the material properties and device utilization of several III-V compounds.

A. Introduction

The III-V compound semiconductors and their alloys cover a wide range of electrical and optical properties which make them potentially useful for a variety of practical applications. These include electro-optic and microwave devices, high-temperature applications, and electron-emitting phenomena. Unfortunately, the synthesis of these materials is frequently complicated by the combination of high melting temperatures and dissociation pressures, and large concentration differences between the isothermal liquidus and solidus in the phase diagrams of these alloy systems. However, many of the difficulties associated with these complications are minimized when vapor phase crystal growth methods are employed, primarily because of the low growth temperatures that are possible with this technique. In addition, vapor-phase growth facilitates preparing these compounds in thin layer geometries which is often essential for optimum use in device structures.

There are many possible approaches to the vapor deposition of III-V compounds, including a variety of evaporation techniques, sputtering, closed-tube and close-spaced chemical transport, and open-tube flow methods. Although most of these methods have been important for specific applications, only the latter offers the flexibility and control needed to prepare many materials, with widely differing properties, and in a variety of geometries. In general, however, even open-tube flow techniques have had limited success, particularly with regard to the preparation of alloys. This is due to the fact that liquids and solids are normally used as the source chemicals, even for the group V elements. Therefore, it is difficult to maintain constant pressures of the reactant species in the growth zone, since the concentrations of these reactants have an exponential dependence on the temperature of the source constituents.

As a result of these considerations, an open-tube flow method (Refs. 12, 17,18,19) has been developed in which the primary source chemicals are predominantly gaseous at room temperature. This minimizes compositional fluctuations and, thereby, insures a high degree of crystalline homogeneity. In addition, the use of gases provides a high degree of flexibility for controlling alloy composition or dopant impurity levels since the reactant concentrations are accurately established by precision flow meters and valves. An important feature of this control is the ability to slowly grade the composition of a growing layer from a substrate composition to that of the terminal compound in order to minimize strains due to the lattice mismatch. In addition, this control accommodates the synthesis of multilayer structures having properties tailored to the needs of specific devices.

To date, the capability of this technique has been demonstrated by the preparation of an outstanding number of materials as single crystalline layers, doped either n- or p-type, and in the form of multilayer structures including p-n junctions. Included in these materials are GaAs, GaP, GaSb, GaN, InAs, InP, AlAs, AlP, AlN, and alloys of $GaAs_{1-x}P_x$, $GaAs_{1-x}Sb_x$, $Ga_{1-x}In_xAs$, $Ga_{1-x}In_xP$, $Ga_{1-x}Al_xAs$, and $InAs_{1-x}P_x$. Further, these materials have found application in a large number of devices, many of which exhibit exceptional characteristics. These include varactor diodes (Ref. 20), transferred electron oscillators (Ref. 21), electroluminescent diodes (Ref. 22), injector lasers (Ref. 23), high-temperature rectifiers (Ref. 24), and transistors (Ref. 25), electro-optic modulators (Ref. 26), secondary-emission dynodes (Ref. 27), and photocathodes (Ref. 28).

This Appendix reviews this vapor-growth technique and the properties of the various materials and devices that have resulted from its use.

B. Experimental

The growth apparatus and technique have been described in detail previously (Refs. 17,19,29), and, therefore, will be only briefly described here. The apparatus consists principally of a straight tube through which the various gases pass. The exact design of this tube depends on the materials to be prepared and on the growth rates desired. One of the more general forms is shown schematically in Figure 6. The group III elements are transported as their subchlorides formed by the reactions of HCl with the elements. The group V elements are introduced to the growth tube as their respective hydrides. N-type doping is accomplished by using H_2Se gas, and zinc vapor provides the p-type dopant. As the gases pass over the substrate they react with its surface to form an epitaxial deposit, the composition and electrical properties of which are determined by the vapor constitution.

The simplicity of this design and technique make it readily adaptable to the synthesis of virtually any III-V compound or alloy, and to many other materials (Refs. 30,31). In all cases, the inherent control afforded by this method assists in maximizing crystalline perfection and in the formulation of device structures.

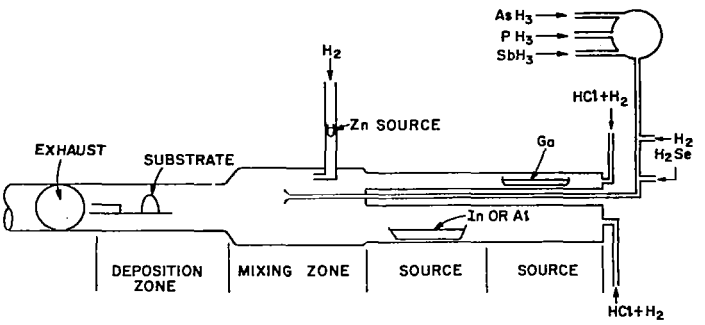

Figure 6. Schematic diagram of apparatus used for growth of III-V compounds and alloys.

C. Characterization of Materials

As cited in the introduction, a very large number of III-V compounds and alloys has been prepared by this growth method, and the properties of many of them have been described in detail previously. Therefore, for the sake of brevity and clarity, only the more important properties will be summarized in this report. The various materials are cataloged below, with an appropriate description of their properties. The references included with the headings provide direction to a more detailed description of these materials.

1. GaAs (Refs. 17,21), GaP (Ref. 26)*, and $GaAs_{1-x}P_x$ (Ref. 17) Alloys. - This group of compounds encompasses energy gaps in the range of about 1.4 to 2.2 eV at room temperature and, therefore, involves optical transitions extending from the near infrared to the middle of the visible spectrum. The energy gaps are direct for values of x up to about 0.45 and are indirect for higher values of x. These materials can be prepared in thicknesses ranging from about 0.5 μm to 1 mm, at growth rates in the range of from 0.5 to greater than 10 μm/min on GaAs substrates, including dielectric materials such as sapphire and spinel.

Undoped samples of GaAs have been prepared with net electron concentrations as low as $9 \times 10^{13} cm^{-3}$ and mobilities as high as 8700 $cm^2/V\text{-sec}$ and 108,000 $cm^2/V\text{-sec}$ at room temperature and 77°K, respectively. All of these compounds can be readily synthesized with net electron concentrations, at room temperature, of less than $5 \times 10^{15} cm^{-3}$. Also, these materials can all be easily doped with donor or acceptor impurities to increase the carrier concentrations into the 10^{18} and $10^{19} cm^{-3}$ range, respectively, without seriously degrading their crystalline quality. It is noteworthy that $GaAs_{1-x}P_x$ alloys prepared by this growth technique were the first to show the proper dependence of the electron mobility on alloy composition which

*Also B. Curtis and R. Sussman, RCA Laboratories, private communications.

provided strong evidence for the now-accepted fact that alloy scattering does not dominate in III-V alloy systems (Ref. 33).

2. InAs, InP, and $InAs_{1-x}P_x$ Alloys (Ref. 18). - These materials are all direct-bandgap semiconductors, and cover the range of about 0.35 to 1.3 eV, at room temperature. Typical growth rates for these compounds range from 0.25 to 0.5 μm/min with the lower rates corresponding to InP-rich alloys. With such growth rates, layers having a thickness as low as about 0.2 μm to as high as 150 μm, dependent on alloy composition, can be prepared. To date, these materials have been prepared on InAs, InP, and GaAs substrates.

Typical electron carrier concentrations for undoped layers are in the range of 5×10^{15} to $1 \times 10^{16}/cm^3$. In general, the electron mobilities of these materials are equivalent to or exceed the highest values reported. Both n- and p-type doping has been achieved to provide carrier concentrations as high as the $10^{19}cm^{-3}$ range while maintaining good crystalline quality.

3. GaSb and $GaAs_{1-x}Sb_x$ Alloys. - This growth technique has permitted the vapor-phase growth of $GaAs_{1-x}Sb_x$ across the entire alloy series for the first time. These compounds have direct transitions across their energy gaps which cover the range of approximately 0.7 to 1.4 eV at room temperature. Because of the low melting point of many of these materials, relatively low growth temperatures are necessary. This restricts the partial pressure of antimony in the growth system to a low value, and results in low growth rates. Typical growth rates for these materials are about 0.2 μm/min, with layer thicknesses normally restricted to the range of about 0.2 to 25 μm, for growth on GaAs substrates.

As-grown layers of these compounds are usually p-type with hole concentrations in the low $10^{16}cm^{-3}$ range. The hole mobilities for GaAs-rich alloys are high, comparable to the highest values reported for unalloyed p-type GaAs. As a result of the strain introduced to GaSb-rich alloys, due to the lattice and thermal expansion mismatch with the GaAs substrates, the mobilities of these materials are slightly lower than reported for melt grown alloys. This problem of strain could be alleviated by using GaSb substrates or by slow compositional grading between the substrate and the alloy layer.

4. GaN (Refs. 12,34). - GaN prepared by this method has provided the first single-crystalline material suitable for good electrical and optical evaluation of this compound. GaN has a direct energy gap, at room temperature, of about 3.5 eV (Ref. 34). Normal growth rates are about 0.5 μm/min and, therefore, layers having thicknesses up to about 150 μm are easily prepared.

Undoped crystals have a very high inherent electron concentration, usually about $10^{19}cm^{-3}$, which is probably due to a high density of nitrogen vacancies. Although conducting p-type samples have been prepared, this result is extremely difficult to reproduce, and the samples have been electrically inhomogeneous.

5. $Ga_{1-x}In_xAs$ (Ref. 8) and $Ga_{1-x}In_xP$ (Ref. 5) Alloys. - $Ga_{1-x}In_xAs$ and $Ga_{1-x}In_xP$ alloys have energy gaps which cover the range 0.35 to 1.4 eV and 1.3 to 2.2 eV, respectively. The $Ga_{1-x}In_xAs$ alloys have a direct energy gap over the entire composition range. Similarly, InP is direct but the $Ga_{1-x}In_xP$ alloys become indirect above about 2.1 eV. The alloy composition is varied for both alloys principally by adjusting the HCl flow ratio to the indium and gallium metal sources. In addition, for the $Ga_{1-x}In_xP$ alloys, the composition is a function of the growth temperature. $Ga_{1-x}In_xAs$ alloys can be prepared by depositing pure GaAs or InAs initially on GaAs or InAs substrates, respectively, which are readily available, and then grading to the final alloy composition to achieve a layer having a low imperfection density and a minimum of strain. A similar procedure can be used for the $Ga_{1-x}In_xP$ alloys by using GaP or InP substrates. However, since GaP and InP substrates have not been readily available, GaAs substrates have also been used; but because of the lattice parameter and thermal expansion mismatches between the epitaxial layer and the substrate, these alloy layers are not as perfect. Donor carrier concentrations as low as $5 \times 10^{14} cm^{-3}$ have been achieved for undoped $Ga_{1-x}In_xAs$ alloys, and both alloy systems can be doped n- and p-type over the broad range required for device applications.

6. AlAs (Ref. 35), AlP (Ref. 29), AlN, and $Ga_{1-x}Al_xAs$. - AlAs, AlP, and AlN are indirect gap compounds with forbidden energy gaps of 2.16, 2.43, and about 4.0 eV, respectively; the latter value has not been well established as yet. GaAs is direct, and the crossover point to indirect gap $Ga_{1-x}AlAs$ alloy has been found to occur at 1.89 eV which corresponds to a composition of about 27% AlAs (Ref. 11). Unlike gallium and indium chlorides, the aluminum chlorides produced by the reaction of HCl with the aluminum metal source have been found to attack the quartz deposition tube, but this can be prevented by using a protective liner of Al_2O_3 or carbon. AlAs and AlP have nearly the same lattice parameters as GaAs and GaP, respectively, thus making the latter materials useful as substrates to attain single crystalline deposits. Further, the constancy of the lattice parameter makes the $Ga_{1-x}Al_xAs$ alloy system of great interest since the attainment of low strain, large bandgap epitaxial layers is more readily achieved than in systems where grading is required. Undoped AlAs layers with donor concentrations as low as $3 \times 10^{17} cm^{-3}$ and room-temperature mobilities as high as 280 $cm^2/V\text{-sec}$ have been achieved, and these represent the best properties reported so far. In addition, AlAs prepared by this method is sufficiently stable in normal ambients so that it can be processed into device structures, such as p-n junctions (Ref. 36), by conventional methods. Previously, AlAs had been considered to be too hygroscopic to permit such device utilization. The enhanced stability of these AlAs layers may be related to improved crystalline perfection and/or higher purity. For undoped AlP, carrier concentrations and room-temperature mobilities are typically $1 \times 10^{18} cm^{-3}$ and 80 $cm^2/V\text{-sec}$, respectively.

D. Device Applications

The most notable accomplishment of this crystal growth method has been the success with which it has been applied to the preparation of device structures. This has involved a broad range of materials and structures, and has accommodated the fabrication of several outstanding devices. The more important devices are listed below with a summary of their properties. The references supplied provide direction to a more complete description of the devices and their characteristics.

1. Varactor Diodes (Ref. 20). - Over 1000 p^+-n-n^+ diode structures were incorporated in complete microwave devices, and provided the highest combination of reverse breakdown voltages and cut-off frequencies ever reported. Breakdown voltages in excess of -50 V are easily achieved, with cut-off frequencies above 150 GHz at -6 V bias.

2. Electroluminescent Diodes (Refs. 22, 37-40). - Complex n^+-n-p-p^+ structures have been studied in $GaAs_{1-x}P_x$ in order to optimize the device parameters of visible electroluminescent diodes. These structures not only involved several changes in dopant type and concentration, but also subtle manipulation of the gross composition of the alloys involved. As a result of this study, diodes emitting in the red region of the spectrum can be reproducibly prepared having brightness values slightly above 30 ft-L at 1 A/cm^2 which is within a factor of 3 of the highest value reported to date.

3. Injection Lasers (Refs. 23,41,42). - Abrupt p-n junction structures prepared in $GaAs_{1-x}P_x$ alloys resulted in the first room-temperature injection lasers operating in the visible region of the spectrum. In fact, these diodes have provided operation at the shortest wavelength ever reported for a room-temperature injection laser, 6750 Å.

4. High-Temperature Rectifiers (Refs. 24,32). - High-power rectifiers capable of operating at temperatures above 300°C have been fabricated from both GaAs and $GaAs_{1-x}P_x$ alloy multi-layer structures consisting of as many as six different layers. To achieve high reverse-bias breakdown voltages and high forward currents, the electron concentration had to be reduced to $< 1 \times 10^{15}$cm^{-3} and micro plasma-free p-n junctions as large as 0.175 in. had to be prepared. The latter was particularly troublesome since the probability of encountering crystal defects which cause micro-plasmas increases with the p-n junction area. Rectifiers fabricated from these wafers have attained reverse-bias voltages as high as 475 V for a 0.050-in.-diameter and 250 V for a 0.175-in.-diameter mesa p-n junction. Further, the 0.175 in. diode passed 50 A in the forward direction at 25°C before and after cycling to 300°C.

5. High-Temperature Transistors (Ref. 25). - GaAs n-p-n and $GaAs_{1-x}P_x$ p-n-p structures with base layers as thin as 1 μm have been used for the fabrication of transistors. So far the GaAs n-p-n structures have given the best results and room-temperature current gains as high as 40 have been achieved. Transistor action has been demonstrated to temperatures as high as 300°C and at this temperature the I-V characteristics are stable. Minority hole and electron lifetimes in GaAs and $GaAs_{1-x}P_x$ p-n junctions are about 10 and 5 nsec respectively for $x < 0.3$.

6. Transferred Electron Oscillators and Amplifiers (Refs. 21, 43-56). - A wide variety of oscillators and amplifiers have been prepared from GaAs and $GaAs_{1-x}P_x$ having outstanding electrical properties, as shown in Table IX. These devices operate in the frequency range of 1 to 40 GHz. Except for coplanar devices, n^+-n-n^+ layer structures have been used and the thickness of the n-layer, which determines the frequency of operation, has ranged from 2 to 100 μm.

7. Electro-Optic Modulators (Ref. 26). - By using a technique of rapid vapor phase growth, GaP crystals doped with Fe to provide high resistivity were prepared with thicknesses suitable for transmitting collimated light beams. These crystals were used to demonstrate electro-optic modulation of visible radiation. However, the utility of these crystals was limited because of problems related to slight crystalline strain, and isolated electrical shorting paths.

8. Secondary Emission Dynodes (Ref. 27). - Highly doped p-type polycrystalline layers of GaP deposited on metallic substrates, were optimized for use as negative-electron-affinity secondary emitters. These layers have provided revolutionary results as dynodes in commercial photomultiplier tubes. Among the most important results are the ability to discriminate between single and multiple photoelectronic events, increased speed of response, and lower dark currents.

9. Photocathodes (Refs. 8,28,57). - Single-crystalline GaAs, $GaAs_{1-x}P_x$, $Ga_{1-x}In_xAs$, $GaAs_{1-x}Sb_x$, and $InAs_{1-x}P_x$ alloys heavily doped with acceptor impurities have been prepared for use as negative electron affinity photocathodes in photomultiplier and image tubes. The bandgap of the alloy determines its spectral response. Thus $GaAs_{1-x}P_x$ alloys with a bandgap of about 1.7 eV have been used to detect ultraviolet and visible radiation up to about 7500 Å with a quantum yield about four times higher than the standard S-10 photocathode surface normally used for this wavelength region. Alloys in the other three systems have been prepared with bandgaps of about 1 eV and have been used to extend the response out to 12,000 Å. So far the $Ga_{1-x}In_xAs$ system has given the best results, with a quantum yield, at 10,000 Å, of more than 10 times that obtainable with the conventional S-1 photocathode. The $GaAs_{1-x}P_x$ alloy photocathode has been incorporated into commercial photomultiplier tubes with outstanding results.

Table IX

CHARACTERISTICS OF TRANSFERRED ELECTRON OSCILLATORS AND AMPLIFIERS PREPARED BY VAPOR PHASE GROWTH

Oscillators	Freq. (GHz)	Mode	Power (W)	Efficiency (%)
High power, GaAs	1	pulsed	120.	32.
High power, $GaAs_{0.8}P_{0.2}$	3	pulsed	200.	27.
CW operation	9	CW	0.7	3.
Series operation of 2 devices	8	pulsed	3.4	28.
Hybrid operation	8	pulsed	19.1	22.
Coplanar (n on semi-insulating GaAs)	1	pulsed	125.	5.
LSA operation	15	pulsed	3.5	8.
Amplifiers				
Stabilized, super-critical GaAs with $n \cdot L > 10^{12} cm^{-2}$	4-8 4-8 8-12	pulsed CW CW	2. 1. 1.	6. 3. 3.

E. Conclusions

A versatile vapor phase growth method has been developed which permits the preparation of virtually all III-V compounds and their alloys in a compatible manner. The quality of the material produced by this technique is, in general, equivalent to or in advance of the state-of-the art of other methods used for the synthesis of III-V compounds.

The crystal growth method has been extended to accommodate the preparation of device structures, and has resulted in the formulation of a number of novel devices having excellent properties.

APPENDIX B

THE PREPARATION AND PROPERTIES OF VAPOR-DEPOSITED SINGLE-CRYSTALLINE GaN

H. P. MARUSKA AND J. J. TIETJEN

Abstract

Single-crystalline, colorless, GaN has been prepared by a vapor-phase growth technique previously used to prepare GaAs, GaP, and GaSb. These crystals are the first reported specimens of GaN suitable for good electrical and optical evaluation of this compound. It has been determined that GaN has a direct energy bandgap of 3.39 eV, and that undoped crystals prepared by this method have a very high inherent electron concentration, typically above $10^{19}/cm^3$, which is probably related to a high density of nitrogen vacancies. Conducting p-type specimens have been prepared using Ge as the dopant; but this result has been difficult to reproduce, and the samples have been electrically inhomogeneous.

A. Introduction

A large amount of work has been expended for the preparation and characterization of III-V compounds having bandgaps corresponding to the spectral range from the infrared to the middle of the visible spectrum. In general this involves compounds formed from the group-V elements As, P, and Sb. In contrast, for the nitrogen-containing compounds which have relatively large bandgaps (extending through the visible and into the ultraviolet) very little work has been reported despite their potential for use as photoconductors, in both cathodo- and electroluminescent devices, and for high-temperature applications.

One nitride of particular interest is GaN since its bandgap corresponds to the edge of the ultraviolet and, therefore, could be applicable to the entire visible spectrum. The work that has been reported has in general described the preparation and properties of polycrystalline deposits, usually prepared by the reaction of NH_3 with Ga (Ref. 58), Ga_2O_3 (Ref. 59), or GaP (Ref. 60). The only report of single-crystalline material involves small needles, only a few microns in length (Ref. 61). It is significant that very little reported work deals with the growth of GaN from the vapor phase. In contrast, vapor-phase growth techniques have played an important role in the preparation and characterization of GaAs (Ref. 62), GaP (Ref. 63), and GaSb (Ref. 64). In particular, a compatible method (Refs. 64,17) has been developed for the preparation of these compounds in which the respective hydrides AsH_3, PH_3, and SbH_3 serve as the sources of the group-V elements, and Ga is transported as its subchloride via a reaction with HCl gas. This technique has now been further extended for the preparation of GaN by using NH_3 as the source of nitrogen. This has resulted in the first reported large-area single-crystalline deposits of GaN, and has led to more precise characterization of its properties.

B. Experimental

1. Apparatus and Materials. - The apparatus is essentially identical to that described previously (Ref. 17) with the exception that NH_3 is used in place of the other group-V hydrides. It is primarily comprised of a straight tube through which the pertinent gaseous species flow to provide chloride-transport of metallic gallium, and subsequent reaction of these transport-products with ammonia to form GaN on a substrate surface.

With the exception of the ammonia* and <0001>-oriented sapphire single-crystalline substrates**, the materials employed in this study are as described previously (Ref. 17). The sapphire substrates were mechanically polished** to a flat mirror-smooth finish, and then heat-treated in hydrogen at 1200°C prior to their introduction to the growth apparatus. Typical substrate dimensions were about 2 cm^2 in area and about 0.25 mm thick.

2. Procedure. - The growth procedure also closely follows that described previously (Ref. 17). Freshly heat-treated substrates are inserted into the deposition zone of the growth chamber and heated in hydrogen at a rate of about 20°C/min. When the final growth temperature is reached, the NH_3 flow is started and, after a 15-min period to allow the NH_3 concentration to reach a steady-state value, the HCl flow is started to provide transport of the Ga and deposition of GaN.

The flow rates of pure HCl and NH_3 are about 5 and 400 cm^3/min, respectively, and an additional 2.5 liters/min of hydrogen are used as a carrier gas. With these flow rates, with a substrate temperature of 825°C, a Ga-zone temperature of 900°C, and a center zone (that region between the Ga- and deposition-zones) temperature of 925°C, growth rates of about 0.5 μm/min are obtained under steady-state conditions. Typical thicknesses for these deposits have been in the range of 50 to 150 μm.

C. Results and Discussion

1. Crystallinity. - X-ray analysis by the Debye-Scherrer technique indicates that these layers are single phase, hexagonal GaN, having the wurtzite structure and lattice parameters a = 3.189 Å, c = 5.185 Å at room temperature. The mean coefficient of thermal expansion in the range of 300° to 900°K is 5.59 x 10^{-6}/°C in the "a" direction. This value was obtained by means of powder patterns taken every 100°K with a Unicam high-temperature camera. Laue back-reflection patterns show this material to be single-crystalline and epitaxial, having a <0001> orientation.

*Scientific Gas Products, Editon, New Jersey.

**Insaco, Quakertown, Pennsylvania.

2. Chemical Properties. - The GaN prepared by this technique was found to be insoluble in H_2O, acids, or bases at room temperature. It dissolves slowly in hot alkalis, a sample weighing 150 mg taking 24 hours to completely dissolve in boiling NaOH. Emission spectrographic and mass spectrometric analyses indicate a total impurity content of less than 10 ppm and less than 1 ppm of any one impurity.

3. Optical Properties. - Room-temperature optical absorption measurements on undoped GaN reveal a very sharp absorption edge, and on the high energy side of this edge the absorption coefficient obeys the general relationship

$$\alpha = \alpha_o(E-E_g)^n \qquad (1)$$

where E is the photon energy, and E_g is the energy of the bandgap (Ref. 65). From the absorption data, E_g and n were determined to be 3.39 eV and 0.62, respectively. The value of 0.62 is indicative of a direct transition across the energy gap and is consistent with values obtained for other direct bandgap III-V compounds (Ref. 66).

4. Electrical Properties. - These epitaxial layers were examined by conventional Hall coefficient and resistivity measurements. Undoped samples are n-type, having typical electron concentrations in the range of 1 to 5 x $10^{19}/cm^3$ and room-temperature mobilities of between 125 and 150 cm^2/V-sec. These high mobility values for such high carrier concentrations also support the contention that GaN is a direct bandgap semiconductor. Since the total impurity content of these crystals is at least two orders of magnitude too low to account for the high inherent donor concentration it is suspected that the donor is related to a native defect, probably a nitrogen vacancy. In this regard, it should be noted that GaN dissociates to liberate nitrogen at temperatures as low as 600°C (Ref. 59).

5. Doping. - Preliminary experiments have been carried out in an effort to dope these GaN layers with acceptor impurities. The impurities studied to date include Zn, Mg, Hg, Si, and Ge. Both Zn and Mg produce high-resistivity material ($\rho > 10^9$ ohms-cm) and color the normally colorless GaN orange and yellow, respectively. Evidently, both of these impurities are introduced as deep acceptor states. Hg-doped samples remained highly conducting n-type, undoubtedly due to a relatively limited solubility of Hg in GaN at the growth temperature. Emission spectrographic analysis revealed that Hg had not been incorporated in the GaN in concentrations greater than 30 ppm.

Consistent with the hypothesis that these GaN layers have a very high density of nitrogen vacancies, the group IV elements, Si and Ge, are attractive candidates as p-type dopants since they are reaily introduced to the growth apparatus in the form of their hydrides, and as substitutes for nitrogen sites should behave as acceptor states. Indeed, the best success was

achieved with these impurities. In the case of Si, substantial compensation was achieved without introducing a color to the GaN indicating that Si is probably a shallow acceptor. However, to date, although the carrier concentration has been reduced to as low as 3 x $10^{16}/cm^3$, Si-doped samples have all been n-type.

With Ge-doping, conducting p-type behavior has been achieved. Two layers have been prepared with resistivities of 0.01 and 0.94 ohms-cm for hole concentrations of 6 x 10^{19} and 6 x $10^{18}/cm^3$, respectively. While this result is encouraging since it demonstrates that a fundamental mechanism does not exist which prevents amphoteric doping of this compound, it has been very difficult to reproduce and the layers are non-uniform, with some regions of the sample being n-type.

This aspect of the research on GaN will be continued to provide a more detailed description of the role of acceptor impurities in this compound, and will be the subject matter of another publication.

D. Conclusions

It has been demonstrated that single-crystalline, colorless, GaN can be prepared in the form of large-area crystals on sapphire substrates by means of a vapor-growth method previously used for the preparation of GaAs, GaP, and GaSb. These crystals represent the first reported single-crystals of GaN of adequate size for good electrical and optical evaluation and have thereby permitted more exact characterization of these properties. The energy bandgap of this compound, 3.39 eV, is slightly larger than the previously reported value of 3.26 eV (Ref. 67), and appears to involve a direct transition. Undoped crystals have a very high inherent donor concentration which is probably related to a high nitrogen vacancy concentration. This implies that the ability to control the electrical properties of this material, especially for providing p-type conductivity, will depend on obtaining better control of its defect structure.

APPENDIX C

THE PREPARATION AND PROPERTIES OF VAPOR GROWN $In_{1-x}Ga_xP$

C. J. NUESE, D. RICHMAN, AND R. B. CLOUGH

Abstract

$In_{1-x}Ga_xP$ has been prepared over the entire alloy system by an epitaxial vapor-phase growth technique. The energy gap dependence on alloy composition for these layers has been determined by optical absorption, Schottky-barrier photoresponse, and electroluminescence measurements. These measurements indicate a non-linear dependence of the (direct) conduction band minimum on $In_{1-x}Ga_xP$ composition, and a direct-indirect energy gap crossover at 2.20 eV and 70% GaP at room temperature.

Zn-diffused p-n junctions have been formed in the $In_{1-x}Ga_xP$ layers, and have been found to be reasonably well-behaved in regard to their I-V and C-V characteristics and their photoresponse. The electroluminescent emission spectra contain a narrow high-energy near-bandgap peak, but are frequently dominated by low-energy impurity peaks. For indirect-bandgap alloys, impurity peaks lie approximately 0.25 and 0.5 eV less than bandgap. A third peak is found at an energy of 1.30 to 1.35 eV independent of composition, for $x \geq 0.4$.

A. Introduction

Reports that the energy band structure of $In_{1-x}Ga_xP$ is direct to energies as high as 2.20 eV make this material particularly attractive for electroluminescent applications, spontaneous and coherent, over a large portion of the visible spectrum. However, difficulties in material preparation have hampered a detailed investigation of this alloy system, and only in recent years have single crystals of $In_{1-x}Ga_xP$ been prepared. In addition, the energy gap dependence on alloy composition has been reported to be quite different by different researchers, Hilsum and Porteous (Ref. 6) and Rodot et al. (Ref. 7) reporting a linear dependence of the direct conduction band minimum on composition, and Lorenz and Onton (Ref. 4) reporting a significant deviation from linearity.

In the present paper we describe the preparation of single-crystal $In_{1-x}Ga_xP$ layers over the entire alloy system by an epitaxial vapor-phase growth technique. These layers have been evaluated electrically and optically to determine their energy gap dependence on alloy composition. In addition, p-n junctions have been formed in the $In_{1-x}Ga_xP$ layers in order to evaluate the quality of the junctions and the electroluminescent potential of the vapor-grown material. Details of the crystal growth, material characterization, and junction evaluation are discussed in the sections below.

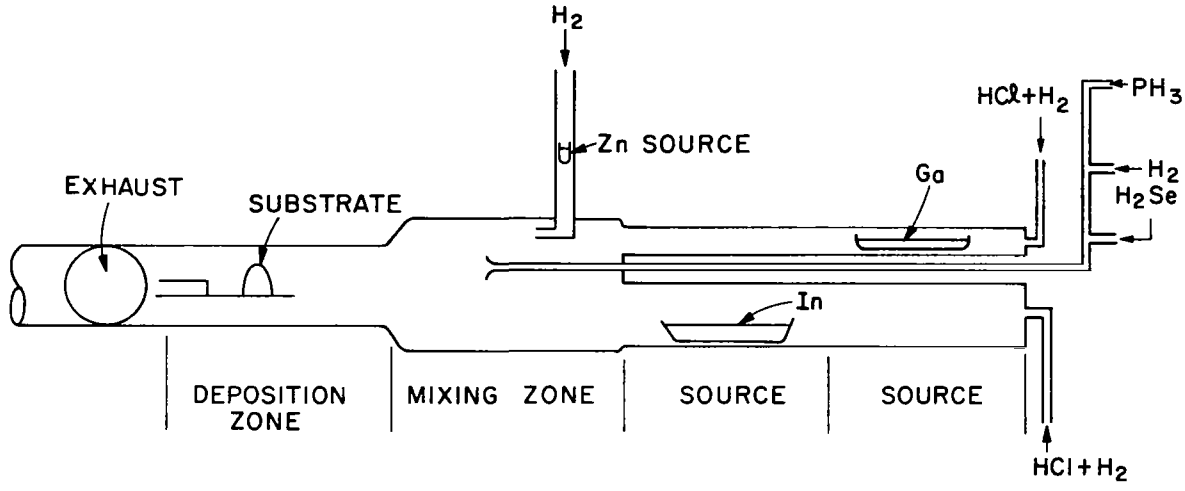

Figure 7. Schematic diagram of growth system used for vapor phase deposition of $In_{1-x}Ga_xP$.

B. Material Preparation and Characterization

The apparatus used to prepare the $In_{1-x}Ga_xP$ alloys used here is a modified version of that described by Tietjen and Amick (Ref. 17), and is shown schematically in Figure 7. The principal modification is the use of separate quartz tubes for the metal sources. In addition, the source zone has been doubled in length. These changes allow independent control of the temperature and the HCl concentrations at each metal source. The substrates used in this work were <100>-oriented GaAs, which were chemically polished with bromine-methanol and Caro's acid prior to insertion into the growth system. The hydrogen carrier gas was palladium-diffused to remove contaminants. The metals, HCl, and phosphine gas (diluted to 5 to 10% in H_2) were the purest commercially available, and were used without further purification. The detailed experimental procedures and apparatus used here are closely similar to those previously reported (Ref. 17), and will not be repeated.

We have investigated the influence of the source, mixing, and deposition zone temperature on the alloy composition. Only the temperature of the deposition zone was found to strongly affect the alloy composition. With all the other variables constant, a decrease in the deposition temperature causes a decrease in the amount of Ga in the $In_{1-x}Ga_xP$ alloy, as shown in Figure 8. We should mention, however, that varying the deposition temperature over the range shown in Figure 8 significantly alters the surface appearance of the epitaxial layers, and is therefore not a practical method for controlling the $In_{1-x}Ga_xP$ alloy composition. For most of the work reported here, the deposition zone was held at 750°C, while the Ga and In sources were maintained at 850° and 950°C, respectively. For these conditions, growth rates between 12 and 25 μm/hr were typically found. The epitaxial layers were generally 25 to 100 μm thick.

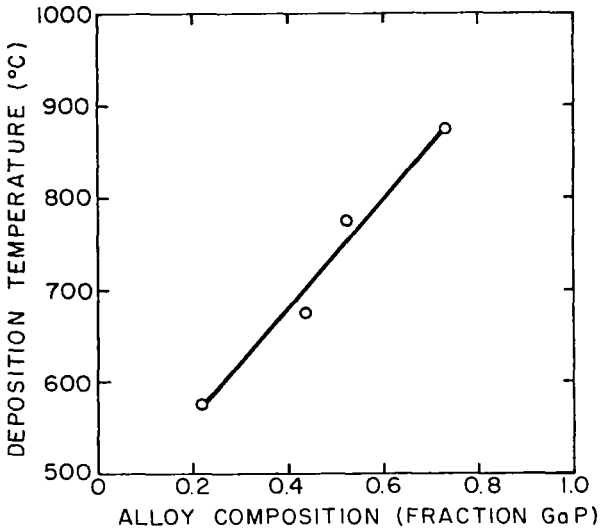

Figure 8. $In_{1-x}Ga_xP$ alloy composition versus deposition temperature. All other growth parameters were held constant.

As expected, the ratio of HCl flow over the two metal sources is of primary importance in establishing the composition of the alloy, as shown in Figure 9. Note here the rapid change in alloy composition for small changes in the HCl ratio. This behavior is not unexpected considering the greater relative stability of InCl to GaCl in the temperature range of this work. The rapid variation of composition with HCl ratio, however, makes the precise control of the gas flows particularly important for achieving homogeneous alloy compositions. For this reason, a mixing bulb was sometimes used to dilute the HCl with hydrogen in order to more accurately control the HCl concentrations over the metal sources. In later experiments a diluted source tank of HCl (10%) was used. Note also in Figure 9 that the $In_{1-x}Ga_xP$ alloy composition is only weakly affected by relatively large changes in the phosphine concentration.

One factor affecting the quality of the alloy layers is the lack of a suitable substrate for all compositions of $In_{1-x}Ga_xP$. The lattice constant of the GaAs substrate matches that of the $In_{1-x}Ga_xP$ epitaxial layer only for a composition, $x = 0.51$. In addition to the lattice constant mismatch, differences in thermal expansion coefficients between the epitaxy and the substrate will introduce strain, and possibly defects, into the alloy layer. We have seen evidence for this in the form of bowing of the epitaxy-substrate composite after removal of the wafer from the growth system, the direction of the bow being concave toward the substrate. Removal of the substrate from the epitaxial layer in some cases has also resulted in severe cracking of the epitaxial layer along (110) crystal planes. These conditions undoubtedly contribute to the low electroluminescent efficiencies obtained for these alloys.

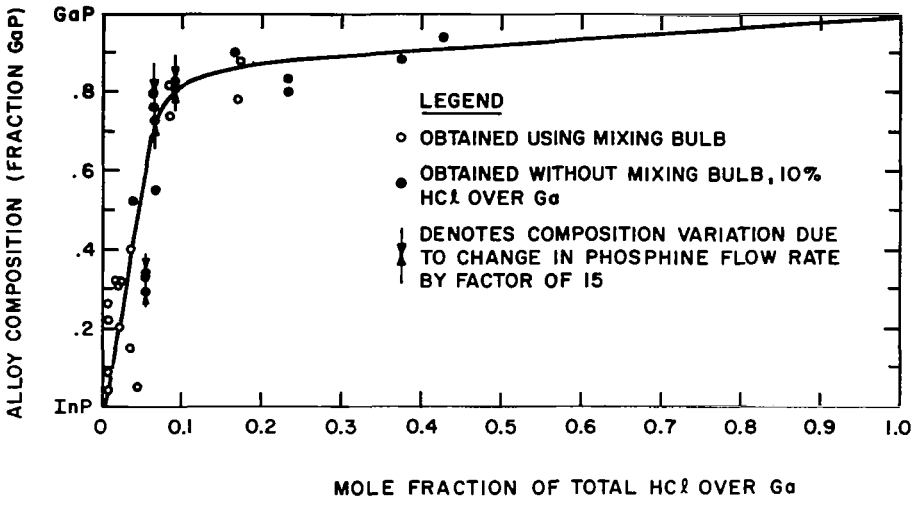

Figure 9. $In_{1-x}Ga_xP$ alloy composition versus the fraction of the total HCl flow over the Ga source. Composition variations produced by changing the phosphine flow rate and by eliminating the use of a mixing bulb (for diluting the HCl) are also shown.

In spite of the warpage and cracking difficulties, it was possible to remove several n-type $In_{1-x}Ga_xP$ layers from their substrate in sufficient size to prepare Hall measurement samples. The results of Hall measurements on three such samples with alloy composition, x, equal to 0.57, 0.65, and 0.75 are shown in Table X. The relatively high mobilities for the samples with x = 0.57 and x = 0.65 suggest that the conduction band structure in these alloys is direct. Conversely, the relatively low mobility for the sample with x = 0.75 suggests an indirect conduction band. It should be noted, however, that the reduced mobility shown in Table X for x = 0.75 is not conclusive evidence for indirect-bandgap material, since the high density of states for the indirect conduction band minima could lead to reduced mobilities even though the zone center minimum could be lowest in energy.

Table X

ROOM-TEMPERATURE HALL MOBILITIES AND CARRIER CONCENTRATIONS FOR $In_{1-x}Ga_xP$

x	Electron Concentration (cm^{-3})	Mobility (cm^2/V-sec)
0.57	5×10^{17}	600
0.65	5×10^{16}	500
0.75	1×10^{17}	92

In addition to undoped layers, which were usually found to be n-type in the 10^{16} electrons/cm^3 range, $In_{1-x}Ga_xP$ layers also were prepared with heavy n- and p-type doping by introducing gaseous H_2Se and Zn (in a hydrogen carrier) into the growth chamber. P-n junction structures also were prepared entirely from the vapor-phase growth; however, their diode characteristics were usually somewhat inferior to those of Zn-diffused $In_{1-x}Ga_xP$ diodes, as discussed further below.

C. Energy Bandgap Determination

The alloy composition of each of a series of $In_{1-x}Ga_xP$ epitaxial layers was determined by measuring the lattice constant by the Debye-Scherrer x-ray technique, and by assuming Vegard's relationship between lattice constant and alloy composition. One of three different techniques was then used to determine the energy gap of each layer at room temperature.

First, for several n-type vapor-grown layers, it was possible to chemically remove the GaAs substrate from the $In_{1-x}Ga_xP$ epitaxial layer, thereby facilitating bulk optical absorption measurements on a Cary Model 14 double-beam spectrophotometer. In these measurements, the dependence of the absorption coefficient on the photon energy was assumed to be of the form

$$\alpha = K\ (h\nu - E_g)^m \qquad (2)$$

For indirect-bandgap alloys, m was found to be about 2; however, because of the steepness of the absorption edge, we could only ascertain that the proper value of m lies between 1/2 and 1 for the direct-bandgap alloys. For such direct-bandgap material, the extrapolated energy-gap values determined by employing either m = 1/2 or m = 1 lie within the energy range covered by the physical size of the data points (circles) in Figure 10 below.

Photoresponse measurements of Schottky-barrier diodes formed by evaporating a thin layer of Au onto n-type $In_{1-x}Ga_xP$ layers were also used for energy gap determination. This technique has been successfully applied to the $GaAs_{1-x}P_x$ alloy system (Ref. 69) and to AlAs and AlSb (Ref. 70) by Mead and Spitzer. The technique assumes that the magnitude of the photoresponse is proportional to the absorption coefficient, and the relationship of Equation (2) is used for either direct- or indirect-bandgap material. The accuracy of the photoresponse and absorption data is estimated to be within 0.04 eV. Photoresponse curves were also generally attained for Zn-diffused p-n junctions in $In_{1-x}Ga_xP$, as discussed in the next section. However, the photoresponse of a p-n junction cannot be used for precise energy gap measurements since its shape depends strongly on minority carrier diffusion lengths, bulk absorption coefficients, and junction depth.

Finally, the high-energy peak of the electroluminescent spectra was also used as an approximation to the energy gap, although it is recognized that this peak could well arise from transitions involving extrinsic states slightly removed from the band edges in energy. In addition, strong absorption of the high-energy emission edge could also shift the observed emission peak to lower values.

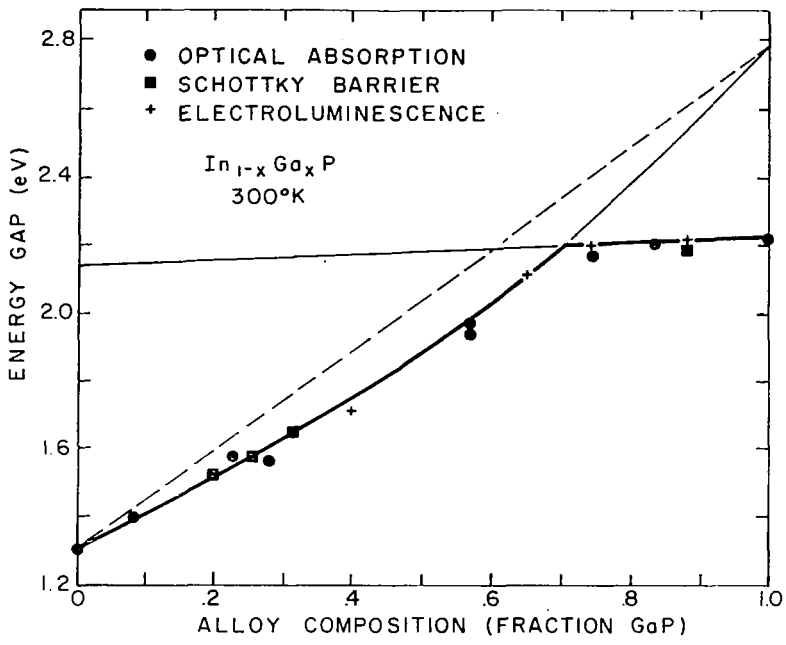

Figure 10. Energy gap at 300°K versus $In_{1-x}Ga_xP$ alloy composition. Direct-indirect transition occurs at 2.20 eV and 70% GaP.

The dependence of the energy bandgap at room temperature on $In_{1-x}Ga_xP$ alloy composition, as determined by the three measurements described above, is presented in Figure 10. For consistency, absorption data taken with InP and GaP are also included as the terminal points of Figure 10. The values obtained for these end points agree with the literature values [2.26 eV for GaP (Refs. 71,72), 1.30 eV for InP] within the accuracy of our measurements. The primary feature of Figure 10 is the clear deviation of the Γ (direct) conduction band minimum from a linear dependence on alloy composition. The curvature of the Γ minimum in Figure 10 generally confirms the cathodoluminescent measurements of Lorenz and Onton (Ref. 4) on bulk $In_{1-x}Ga_xP$ prepared by a modified Bridgeman growth technique, but differs from the linear energy gap dependence first observed by Hilsum and Porteous (Ref. 6) on platelets grown from solution, and later confirmed by Rodot et al. (Ref. 7).

From Figure 10 the direct-indirect energy gap crossover occurs at 2.20 eV for an alloy consisting of 70% GaP. This composition at the crossover is reasonably close to that determined by Lorenz and Onton (Ref. 4) (74% GaP), but somewhat higher than that determined by Hilsum and Porteous (Ref. 6) and by Rodot et al. (Ref. 7) (60% GaP). A crossover near 60% GaP has also been suggested by the photoluminescence measurements of Williams et al. (Ref. 73) and White et al. (Ref. 74) (60 $\pm$ 5% GaP) and by pressure experiments with $In_{1-x}Ga_xP$ diodes by Hakki et al. (Ref. 75) (63% GaP).

It is conceivable that the deviations from linearity observed by some workers, but not by others, is a result of internal crystal strain, which under certain circumstances or at some alloy compositions, could shrink the effective energy gap. In this regard, the vapor-grown $In_{1-x}Ga_xP$ layers prepared epitaxially in our research are thought to be significantly strained, as evidenced by a bowing which is frequently observed on the epitaxy-substrate composite following growth. In addition, the x-ray diffraction patterns observed for the $In_{1-x}Ga_xP$ layers were usually somewhat broadened at intermediate compositions, but sharp near the In-rich and Ga-rich terminal compositions. Such behavior could be caused by strain or by slight inhomogeneities in the alloy composition. Either of these effects could cause the bandgap curve to deviate from linearity.

The data for the (direct) conduction band minimum in Figure 10 extrapolates roughly to an energy value of 2.78 eV in GaP, consistent with Zallen and Paul's determination of the Γ minimum in GaP from high-pressure experiments (Ref. 76). The data for the indirect minima in $In_{1-x}Ga_xP$ extrapolate to an energy value of 2.15 eV for the indirect subsidiary minima in InP. Calculations (Ref. 77) and recent experimental observations (Ref. 78) suggest that these minima lie about 0.90 eV above the direct conduction band minimum, or at approximately 2.20 eV. The direct nature of the $In_{1-x}Ga_xP$ band structure to energies as high as 2.20 eV illustrates the potential of this alloy system for electroluminescent applications through most of the visible portion of the spectrum.

D. P-N Junctions

As mentioned previously, p-n junctions have been formed in epitaxial layers of $In_{1-x}Ga_xP$ both by changing extrinsic dopants (Se and Zn) during vapor-phase growth, and by subsequent diffusion of Zn into n-type layers of $In_{1-x}Ga_xP$. In general, the junctions formed by Zn diffusion were found to be of somewhat higher quality than the vapor-grown junctions for reasons which are not yet clear.

The Zn diffusions were carried out in an evacuated (10^{-6} Torr) quartz ampoule which contained sufficient elemental phosphorus to provide 1 atm. pressure of P_4 at the specific diffusion temperature used, typically 750°C. The surface appearance of the $In_{1-x}Ga_xP$ layers was not perceptibly affected by the diffusion process.

Contacts to the uppermost p-type layer of $In_{1-x}Ga_xP$ were made by evaporating Ag-Mn dots (Ref. 79) and sintering at 600° to 700°C in H_2. Au-Sn was used to contact either the n-type GaAs substrate or the n-type layer of $In_{1-x}Ga_xP$ in cases where the epitaxial layer was thick enough (> 75 μm) to remove the substrate. Removal of the GaAs from the $In_{1-x}Ga_xP$ was accomplished by immersing the wafer in an acid solution of 4 HNO_3:1 HF, which does not etch $In_{1-x}Ga_xP$ alloys containing a significant fraction of GaP.

The room-temperature I-V characteristics of p-n junctions formed by Zn diffusion into n-type $In_{1-x}Ga_xP$ were generally found to be well-behaved, with forward voltage saturation beginning at approximately 1.5 V, as expected for the relatively large energy gaps of these alloys. Reverse breakdown voltages for such diodes were in the range of 5 to 20 V, depending on the donor concentration in the n-type layer prior to diffusion. In general, at decreasing temperatures between 300° and 77°K carrier freeze-out frequently (but not always) occurred, as observed in the form of a significant increase in the series resistance of the forward I-V characteristics. Despite the effect of carrier freeze-out on impurity or defect states, the p-n junctions formed in the epitaxial layers of $In_{1-x}Ga_xP$ were reasonably well-behaved in several other respects, as described further below.

A photoresponse was detected for all of the $In_{1-x}Ga_xP$ junctions examined, with the low-energy intercept of the spectral response occurring at approximately the bandgap energy of the $In_{1-x}Ga_xP$ alloy. In addition, the photoresponse was found to shift with temperature in a fashion appropriate for the change in the semiconductor energy gap with temperature, as shown in Figure 11, for an

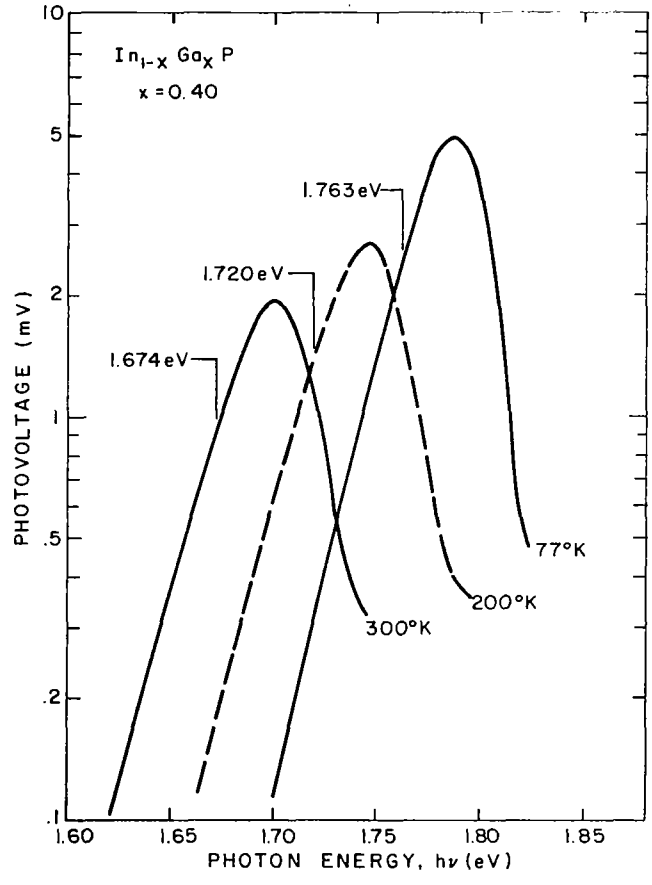

Figure 11. Photovoltage response of an $In_{.60}Ga_{.40}P$ p-n junction at T = 77°, 200°, and 300°K.

$In_{.60}Ga_{.40}P$ p-n junction. Here, for temperatures between 200° and 300°K, the half-amplitude point of the photoresponse shifts with a temperature dependence of about 4.6×10^{-4} eV/K, in excellent agreement with the temperature dependence of the direct conduction band minimum in InP (Ref. 80). The sharp fall-off on the high-energy side of the photoresponse curves in Figure 11 is due primarily to the strong absorption of the high-energy illumination in the region between the crystal surface and the p-n junction, and was much more gradual for the Schottky barrier diodes (used in the energy gap determination of Figure 10), where most of the incident radiation reaches the depletion region of the barrier. The decrease in the magnitude of the photoresponse with increasing temperature in Figure 11 is probably due to larger absorption losses at room temperature, which prevent much of the radiation from reaching the vicinity of the junction.

Finally, from one layer which was thick enough for Hall sample preparation, the carrier concentration determined from C-V measurements of the p-n junction could be compared with that determined from Hall measurement. From the slope of the $1/C^2$ vs V characteristics, an electron concentration of $2.4 \times 10^{17} cm^{-3}$ was obtained, in good agreement with a value of $1.4 \times 10^{17} cm^{-3}$ from the Hall measurement.

E. Electroluminescence

The electroluminescent spectra of the $In_{1-x}Ga_xP$ p-n junctions were usually dominated by low-energy impurity peaks, as shown in Figure 12. Here, the room-temperature spectra of typical p-n junctions are illustrated for alloys with $x = 0.40$ and $x = 0.88$. In both spectra, a narrow near-bandgap peak is observed at the shorter wavelengths (high energy) as well as two impurity peaks at longer wavelengths. An impurity peak at 1.31 to 1.33 eV is present in both spectra, and was also found in junctions prepared over a wide range of $In_{1-x}Ga_xP$ alloy compositions. Emission at 1.30 to 1.35 eV has also been observed in our vapor-grown $GaAs_{1-x}Ga_xP$ and AlAs, however, the origin of the recombination center is not known.

The peak at 1.77 eV for $In_{.12}Ga_{.88}P$ lies approximately 0.5 eV below the bandgap energy, and is similar to the 1.78 eV peak that provides the red emission in GaP. Since the 1.78 eV GaP peak is known to result from Zn-O transitions (Ref. 82), and since oxygen was in fact detected in our vapor-grown layers by spark source mass spectrographic analysis, we can ascribe the 1.77 eV peak in Figure 12 to Zn-O transitions in $In_{1-x}Ga_xP$.

The spectrum of the $In_{0.6}Ga_{0.4}P$ sample also illustrates a shoulder at 1.43 eV, which is about 0.25 eV less than bandgap. The origin of this center has not yet been identified.

In general, over a wide range of indirect-bandgap alloy compositions, low-energy impurity peaks are observed at energies approximately 0.25 and 0.5 less than bandgap, as shown in Figure 13. The invariant energy of these peaks with alloy composition is consistent with the similarly weak energy gap dependence for the alloy system with $x > 0.7$. The third impurity peak at 1.30 to 1.35 eV

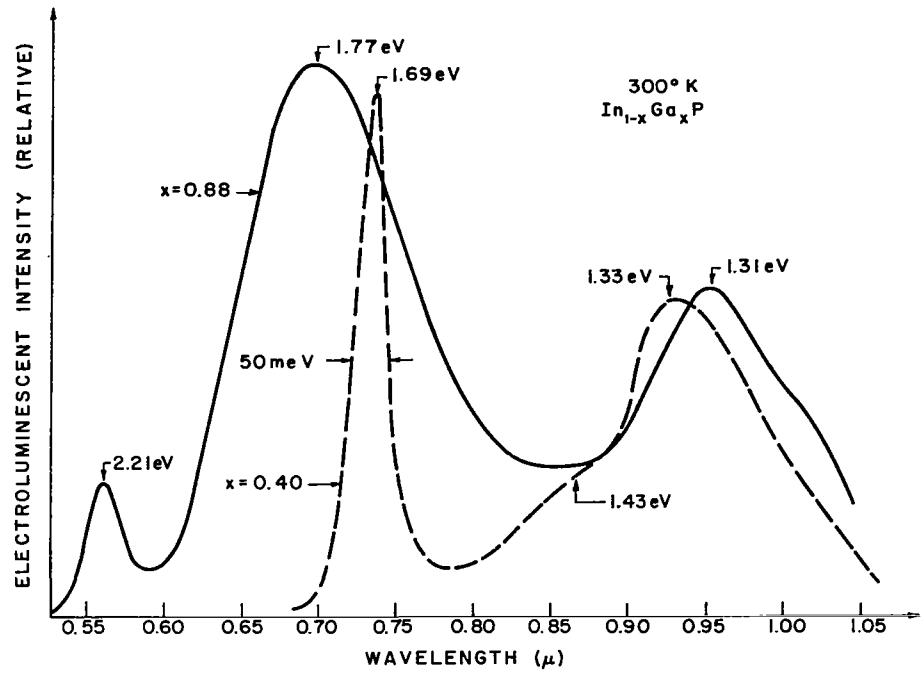

Figure 12. Room-temperature emission spectra of $In_{1-x}Ga_xP$ electroluminescent diodes with x = 0.40 and x = 0.88. Spectra are not corrected for S1 photomultiplier response. $J \approx 50$ A/cm^2.

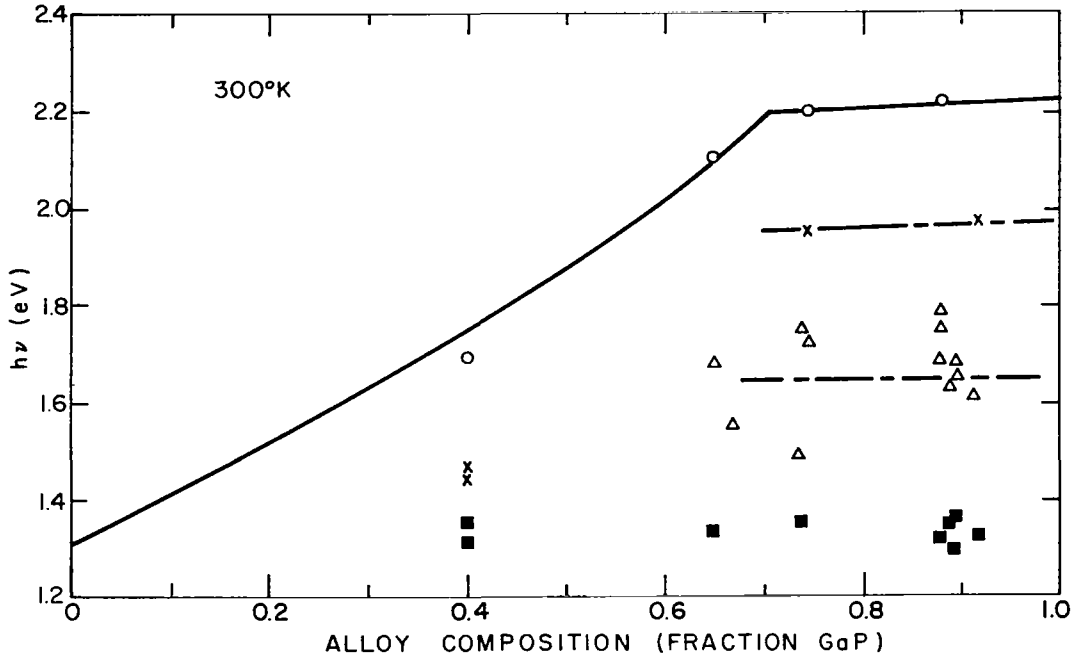

Figure 13. Near-bandgap and impurity peaks in $In_{1-x}Ga_xP$ electroluminescent diodes, $x \geq 0.4$. T = 300°K.

appears to be independent of alloy composition for $x > 0.4$, although further data is required to determine the nature of this peak for In-rich alloys. For all of the electroluminescent junctions studied here, the donor concentrations were in a range of 2×10^{17} to $2 \times 10^{18} cm^{-3}$, therefore the possible influence of donor concentration on the impurity peaks was not established.

The fact that the recombination mechanisms of the near-bandgap and the low-energy peaks differ was confirmed by examining the spectral intensities of the various peaks as a function of the applied forward bias. In all cases, the current dependence was significantly stronger for the near-bandgap recombination, suggesting a higher order recombination process for the near-bandgap peak. Similar observations have been reported for a variety of III-V compounds, and have been previously explained by Mayburg and Black (Ref. 83). The fact that two of the high-energy spectral peaks lie very close to the semiconductor energy gap at alloy compositions close to GaP may be consistent with the near-bandgap exciton recombination reported for the green emission in GaP at room temperature (Ref. 84).

Although impurity peaks have indeed been typically large in the $In_{1-x}Ga_xP$ layers prepared to date, the fact that this is not fundamental to vapor-grown $In_{1-x}Ga_xP$ is illustrated in the spectra of an $In_{.35}Ga_{.65}P$ p-n junction shown in Figure 14. Here, the magnitude of the impurity peaks are no more than 10% that of the near-bandgap peak, even though this particular alloy is very close to the direct-indirect energy gap transition. The crystalline perfection of the layer in which this junction was formed was superior to most others similarly examined in regard to surface smoothness and freedom from warping. The external quantum efficiency of the diode whose spectrum is shown in Figure 14 was 2×10^{-6} at room temperature. In general, the total electroluminescent efficiencies of the $In_{1-x}Ga_xP$ diodes examined here ($x \geq 0.4$) were in the range of 10^{-5} to 10^{-6} at 300°K and 10^{-3} to 10^{-4} at 77°K for current densities on the order of 1 to 10 A/cm^2.

F. Conclusions

Single-crystal epitaxial layers of $In_{1-x}Ga_xP$ can be prepared across the entire alloy series by the vapor-phase growth technique described in this paper. The principal growth parameter for controlling the alloy composition of the $In_{1-x}Ga_xP$ layers is the relative flow rate of HCl over the Ga and In sources. Because of the high relative stability of the InCl as compared to that of the GaCl at typical growth temperatures, much larger HCl flow rates are required over the In than over the Ga in order to prepare intermediate $In_{1-x}Ga_xP$ alloy compositions.

The dependence of the direct conduction band minimum on $In_{1-x}Ga_xP$ alloy composition is nonlinear, with the direct-indirect crossover in the energy gap occurring at 70% GaP and 2.20 eV. This nonlinear dependence is in reasonable agreement with the measurements of Lorenz and Onton, but differs significantly from the linear bandgap dependence determined by Hilsum and Porteous and by Rodot et al.

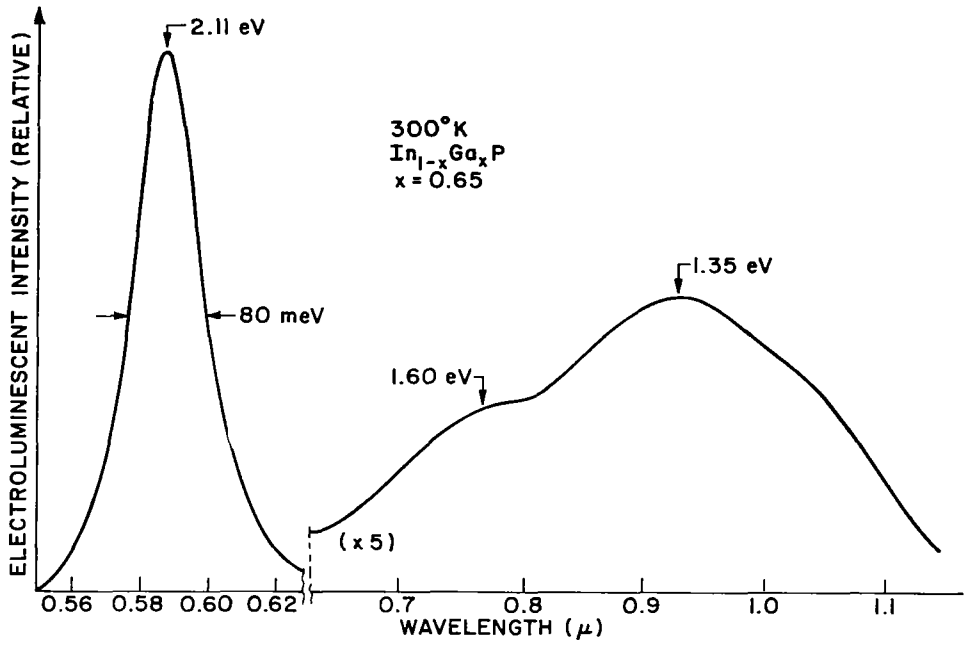

Figure 14. Electroluminescent emission spectrum of $In_{.35}Ga_{.65}P$ Zn-diffused p-n junction at room temperature. Spectrum is not corrected for S1 photomultiplier response. $J \approx 10$ A/cm^2.

P-n junctions formed by diffusing Zn into n-type $In_{1-x}Ga_xP$ layers behave reasonably well in regard to their I-V and C-V characteristics, and their junction photoresponse. However, the electroluminescent spectra of the diodes are generally dominated by low-energy impurity peaks, which are probably caused either by contamination or by strain-induced lattice defects. Three main impurity peaks are frequently observed in the room-temperature spectra of Ga-rich $In_{1-x}Ga_xP$ alloys, one about 0.25 eV below bandgap, another 0.5 eV below bandgap, and a third at about 1.30 to 1.35 eV for $x > 0.4$. Electroluminescent efficiencies in this compositional range are on the order of 10^{-5} to 10^{-6} at room temperature and 10^{-3} to 10^{-4} at 77°K.

APPENDIX D

VAPOR GROWTH OF $Ga_{1-x}In_xAs$ ALLOYS FOR INFRARED PHOTOCATHODE APPLICATIONS

R. E. ENSTROM, D. RICHMAN, M. S. ABRAHAMS, J. R. APPERT,
D. G. FISHER, A. H. SOMMER, AND B. F. WILLIAMS

Abstract

Vapor phase epitaxial growth has been used to prepare $Ga_{1-x}In_xAs$ alloy layers ($0 < X < 0.6$) for use as reflection and transmission photocathodes sensitive in the infrared. Reflection cathodes about 20 μm thick incorporated graded layers to reduce strain which, however, could not be completely eliminated. Alloy layers as thin as 1 μm were prepared for use as transmission photocathodes. Minority carrier diffusion lengths greater than 1 μm were measured for GaAs and $Ga_{0.94}In_{0.06}As$ layers doped to about 1×10^{19} holes/cm^3. The photoemissive properties were found to be strongly dependent upon alloy composition, with the white light sensitivity decreasing monotonically with increasing InAs content and the quantum yield and I.R. sensitivity passing through maximum values. Alloys with clean surfaces and the proper composition and acceptor concentration were activated with cesium and oxygen to quantum efficiencies at 1.06 μm of about 2.0% in reflection and 1.0% in transmission. In addition, bandgap limited emission out to 1.3 μm was observed.

A. Introduction

$Ga_{1-x}In_xAs$ alloys are of interest for use as negative electron affinity (NEA) photocathodes sensitive in the infrared to beyond 1.2 μm (Refs. 85, 86,87,57). In particular, detection of radiation at 1.06 μm has been emphasized because of the availability of high-power Nd:YAG and Nd:glass lasers that emit at this wavelength. At present, the only cathode available for detection of radiation in this spectral range is the Ag-O-Cs (S-1) photocathode that was developed about 40 years ago. Unfortunately, the quantum efficiency (Q.E.) of this photocathode at 1.06 μm is only about 0.04% electrons/incident photon. The present research shows that efficiencies of about 2.0% at 1.06 μm (more than 30 times higher than the S-1 surface), and correspondingly higher efficiencies at shorter wavelengths can be attained in the reflection mode with negative electron affinity $Ga_{1-x}In_xAs$ alloy photocathodes. Further, and of equal importance, transmission photocathodes, in which the light enters on one side of the cathode and the electrons are emitted on the opposite side, have been prepared that have given quantum yields of about 1.0% at 1.06 μm.

The high efficiency of these devices is based on attaining a negative electron affinity at the surface of the p^+ semiconductor crystal. This is achieved by reducing the work function of the semiconductor surface with cesium and oxygen so that the vacuum level lies below the bottom of the conduction band in the bulk. In this way, electrons photoexcited in the bulk crystal and subsequently thermalized in the conduction band have a higher

energy than needed to be emitted into vacuum. Accordingly, they can be emitted into vacuum as long as they are within approximately a diffusion length of the surface. The diffusion length for electrons in the p-type alloy can be about 1 μm. By contrast, in a non-NEA photocathode such as the S-1, only "hot" electrons can escape and the corresponding escape depth is about 100 to 300 Å. Since only those electrons photoexcited near the surface can escape, the quantum efficiency is necessarily low.

The spectral response of the NEA photocathode is determined by the bandgap of the semiconductor, and for response out to 1.3 μm materials with bandgaps of less than 1.0 eV have been investigated. To achieve high quantum yields at long wavelengths, we have found that the crystals must be homogeneous and have a very clean surface after growth, and the bandgap of the alloy and the acceptor concentration must be optimized. In addition, the activation procedure has to be sufficiently sophisticated so that NEA can be achieved on the surface of the low bandgap alloys. The effects of these and other materials growth parameters on photocathode response are discussed in the following sections.

B. Experimental Procedure

The $Ga_{1-x}In_xAs$ alloy samples were vapor grown using the arsine method described previously (Ref. 17), but with provision for separate metallic Ga and In sources as shown in Figure 15. Pd-diffused high purity hydrogen was

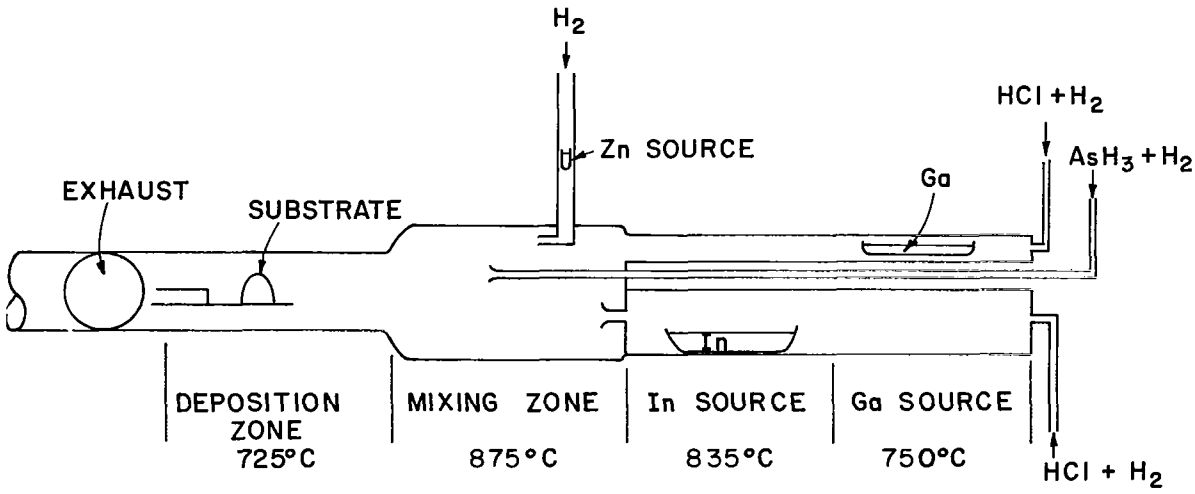

Figure 15. Schematic representation of apparatus used for the growth of $Ga_{1-x}In_xAs$ alloys.

used as the carrier gas. High-purity HCl transported the Ga and In as metal chlorides to the deposition zone where they reacted with the thermal decomposition products of AsH_3, to form a $Ga_{1-x}In_xAs$ alloy single crystalline layer on the surface of a GaAs substrate. A metallic Zn source was used to achieve acceptor concentrations ranging from about 1×10^{19} to $6 \times 10^{19} cm^{-3}$. The Zn concentration was controlled by adjusting the temperature of the doping sidearm, and good reproducibility was achieved on successive runs. Precautions were taken to ensure that the alloy crystal surface after vapor growth remained as clean as possible.

The alloys were grown on (100)-oriented single-crystalline GaAs substrates having areas of 1 to 2 cm^2. For practical photocathode applications, the large-area surface is desirable, rather than cleaved edges as used in prior studies (Refs. 85,88). Prior to growth, the substrates were chemically polished in a solution containing H_2SO_4, H_2O, and H_2O_2 in the ratio 4:1:1. The alloy surfaces were cleaned in vacuum by heating and were activated with cesium and oxygen in successive, alternate steps until a peak in the white light photosensitivity was obtained. Up to 12 samples were activated and tested successively in an ultra-high vacuum stainless-steel chamber capable of pressures less than 10^{-10}Torr. In addition to the white light sensitivity, the infrared sensitivity (in μA/lumen) was measured with a Corning 7-56 infrared transmitting filter placed between the photocathode sample and the standard white light lumen source, and was found to be a convenient figure of merit of the infrared response.

C. Experimental Results

1. Control of Alloy Composition and Homogeneity. - To prepare homogeneous alloys with the two metal sources, the HCl flows must be carefully controlled. As shown in Figure 16 a linear relationship is found between the InAs concentration and the HCl_{In}/HCl_{Ga} ratio. Therefore, the InAs concentration can be easily adjusted over a wide range and excellent reproducibility at a given composition can be achieved. To prevent incomplete reaction of the HCl with the In metal source*, especially at the higher HCl_{In} flow rates, a sufficient volume of In metal is used.

The growth rate is a function of alloy composition above 20% InAs and varies from about 20 μm/hour at 20% to about 12 μm/hour at 50% InAs under our usual conditions of gas flow and furnace temperatures. However, by adjusting growth conditions, growth rates above 20 μm/hour can be attained for alloys containing up to 50% InAs.

The homogeneity of the alloy samples is good as evidenced by the sharpness of the x-ray powder diffraction lines. Electron-microprobe measurements confirm the good homogeneity of vapor grown layers. For a 16.5% InAs alloy, it was found that the composition is within ± 1% of the average value over a

*Ban, V., RCA Laboratories, private communication.

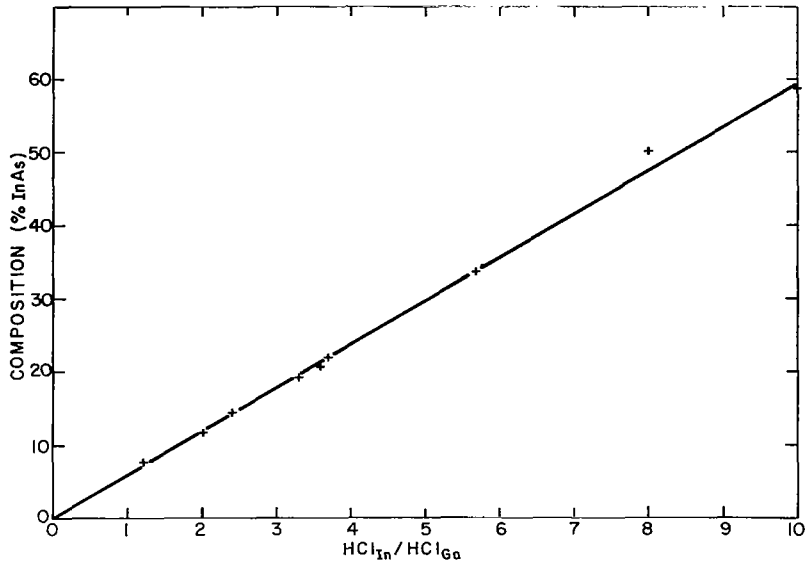

Figure 16. Composition of $Ga_{1-x}In_xAs$ alloy as a function of the HCl flow ratio to the In and Ga sources.

distance of 1 cm on the surface, and identical composition values were found over distances of several mm. Good homogeneity is required to obtain the long minority carrier lifetimes and diffusion lengths needed for high yield photocathodes.

2. Microstructure. - Strain can be a problem in the vapor growth of $Ga_{1-x}In_xAs$ alloy layers because of the large differences in lattice parameters of GaAs (5.6535 Å) and InAs (6.0585 Å). We have attempted to minimize strain resulting from differences in lattice parameter of the GaAs substrate and the alloy layer by grading from the GaAs substrate to the final composition. However, while the magnitude of the strain has been reduced, the strain has not been completely eliminated. This was shown by the curling of a thin 14% InAs alloy layer, indicating the relief of an internal stress, when the GaAs substrate was removed. The sense of the curl was opposite to that found for $GaAs_{1-x}P_x$ alloys on GaAs substrates (Ref. 89). This is in agreement with the lattice parameter difference for GaP (5.4506 Å) which is smaller than that of GaAs, in contrast to InAs which is larger.

The alloys are very smooth and reflective, and are comparable in appearance to GaAs layers prepared under good growth conditions, except for the appearance of a checker-board pattern on the (100) surface. This feature is shown in Figure 17 and is probably associated with the grading dislocation network shown in Figure 18 that exists in the graded composition region between the substrate and the constant composition layer. These lines are oriented parallel to <100> directions and thus appear orthogonal on the (100) crystal surface. The grading dislocations serve to take up the strain associated with

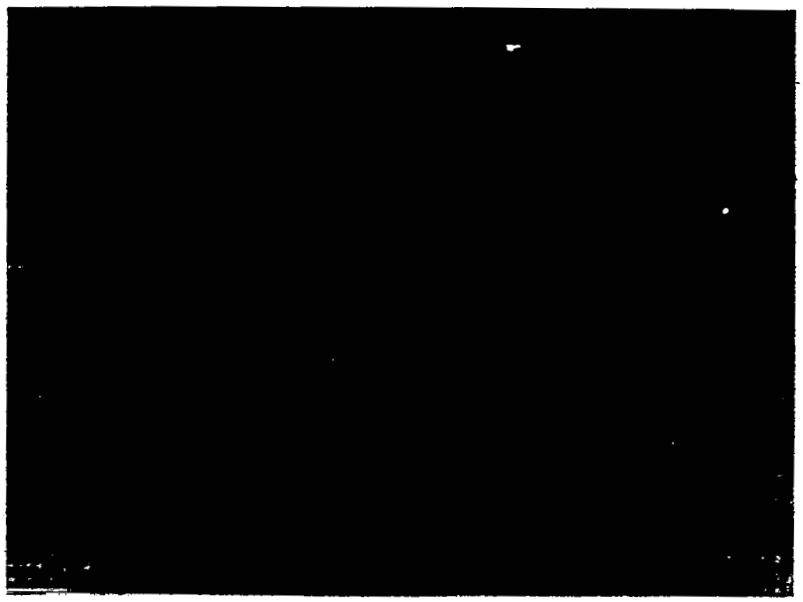

Figure 17. Surface of $Ga_{1-x}In_xAs$ alloy layer showing checker board pattern associated with grading dislocations. 50 X magnification.

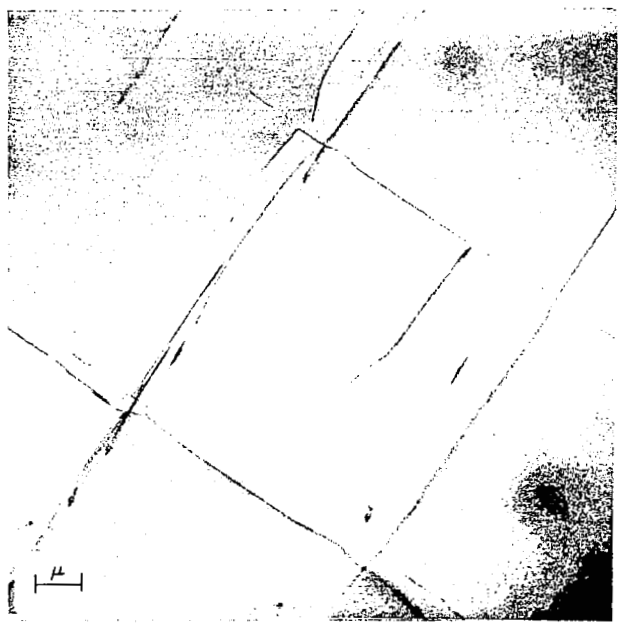

Figure 18. Transmission electron micrograph of the graded region of a $Ga_{.86}In_{.14}As$ alloy doped with zinc acceptor impurities to about $1 \times 10^{19} cm^{-3}$. Grading dislocations, but no precipitates are visible.

changes in lattice parameter (Ref. 90). The grading rate for the sample in Figure 18 is about 1% InAs/μm and the dislocation structure is similar to that found for a $GaAs_{1-x}P_x$ alloy graded at the rate of about 1.7% GaP/μm (Ref. 90) perhaps because the lattice parameter change per μm is about the same for both alloys. The transmission electron micrograph of the constant composition layer of the same sample, Figure 19, shows inclined dislocations, but no grading dislocations or stacking faults. The inclined dislocation density (Ref. 90) is about $10^6 cm^{-2}$. It is of special interest to note in Figures 18 and 19 that no zinc or zinc arsenide precipitates are present which might tend to reduce the minority carrier diffusion length and also the photoemissive yield (Ref. 91).

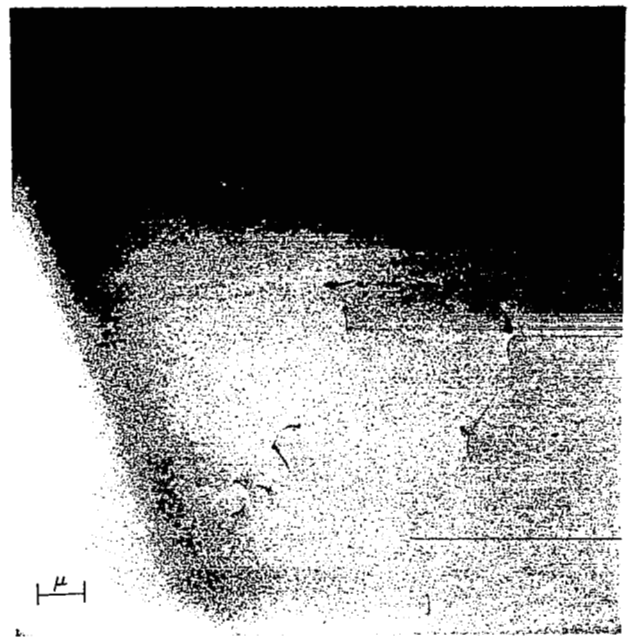

Figure 19. Transmission electron micrograph of the constant composition region of a $Ga_{.86}In_{.14}As$ alloy doped with zinc acceptor impurities to about $1 \times 10^{19} cm^{-3}$. Inclined dislocations, but no stacking faults, grading dislocations or precipitates are observed.

The cross-sectional structure of a 15% InAs alloy graded at the rate of about 0.3% InAs/μm and etched with the A-B etchant (Ref. 92) is shown in Figure 20. It may be seen that numerous grading steps can be discerned. These are associated with the discrete, small increases of HCl to the In metal source as the InAs composition is increased during the grading period.

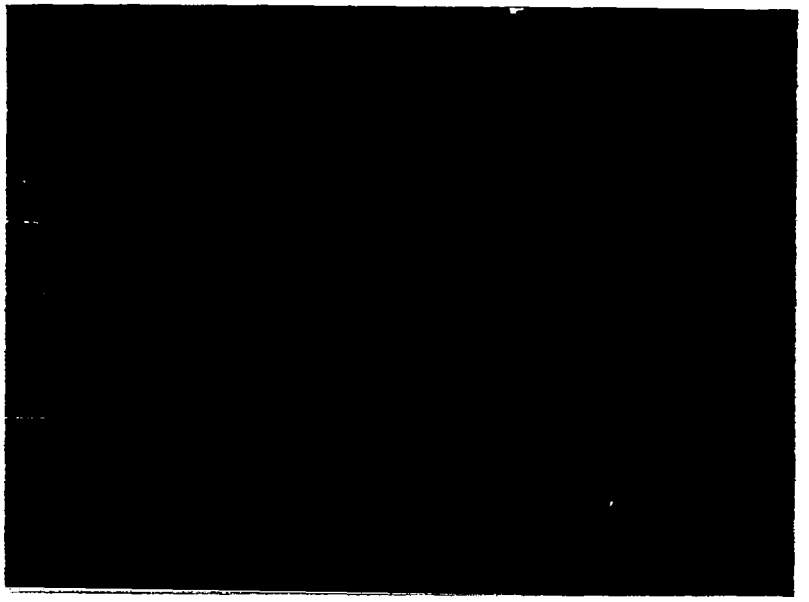

Figure 20. Micrograph of the (110) cleaved face of a Zn-doped $Ga_{.85}In_{.15}As$ alloy graded at the rate of about 0.3% InAs/μm. Etched with the A-B dislocation etchant to reveal the microstructure. 500 X magnification.

3. Electrical Properties. - The electrical properties are a measure of the quality of the vapor grown material and therefore these have been examined.

The electrical properties as determined by Hall effect measurements of typical materials are shown in Table XI. Undoped GaAs samples contain about

Table XI

ELECTRICAL PROPERTIES OF VAPOR GROWN $Ga_{1-x}In_xAs$ ALLOYS

Run	Composition	Carrier Type		μ300°K cm^2/V-sec	μ77°K cm^2/V-sec
572-II	GaAs	n	5.2×10^{14}	7500	98,000
603-II	GaAs-Zn doped	p	8.7×10^{18}	69	109
463-II	$Ga_{0.833}In_{0.167}As$	p	4.2×10^{18}	76	67
462-II	$Ga_{0.833}I_{0.167}As$	p	3.7×10^{19}	46	75
471-II	$Ga_{0.523}In_{0.477}As$	n	8.5×10^{15}	5900	13,000

5×10^{14} electrons/cm^3, and it may be seen that good mobility values have been achieved both at 300° and 77°K. A further indication of the quality of our material is the high value of the mobility at 77°K, 13,000 cm^2/V-sec, for an n-type alloy containing 48% InAs. For most of the photocathode samples, a hole concentration of about $1 \times 10^{19} cm^{-3}$ is used. Thus, the room-temperature mobility for p-type GaAs and $Ga_{1-x}In_xAs$ alloy layers is between 60 to 70 cm^2/V-sec over the compositional range of interest.

The photoemissive properties are strongly affected by the diffusion length of the photoexcited electrons. Therefore, a study has been made of minority carrier lifetimes and diffusion lengths and the details of this work will be published elsewhere by Enstrom, Coutts, Dean, Goldstein, and Nuese. Briefly, it was found, using a scanning electron microscope technique (Ref. 93) for the determination of the minority carrier properties, that the diffusion lengths for minority carriers (electrons) in GaAs, $Ga_{.94}In_{.06}As$ and $Ga_{.80}In_{.20}As$ layers doped to 1×10^{19} holes/cm^3 are 1.6, 1.2, and 0.8 μm, respectively. The value for GaAs is consistent with that determined from photoemissive yield data (Ref. 94). Thus, we see that the minority carrier diffusion length is only weakly affected by alloying with InAs.

It will be shown in a subsequent section that the photoemissive properties are a strong function of composition, and theoretical analysis requires knowledge of the alloy bandgap. Therefore, it is important to know the exact dependence of the energy gap, E_g, on composition in the range 1.4 to 1.0 eV in order to select the proper alloy for response at a given wavelength. Prior work (Refs. 95,96) established the dependence of E_g on composition for values of E_g less than 1 eV but for higher values the curve was not well established. In the present work we have measured E_g by extrapolating to zero the best straight line fit of the square of the optical density versus photon energy, $h\nu$, for undoped samples with compositions between 0 and 50% InAs. The composition was determined from measurements of the lattice parameters since Vegard's law has been found to be valid for the GaAs-InAs alloy system (Ref. 95).

The results of the present work are shown in Figure 21, and are compared with the results obtained previously (Ref. 96). Our results show a uniform decrease of E_g with composition unlike Woolley's curve which shows a more rapid decrease in the range of 0 to 20% InAs. For compositions of 50 to 60% InAs, good agreement is found between the two curves. The present curve is 0.07 to 0.1 eV higher than, but parallel to, the curve determined in Ref. 95. It should be noted that for alloys doped with Zn acceptor impurities, the energy gap would be about 0.05 eV lower.

4. Photoemissive Properties. - The effect of various growth parameters on the photocathode response has been examined.

a. Substrates. - A variety of substrate materials can be considered for the preparation of reflection photocathodes but for transmission photocathodes, substrates transparent to radiation of interest (e.g., 1.06 μm) must be used.

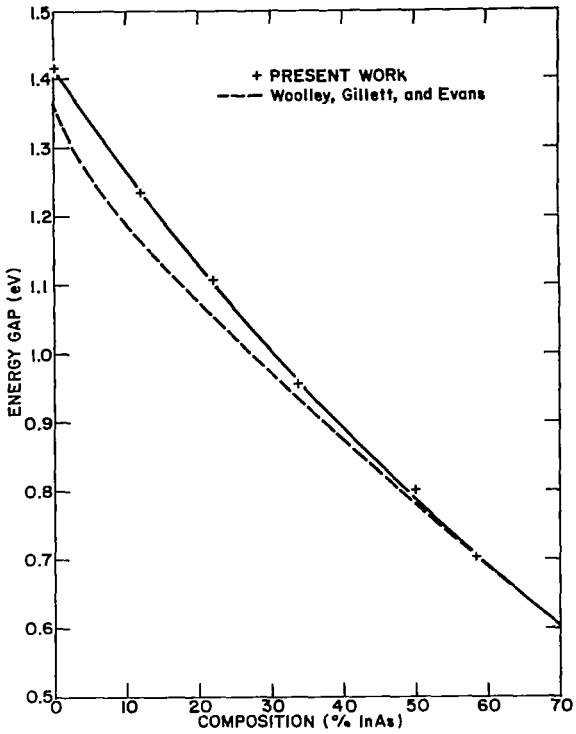

Figure 21. The energy gap for undoped $Ga_{1-x}In_xAs$ alloys as a function of composition.

For the latter, GaAs is the most practical substrate, and we have found that both undoped ($n \sim 1 \times 10^{16} cm^{-3}$) and Cr-doped high resistivity ($\rho \sim 10^7$ ohms-cm) substrates have low absorption coefficients (2 to 5 cm^{-1}) at 1.06 μm. High conductivity p-type substrates cannot be used for transmission photocathodes because of the very high free carrier absorption.

It was found that Zn-doped substrates from different boules, as well as substrates doped with Cr or Si, gave nearly the same sensitivities, and values as high as 920 μA/lumen (110 μA/lumen with a 7-56 IR passing filter) were measured for 14% InAs samples. On the other hand, a layer grown on a (111) As surface had a poorer sensitivity, particularly in the IR compared to a layer grown simultaneously on a (100) oriented substrate.

b. Acceptor Concentration. - The acceptor concentration affects both the minority carrier lifetime and the width of the bent band region at the crystal surface. A lower acceptor concentration favors increased lifetime and diffusion length, but increases the width of the bent band region about a factor of three for each factor of ten decrease in the acceptor concentration. Therefore a compromise must be made between these two competing factors. It was found that decreasing the acceptor concentration from $6 \times 10^{19} cm^{-3}$ to

$1 \times 10^{19} cm^{-3}$ for a 21% InAs sample increased the IR sensitivity and yield at 1.06 μm by a factor of about two. Therefore, the increased diffusion length with lower acceptor concentration appears to dominate.

c. Composition. - The photoemissive properties are a strong function of alloy composition. The threshold for photoemission shifts to longer wavelengths, but the white light sensitivity decreases from about 1200 μA/lumen for pure GaAs to about 180 μA/lumen as the concentration is increased to 30% InAs. GaAs is not sensitive to radiation at 1.06 μm. But, with increasing InAs content, the yield at 1.06 μm continues to increase to quantum efficiencies of about 2.0% and then begins to decrease monotonically so that the performance at 30% ($Y_{1.06\ \mu m} = 0.06\%$) is poorer than that at 25% InAs ($Y_{1.06\ \mu m} = 0.8\%$). The IR sensitivity measured through a 7-56 filter has a similar compositional dependence. The decrease in the IR sensitivity and the quantum efficiency at 1.06 μm as a function of composition is thought to be associated with the decreasing magnitude of the NEA for lower bandgap alloys. Photoexcited electrons having traversed the bent band region have a broadened energy distribution. As the magnitude of the NEA becomes smaller than the width of this distribution, some of the electrons are prevented from escaping into vacuum. Hence, the escape probability is reduced, and the photoemissive properties decrease (Ref. 97).

It should be noted that the quantum efficiency achieved with these $Ga_{1-x}In_xAs$ alloys is more than 30 times the quantum yield of a good S-1 photocathode surface at 1.06 μm thereby indicating that these materials should find important commercial and scientific application. Further, the valence band emission threshold for the p-type 30% InAs alloy ($E_g = 0.96$ eV) is 1.3 μm, which is comparable to that measured on a bulk-grown $Ga_{1-x}In_xAs$ alloy sample (Ref. 86). However, the quantum yield near threshold is about 2 orders of magnitude higher for the present vapor-grown sample.

d. Thickness. - For the preparation of reflection photocathodes, the grading layer and the constant composition layer are each about 20 μm thick. For transmission photocathodes, alloy layers about 1 μm have been grown and these have been prepared principally on Cr-doped GaAs substrates. Since the growth rate is about 0.3 to 0.5 μm/min, this involves growth times of about 2 minutes, which is feasible with the described growth method. Layers with about 21% InAs have white light sensitivities as high as 800 μA/lumen in the reflection mode and quantum efficiencies up to 1.0% at 1.06 μm in the transmission mode, thereby demonstrating that transmission photocathodes prepared from $Ga_{1-x}In_xAs$ alloys should find important applications as IR detectors and image converters.

D. Summary

Homogeneous single-crystalline $Ga_{1-x}In_xAs$ alloy layers were prepared over the range $0 < X < 0.6$ by vapor phase growth using separate In and Ga metallic sources and AsH_3 gas. Excellent control and reproducibility of the composition was achieved by precise adjustment of the HCl_{In}/HCl_{Ga} ratio. Evidence for strain in the alloy layers on GaAs substrates was found, but minority carrier diffusion lengths greater than 1 μm were measured for both GaAs and $Ga_{0.94}In_{0.06}As$ alloys doped to about 1×10^{19} holes/cm^3. These good minority carrier properties are probably a result of the absence of precipitates and stacking faults in the constant composition layer. Equally high white light photoemissive sensitivities were measured for layers deposited on Zn-, Si-, and Cr-doped substrates, thereby indicating that the type of substrate dopant does not affect photocathode response. On the other hand, the photocathode properties are a strong function of alloy composition. The white light sensitivity is a monotonically decreasing function of increasing InAs content while the IR sensitivity (7-56 filter) and the quantum efficiency at 1.06 μm pass through maximum values. These properties are also affected by the acceptor concentration. By proper growth and activation procedures, $Ga_{1-x}In_xAs$ alloy layers with excellent photoemissive properties at 1.06 μm have been attained including quantum efficiencies of about 2.0% and 1.0% in the reflection and transmission modes, respectively. Further, bandgap limited photoemission with threshold values out to 1.3 μm was observed.

APPENDIX E

VAPOR GROWTH AND PROPERTIES OF AlAs

M. ETTENBERG, A. G. SIGAI, A. DREEBEN, AND S. L. GILBERT

Abstract

Aluminum arsenide epitaxial layers on GaAs substrates have been prepared by a continuous-flow vapor-transport technique employing AlCl and AsH_3. It has been found that for all practical experimental conditions the reaction of AsH_3 and AlCl takes place at the point of mixing of the reactive gases. This behavior is consistent with a thermochemical analysis of the AlAs growth. The bandgap of AlAs was determined by optical absorption to be 2.17 eV and indirect. Hall and resistivity measurements made on epitaxial layers removed from the substrates indicate that the as-grown material is n-type with electron concentrations ranging from 6×10^{18} to $4 \times 10^{17} cm^{-3}$ with corresponding room temperature mobilities varying between 75 and 280 $cm^2/V\text{-sec}$. The value of 280 $cm^2/V\text{-sec}$ is the highest measured electron mobility yet reported for AlAs. While the material does degrade in air it has been found stable enough to allow ample time for device fabrication and protection.

A. Introduction

The large bandgap (> 2.1 eV) (Ref. 98) of AlAs makes it an especially interesting material for high-temperature device applications or optical applications in the visible region of the spectrum. The high melting point of this compound and the reactivity of aluminum have created problems in its high purity preparation. The major limitation to material characterization or device fabrication, however, has been the instability of AlAs in air. Reported complete degradation of grown layers in 10 minutes (Ref. 99) would indicate a limited usefulness.

This study was made using the open-flow vapor growth system (Ref. 17) employing the Group V hydride and the Group III chloride, modified to accommodate the growth of aluminum III-V compounds. In this system growth takes place at temperatures significantly below the melting point of the compound grown, thus reducing many of the problems associated with the reactivity of aluminum and general contamination. This technique has yielded n-type AlAs having increased stability and the highest electron mobilities yet reported (Refs. 100,101).

B. Experimental

The growth system, shown in Figure 22, consists of a quartz tube which accommodates a pure alumina liner containing alumina boats filled with 99.999% aluminum. The alumina is 99.7% Al_2O_3 with 0.05% SiO_2, 0.1% Fe_2O_3, 0.2% Na_2O, and 0.05% K_2O as major impurities. Aluminum monochloride is formed by passing Pd diffused H_2 carrier gas containing 0.2% HCl by volume over the liquid

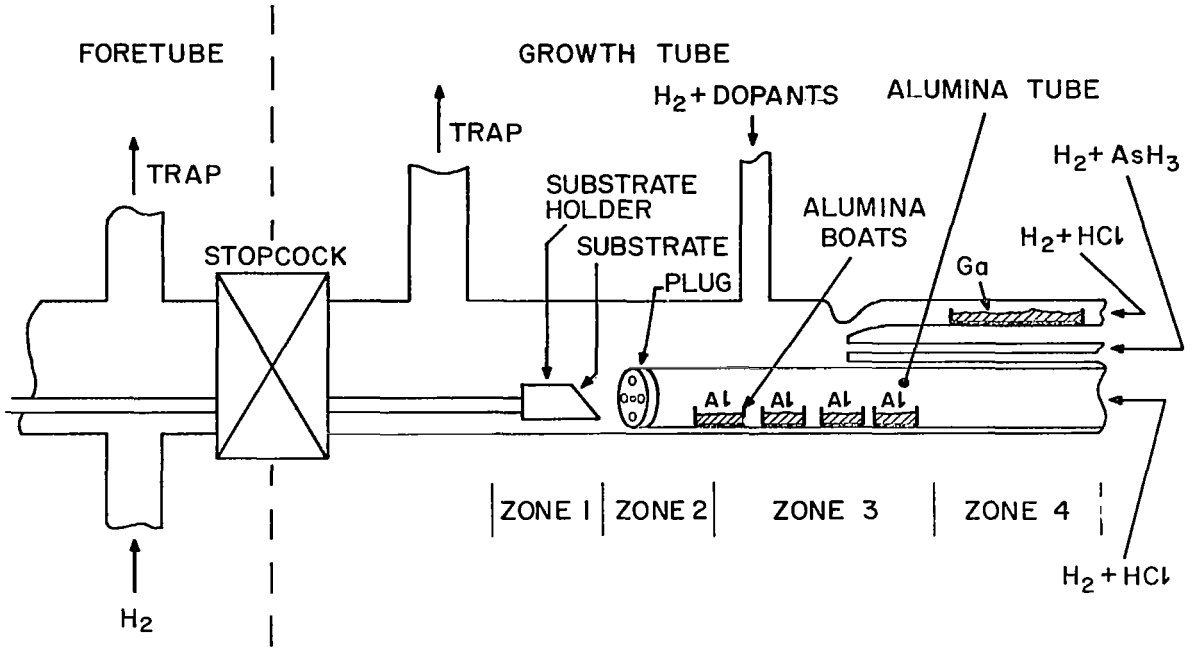

Figure 22. Aluminum arsenide vapor growth system.

aluminum at 1000° to 1050°C. The AlCl is then mixed with AsH_3 and the AlAs formed was deposited on GaAs substrates at a temperature between 1000° and 1050°C. The AsH_3, which contains 1 ppm total impurities, is 2% by volume in the H_2 carrier gas. This configuration (Figure 22) includes provision for a gallium boat so that $Al_xGa_{1-x}As$ alloys may be grown as well as pure AlAs by simultaneously passing HCl over gallium. This basic system may also be employed to grow AlN using NH_3 instead of AsH_3 and AlP using PH_3. The long aluminum zone, containing up to six aluminum filled boats, allows the first two aluminum boats to act as getters removing any traces of H_2O, O_2 or other impurities contained in the HCl and H_2 stream. The remaining boats serve to insure complete equilibration of the HCl with aluminum. The exposed quartz in the deposition zone is protected from attack by the initial deposits of AlAs. More recently, a tungsten liner has been employed in the deposition region to facilitate cleaning and to further reduce Si contamination.

Reaction of the AsH_3 and AlCl to form AlAs takes place at the point of mixing of the two gases, independent of reactive gas concentrations up to at least changes of a factor of five in AlCl or AsH_3 concentrations. Furthermore the location of the reaction zone does not change for various combinations of aluminum and reaction zone temperature between 850° and 1050°C. In order to move the reaction zone from the mouth of the alumina tube, an alumina plug (99.7% Al_2O_3), with small holes (1/16" dia) drilled through it, was added to the mouth of the alumina tube, decreasing the effective cross section and thus increasing the gas velocity at the point of reaction. This spread the reaction over a 4-in. length, allowing a suitable substrate to be conveniently placed in the reaction zone.

Growths were usually made on chemically polished GaAs substrates oriented 3° from the (100) plane. Substrates were cleaned for 20 minutes in Caro's acid etch and 1 minute in 1% Br-methanol solution just prior to insertion in the system. Growth rates could be varied between 10 and 100 μm/hr depending on reactant concentrations and volumes. Depositions at growth rates less than 60 μm/hr on GaAs substrates at temperatures exceeding 980°C were invariably good single crystalline layers as evidenced by Laue back reflection photographs. Layers grown at temperatures below 980°C or at high growth rates (> 60 μm/hr) were usually highly oriented large-grain polycrystals.

C. AlAs Properties

One of the significant factors limiting the potential usefulness of AlAs is its reported instability in air (Ref. 99); contrary to this report, some of the single crystalline epitaxial layers reported here were stable in air for periods of up to one month and could be maintained in vacuum indefinitely. Unprotected diffused diodes fabricated from this material (Ref. 36) maintained their I-V characteristics for several weeks. This stability is attributed to the higher purity and good crystallinity of the AlAs prepared by this technique.

The optical bandgap for the material has been ascertained to be indirect and 2.17 $\pm$ 0.02 eV at 300°K, in good agreement with prior studies (Refs. 98, 36,14). This value has been obtained by analysis of optical absorption data from several AlAs layers from which the GaAs substrate was removed. Similar results were obtained with polycrystalline layers grown on (0001) sapphire substrates.

Hall effect and resistivity measurements made on epitaxial aluminum arsenide layers while still on semi-insulating Cr-doped GaAs substrates (> 10^5 ohms-cm), yielded mobility values, which were inordinately high for a large indirect bandgap material (in excess of 3000 cm^2/V-sec). Attempts to remove the AlAs from the substrate were hampered by cracking of the sample as it was thinned. By preferential removal of the AlAs in aqueous HCl it was ascertained from Hall measurements that there existed, in some samples, a thin layer of highly conducting GaAs at the surface of the semi-insulating GaAs substrate. The Hall mobility of such a layer was measured to be $\approx$ 2000 cm^2/V-sec. By sandblasting the GaAs surface with alumina powder, the conducting GaAs layer could be removed; it was estimated that the thickness of these interfacial layers were between 2 and 10 μm. In Table XII the impurity concentrations at the surface of a Cr-doped GaAs substrate are compared before and after removal of the interfacial layer by sandblasting.

As can be seen from the table, there is a high concentration of impurities at the interfacial layer. These impurities probably have diffused into the GaAs from the AlAs during growth. The impurity concentration of silicon is sufficiently in excess of the Cr compensation to make the semi-insulating Cr-doped GaAs n-type. Furthermore, calculations have shown that typical growth rates may be comparable to the diffusion rate of Si at growth temperatures, indicating that the Si contamination of the semi-insulating GaAs

substrate could arise from Si impurities present in the AlAs. Thus, it may be concluded that contrary to the results for other III-V compounds, reliable electrical measurements on vapor grown AlAs cannot be made on compensated semi-insulating substrates when diffusion of impurities is likely.

Table XII

IMPURITY ANALYSIS

Sample	Technique	Fe	Cr	Si	Cu
Interfacial Layer	Mass Spec.*	2	2	31	6 ppma
Cr-doped GaAs	Mass Spec.*	.1	2	.5	.1 ppma

*In all the mass spectrographic analyses, impurity levels of C, O, and F were consistently observed. These levels are thought to be associated with surface contamination since their concentrations decreased as more of the surface is removed during analysis.

As a result, emphasis was placed on electrical data derived from thicker AlAs layers (> 4 mils) from which the GaAs substrates could be removed. Ohmic contacts were made to the AlAs by a combination of ultrasonic soldering with indium followed by an anneal in H_2 at 800°C for 2 minutes. In Table XIII are listed electrical properties and impurity analyses of AlAs epitaxial layers with the GaAs substrates removed. Table XIII indicates that silicon is the main donor in this vapor grown AlAs.

The room-temperature electron mobility of 280 cm^2/V-sec obtained for sample C is higher than the highest previously reported value of 180 cm^2/V-sec obtained by Whitaker (Ref. 101). The higher mobility value found in this study may still be representative of compensated material, perhaps due to Si self-compensation such as found in $Al_{1-x}Ga_xAs$ grown from Ga solution (Ref. 102). This hypothesis is consistent with the mass spectrographic analysis which shows that the amounts of species which are probably compensators (Fe, Cu, Mg) are quite low in sample B, while the silicon contamination is quite high.

The cracking of the thinner epitaxial AlAs layers upon attempts to remove the GaAs substrate is indicative of strain at the interface. It is noteworthy that at the growth temperature the lattice match between AlAs and GaAs is almost perfect (Ref. 103) indicating that this is not the source of the strains. Instead, the strain is probably due to the differential thermal contraction (Ref. 103). This hypothesis is consistent with the fact that the dislocation densities found by electron microscopy in the grown AlAs layers are comparable to that of the starting substrates ($\sim 10^5/cm^2$).

Table XIII

ELECTRICAL PROPERTIES AND CHEMICAL ANALYSES OF VAPOR GROWN AlAs REMOVED FROM GaAs SUBSTRATES

Sample	Temp. °K	N_D-N_A Electrons/cm^3	μm cm^2/V-sec	Impurity Analysis Technique	Fe	Cu	Mg	Si
A	298	$1.4x10^{18}$	95	Mass Spec.*	1.7	0.6	1.0	110 ppma
B	298	$6.4x10^{18}$	75	Mass Spec.*	1.2	1.0	1.6	200 ppma
	77	$2.0x10^{17}$	18					
C	298	$3.6x10^{17}$	280	Emission Spec.	2	2	15	30 ppma
D	298	$5.4x10^{17}$	220					

*In all the mass spectrographic analyses, impurity levels of C, O, and F were consistently observed. These levels are thought to be associated with surface contamination since their concentrations decreased as more of the surface is removed during analysis.

D. Thermochemical Analysis

Analysis of the thermochemistry of the aluminum arsenide vapor growth was made to better understand the growth of AlAs and provide a compiled data source to give insight for the future growth of $Al_xGa_{1-x}As$ and other mixed aluminum compounds.

Three primary sources of data were employed. The Janef tables (Ref. 104 were used for data on AlCl, $AlCl_3$, and HCl; the values derived from this source for the important reactions present in the system are shown as solid lines in Figures 23 and 24. Values derived from recent work by Kikuchi, et al. (Ref. 105), more in agreement with the bulk of previous measurements, are indicated as dashed lines in Figures 23 and 24. The free energy of formation of AlAs is given by Hoch and Hinge (Ref. 106), who used a Knudsen effusion cell to measure vapor pressures between 1350° and 1530°K. On this basis the reliability of extrapolated values is estimated to be reliable within $\pm$ 50°C about the measured temperature range. The free energy of formation was reduced to the liquid aluminum standard state by taking values for the free energy of evaporation from Hultgren, et al. (Ref. 107).

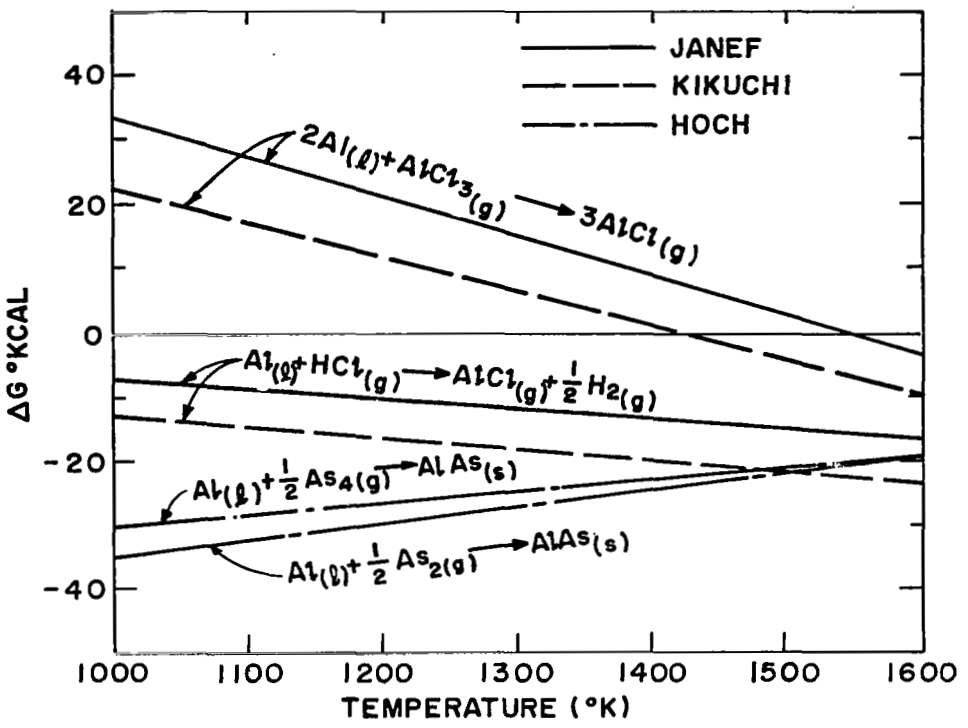

Figure 23. Standard free energy changes for aluminum reactions.

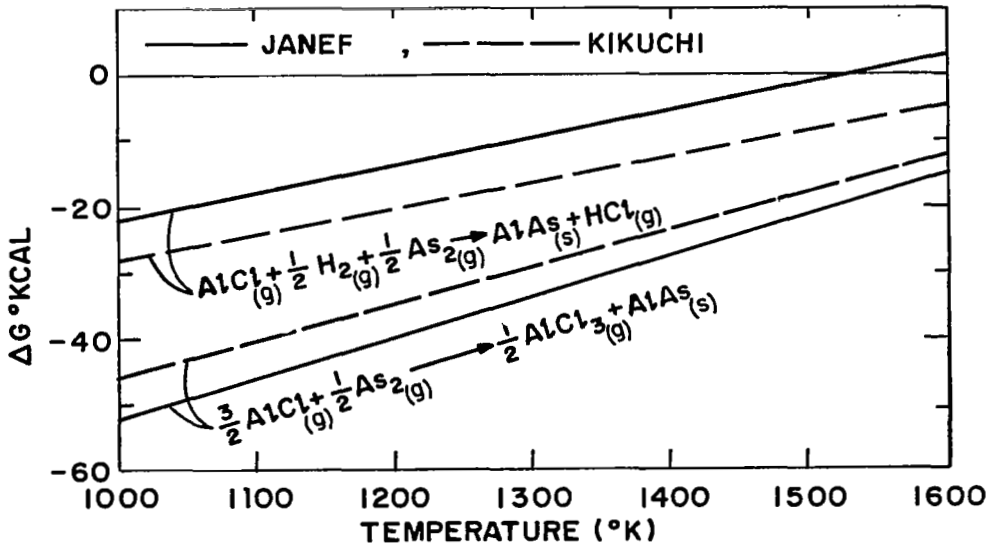

Figure 24. Standard free energy changes for formation of AlAs in vapor growth system.

Although there are some discrepancies between the various sources of thermodynamic data, certain conclusions may still be drawn. It is assumed that the volume fractions of the various gases, in the growth tube, are equal to their partial pressures. This is a valid assumption since the system is held at a constant pressure of one atmosphere by a small head of silicone oil at the gas exit, and the volume fraction of the gases are all measured at room temperature.

It must first be ascertained what gaseous species enter the growth or mixing chamber. If it is assumed that the various species have come to equilibrium, according to data accumulated by Ruehrwein, at 1000°C and an incoming AsH_3 pressure of 2×10^{-2}atm,* the AsH_3 has completely decomposed ($<<$ 0.01% undecomposed) and the amount of As_2 and As_4 coexisting are 20 and 80%, respectively. Employing the data of Stull and Sinke (Ref. 108) 70% As_2 and 30% As_4 exist at 1000°C at equilibrium. In both cases, little of the As specie is present ($<$ 0.1%). Even though the calculations do not clearly indicate the predominant arsenic specie, As_2 is used as the standard state for the reactions considered in Figures 23 and 24. The assumption is justified because departures from equilibrium will tend to favor the simpler As_2 molecule; also, as shown in Figure 23, there is only a small difference in free energy of formation of AlAs between the As_2 and As_4 standard states.

In the aluminum zone the picture is much clearer; in equilibrium at 1000°C and an incoming HCl pressure of 2×10^{-3} atm, AlCl is the predominant specie. Using the Janef tables, calculations show that 99.5% is AlCl and 0.5% is $AlCl_3$, while from the data of Kikuchi 99.8% of the reactive gas is AlCl. Calculations with both data indicate that a negligible amount of HCl will remain unreacted at equilibrium.

The equilibrium products for the reactions taking place on mixing of the As_2 and AlCl at 1000°C can now be calculated. The two possible reactions forming AlAs are:

$$AlCl + \frac{1}{2} H_2 + \frac{1}{2} As_2 \rightarrow AlAs + HCl \qquad (3)$$

$$3AlCl + As_2 \rightarrow 2AlAs + AlCl_3 \qquad (4)$$

Ignoring the small diluent effect of mixing the As_2 and AlCl from the Janef data both reactions will result in almost complete reaction of AlCl to form AlAs, 85% if HCl is the only product and 96% for $AlCl_3$ product. Kikuchi's data indicates 99% conversion for HCl and 90% for an $AlCl_3$ product. Due to the differences in free energies from the two sources a dominant reaction cannot be chosen. The overall reaction in the mixing zone is:

*R. A. Ruehrwein, Monsanto Research Corp., private communication.

$$5AlCl + 2As_2 + H_2 \rightarrow 4AlAs + 2HCl + AlCl_3 \quad (5)$$

This reaction does go to completion but the ratio of HCl to $AlCl_3$ is ambiguous from the available data.

It should be noted that a simple examination of the signs of the free energies changes for the various reactions taking place in the AlAs growth system will not lead to proper conclusions about the gaseous species involved. One of the prime factors controlling these reactions are the low partial pressures of the reactive gaseous compounds.

Although it is difficult to make precise quantitative statements from the available data, it should be possible to predict some temperature range, where at the present flow rates, the reactants forming AlAs should not react completely. The reactive gases may then be mixed in one temperature zone and the product deposited at some lower temperature as is done for the growth of GaAs. By simple examination of Figure 24 it may be seen that at temperatures in excess of 1300°K the dominant reaction is the one that yields HCl as the product. An arbitrary temperature to employ as a mixing temperature would be the point at which the reaction only proceeds 25% to completion. This temperature is $\sim$ 1160°C from the Janef data and $\sim$ 1300°C from Kikuchi's data. The temperatures necessary to test this hypothesis were not attainable in the present growth system; and in use, equilibrium was only approached. Although quantitative data is difficult to derive from this growth system, it has nevertheless been observed that as the temperature is raised in the reaction zone the growth region tends to spread out. Thus, as indicated by the equilibrium analysis, complete reaction is not taking place at the point of mixing of reactive gases.

In conclusion, the vapor growth of AlAs from AsH_3 and AlCl in the temperature range accessible in the present experiments and reactant concentration necessary for single crystal growth occurs at the point of mixing of the two reactant gases. This is distinct from GaAs vapor growth where mixing occurs at one temperature and deposition occurs at some lower temperature. This immediate deposition of AlAs is consistent with the given thermochemical analysis. AlAs has been shown to be a wide bandgap semiconductor with a higher electron mobility than GaP and a stability which allows sufficient time for device fabrication and protection.

APPENDIX F

PHOTO- AND CATHODOLUMINESCENCE IN VAPOR-GROWN AlAs

H. KRESSEL, F. H. NICOLL, M. ETTENBERG, W. M. YIM, AND A. G. SIGAI

Abstract

This Appendix reports the first observation of luminescence in n-type single-crystal AlAs grown by vapor-phase epitaxy. Silicon is the dominant donor, and Mg is the dominant acceptor. At 77°K, the emission spectra are dominated by bands at 2.16 and 1.73 eV, while at 7°K the emission is mostly via a band at $\sim$ 2.1 eV. It is estimated that the "optical" ionization energy of Si donors in AlAs is $\sim$ 73 meV and that of Mg acceptors is $\sim$ 60 meV.

A. General

This appendix reports the first observation of luminescence in n-type single crystal AlAs grown by vapor-phase epitaxy. From the luminescence data, we estimate that the "optical" ionization energy of Si donors in AlAs is $\sim$ 73 meV and that of Mg acceptors is $\sim$ 60 meV.

The samples studied were prepared by vapor-phase epitaxy using the basic growth apparatus used previously for GaAs synthesis (Ref. 17). The details of the method used for the AlAs growth will be separately described (Ref. 109,35) The dominant impurities in the n-type samples were Si, Mg, Cu, and Fe. Oxygen may be present but was not positively identified. The range of impurity levels of the purest samples (as determined by emission spectrographic analysis) was 1 to 10 ppm Si, 1.5 to 15 ppm Mg, 0.03 to 0.3 ppm Cu, and $<$ 2 ppm Fe.

The photoluminescence measurements were obtained using argon laser excitation (4880 Å line). The cathodoluminescence data were obtained using a 15 KV electron beam in an apparatus described elsewhere (Ref. 110). The highest electron beam current density was $\sim$ 5 A/cm^2 which results in the formation of 10^{17} to 10^{18} electron-hole pairs cm^{-3}. The maximum excitation level for the photoluminescence measurements was smaller, with the estimated non-equilibrium carrier density only in the 10^{13}cm^{-3} range.

The photoluminescence spectrum at 7°K of a relatively pure AlAs sample (#37) with a free electron density of $\sim 10^{17}$cm^{-3} is shown in Figure 25. The emission is dominated by a relatively broad band at 5890 Å (2.105 eV), which is 132 meV below the bandgap energy. [Bandgap energy values for AlAs were recently determined (Ref. 111)]. Studies of other samples similarly grown but containing more impurities (particularly Si) show that the band at about 2.1 eV is always seen; however, the weaker bands at higher energies are not resolved in the less pure samples.

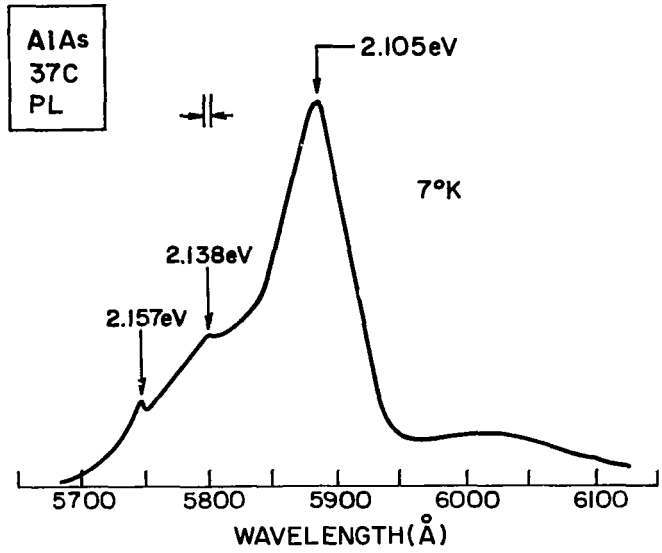

Figure 25. Photoluminescence at 7°K of a sample (#37) with a free electron concentration at room temperature of $\sim 10^{17}cm^{-3}$. The mobility of this sample was not determined, but similar samples have 300°K mobilities of $\sim$ 300 cm^2/V-sec. The bandgap energy is 2.238 eV at 2°K and decreases only slightly to 2.233 eV at 77°K (Ref. 111). Thus the bandgap is $\sim$ 2.237 eV at 7°K.

The 77°K cathodoluminescence spectra of sample 37 consist of two main bands and a "shoulder" in the vicinity of the bandgap energy as shown in Figure 26. The "shoulder" in the vicinity of E_g is very likely due to a combination of free carrier and exciton recombination. The 5740 Å (2.16 eV) band is 73 meV below E_g while the much broader 7170 Å (1.73 eV) band is 0.5 eV below E_g.

The interpretation of the main emission lines requires some consideration of the probable behavior of Si, Mg, Cu, and Fe in AlAs. The only published results concern Si, which was found to be a shallow donor (Ref. 10), and is thought to be responsible for the n-type conductivity of our samples. With regard to Mg, we expect an ionization energy comparable to that of Zn for the following reason. In GaAs, Mg has recently been shown to introduce an acceptor level of $\sim$ 30 meV, a behavior similar to that of Zn (Ref. 112). Arguing from the comparable behavior of Zn in GaAs and AlAs, for both of which Zn is a relatively shallow acceptor with the respective levels of $\sim$ 0.03 and $\sim$ 0.06 eV, (Ref. 13), we expect that Mg should have an ionization energy close to that of Zn in AlAs or $\sim$ 0.06 eV. As will be shown below, this hypothesis is consistent with the data. Finally, Cu and Fe are expected to introduce deep recombination centers, as is the case in many other III-V compounds.

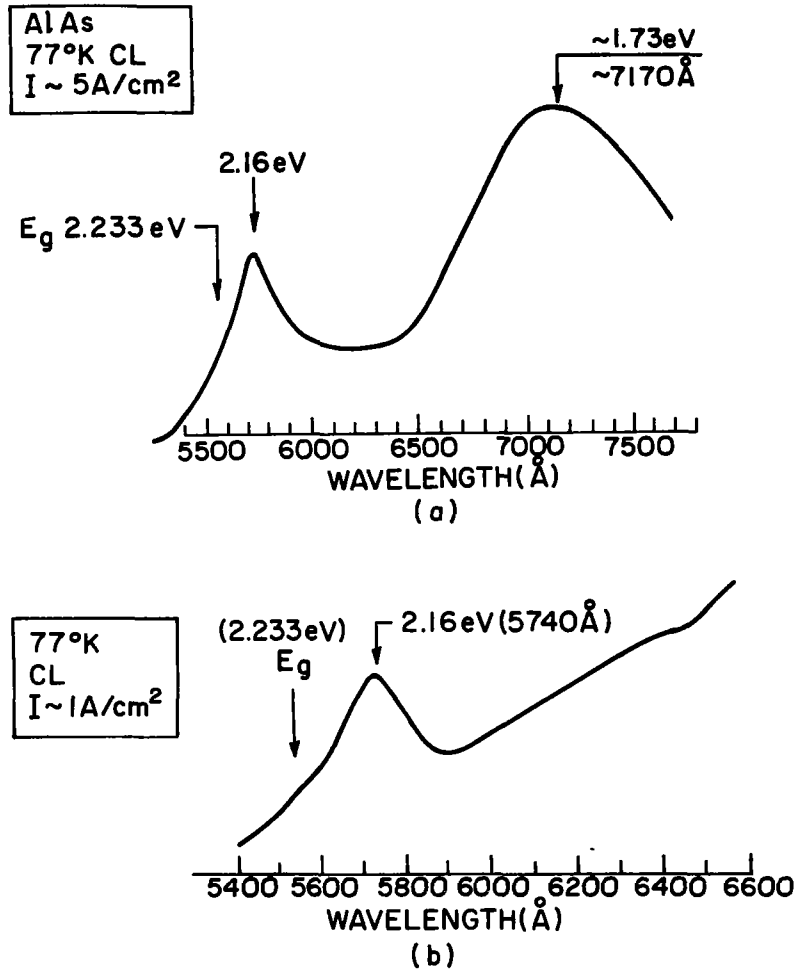

Figure 26. Cathodoluminescence of the same sample shown in Figure 25 at two different electron beam excitation levels: (a) 5 A/cm^2 and (b) 1 A/cm^2. Note the change in wavelength scale.

The analysis is best begun with the low temperature data of Figure 25. At these low temperatures and low excitation levels, donor-acceptor pair recombination is expected to be the dominant process. The most intense band, which peaks at 2.105 eV (E_g - 0.132 eV), is tentatively attributed to Si-Mg pair recombination which, as previously indicated, are the impurities expected to give the shallowest recombination centers. We can estimate $E_a + E_d$ from the expression for the donor-acceptor band peak energy, which is of the form (Ref. 113)

$$h\nu_p = E_g - (E_a+E_d) + \frac{e^2}{\epsilon R} , \qquad (6)$$

where R is the average distance of the interacting pairs with ionization energy E_a and E_d, respectively, and ϵ is the dielectric constant. Neglecting the Coulomb term in the above equation, we estimate that $E_a + E_d \cong 132$ meV.

One way of obtaining the ionization energy of the donors is to study luminescence at high excitation levels where the donor-acceptor recombination process can be saturated, giving way to dominant donor-valence band transitions and eventually free carrier or exciton recombination. While such high excitation was not experimentally feasible at low temperatures, we did strongly excite the samples with the electron beam at 77°K, with the results shown in Figure 26 at two different high excitation levels. The data of Figure 26 show that the dominant near-bandgap recombination band is centered at 2.16 eV (73 meV below the bandgap energy). We tentatively attribute this band to electron transitions from the Si donors to holes in the valence band because the non-equilibrium electron-hole population is in excess of the Mg concentration, thus leading to a saturation of the recombination process via the Mg centers. This suggests then that the Si donor ionization energy $E_d \sim 73$ meV, a value much greater than the 18 meV previously estimated from Hall measurements (Ref. 10). Since we estimated above, from the low temperature data, that $E_a + E_d \cong 132$ meV, we tentatively conclude that the Mg ionization energy is $132\text{-}73 \cong 59$ meV, a value similar to the estimated ionization energy of Zn in AlAs (60 ± 5 meV).

With regard to the other emission lines observed at 7°K, no conclusions can as yet be drawn from the available data. The 1.73 eV band, so prominent at 77°K, is probably due to donor-acceptor transitions involving Si donors and Fe or Cu acceptors. However, the possibility that the crystals contain some oxygen is not excluded and this band may, therefore, involve Mg-O recombination similar to the well-known Zn-O recombination in GaP.

APPENDIX G

THERMAL EXPANSION OF AlAs

M. ETTENBERG AND R. J. PAFF

Abstract

The lattice parameter of AlAs has been very accurately measured as a function of temperature between 15° and 840°C and the coefficient of thermal expansion has been determined. The lattice parameter at 0°C is 5.6605 ± 0.0005 Å and the coefficient of thermal expansion is (5.20 ± 0.05) x 10^{-6}/°C. A comparison is made to GaAs which indicates that there is a perfect lattice match at about 900°C and 0.14% lattice mismatch at room temperature.

A. Introduction

The excellent lattice match, at room temperature, between AlAs (5.660) (Ref. 98) and GaAs (5.653) (Ref. 114) make GaAs an excellent substrate for the growth of epitaxial layers of AlAs or $Al_xGa_{1-x}As$. Since epitaxial growth techniques involve elevated temperatures, it would be of direct interest to investigate the variation of the AlAs-GaAs lattice match with temperature. Assuming Vegard's Law is obeyed in the $Al_xGa_{1-x}As$ system at elevated temperatures, these results would give insight into the mechanical state of epitaxial $Al_xGa_{1-x}As$ alloy layers as well as AlAs layers grown on GaAs.

B. Experimental Procedure

The AlAs studied was synthesized using an open-flow vapor phase growth system, where aluminum is transported as the chloride and As is provided as the decomposition product of arsine. The basic growth system has been previously described (Ref. 17). The AlAs has been shown to have less than 200 ppm total nongaseous impurities by mass and emission spectroscopy. The major impurity was silicon with trace amounts of Mg and Fe.

Samples of AlAs were ground to pass through a 325 mesh screen and loaded into a 0.3 mm I.D. quartz capillary. The capillaries were sealed and loaded into a Unicam high-temperature x-ray powder camera, model S-150 with a 19-cm diameter. To improve accuracy, by eliminating film shrinkage errors, the camera cassette was modified to accommodate single film Straumanis loading rather than the supplied twin-film knife edge placement.

The temperature was monitored during a run by employing a Pt/Pt-13% Rh thermocouple absolutely calibrated by measuring the accurately determined lattice parameter of silver (Ref. 115) as a function of thermocouple EMF. The temperature was maintained within ± 3°C over the duration of an exposure.

Nickel filtered copper radiation was used and the exposure time was approximately 16 hours per pattern. During an exposure the camera was evacuated to less than 10^{-3} Torr by a mechanical pump.

The line positions were read using a standard film reader to an accuracy of $\pm$ 0.05 mm. The line position data was transmitted to a computer where a previously stored program applied Cohen's method (Ref. 116) to the back reflection lines and determined an accurate lattice parameter. Assuming α to be linear with temperature the standard formula for thermal expansion is:

$$a_T = a_0(1 + \alpha T) \tag{7}$$

where a_T is the lattice constant at any temperature T in °C. The computer was also employed to determine the best straight line fit to a plot of lattice parameter vs. temperature. The slope of this line is the coefficient of thermal expansion (α) multiplied by the lattice parameter at 0°C, (a_0).

C. Results and Discussion

The results are listed in Table XIV for the two separate samples measured.

Table XIV

AlAs LATTICE PARAMETER

Sample 1		Sample 2	
Temp. °C	L.P. Å	Temp. °C	L.P. Å
15	5.6610	16	5.6611
130	5.6634	185	5.6653
263	5.6677	358	5.6703
500	5.6750	484	5.6738
660	5.6786	611	5.6768
840	5.6847	812	5.6848
15	5.6605	15	5.6611

The lattice parameter of each sample was first measured at room temperature, then at elevated temperatures, and then redetermined at room temperature. The agreement in the two room-temperature determinations, within the estimated error of 1 part in 10,000, indicate that the sample has not been altered at the elevated temperatures. A careful examination of the computer calculations showed that no extra lines were present on the film and that no line deviated significantly from its expected position. The a_0 for AlAs is 5.6605 ± 0.0005 Å in excellent agreement with previous work (Refs. 98,10). The calculated coefficient of thermal expansion (α) is $(5.20 \pm 0.05) \times 10^{-6}/°C$ and is quite linear over the measured temperature range as can be seen in the lattice parameter, temperature plot presented in Figure 27. This result is in disagreement with a more limited study (Ref. 117) which indicated that α varied from 3.66×10^{-6} to 4.92×10^{-6} between 30° and 230°C.

If the lattice parameters of AlAs and GaAs (Ref. 118)* are compared as a function of temperature (Figure 27), it can be seen that at the normal epitaxial growth temperatures of 800° to 1100°C, there is almost a perfect lattice match. As an epitaxial layer of AlAs on GaAs is cooled, lattice strain will be introduced at the interface and reach a maximum at room temperature of 0.14%.

One question important to device fabrication is whether epitaxial layers of AlAs or $Al_xGa_{1-x}As$ on GaAs contain simple strain or strain-relieving dislocations at the interface. Previous work on silicon (Ref. 119) shows that plastic deformation does not take place below 600°C. Because of the greater melting point of AlAs (> 1700°C) (Ref. 98), plastic deformation probably does not take place below 800°C. Since almost no strains are introduced at the interface until the temperature is below this point, dislocations will not tend to move from the surface to take up the interfacial strain.

It must, therefore, be presumed that dislocation-free but slightly strained AlAs or $Al_xGa_{1-x}As$ can be grown epitaxially on dislocation-free GaAs substrates and that this condition of strain decreased proportionately with decreasing aluminum content.

---

*Also M. Abrahams, J. J. Tietjen, and R. Paff, RCA Laboratories, private communications.

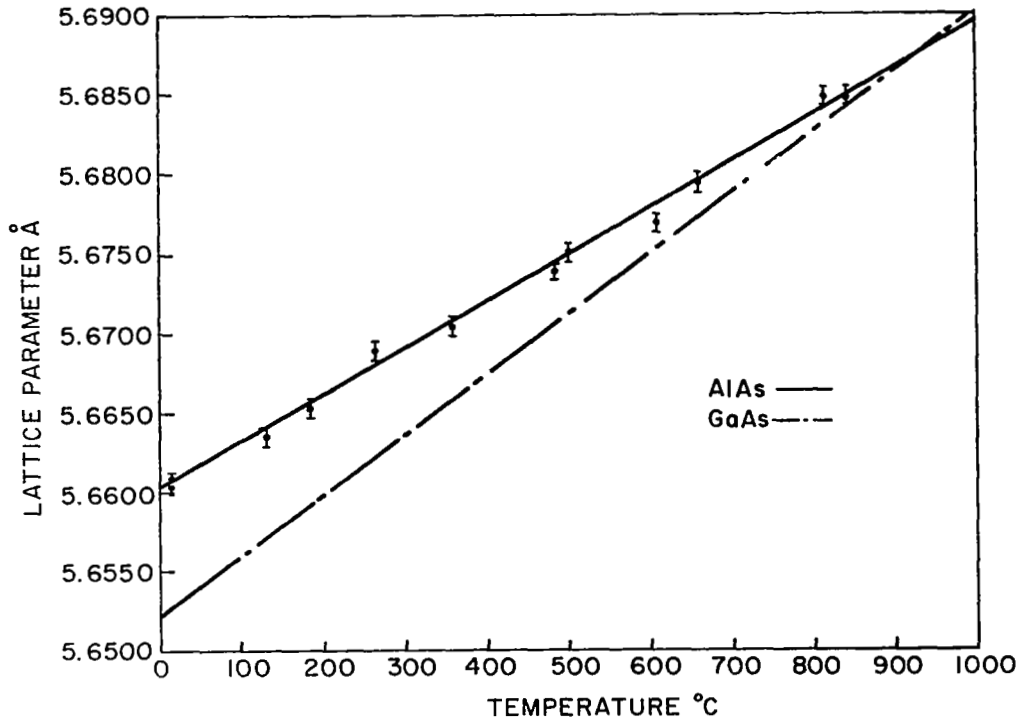

Figure 27. Lattice parameter of AlAs vs. temperature.

APPENDIX H

THE PREPARATION OF VISIBLE-LIGHT-EMITTING P-N JUNCTIONS IN AlAs

C. J. NUESE, A. G. SIGAI, M. ETTENBERG,
J. J. GANNON, AND S. L. GILBERT

Abstract

P-n junctions have been formed for the first time in AlAs by diffusion Zn into single-crystal n-type vapor-grown AlAs layers. I-V, C-V, and photovoltage measurements indicate well-behaved junctions at room-temperature, with external electroluminescent efficiencies on the order of 10^{-5}. The room-temperature forward-bias emission spectrum consists of a narrow yellow-green peak at 2.146 eV and two broad infrared peaks at 1.66 and 1.35 eV. At 600°K and 3 V reverse-bias, current densities of 10^{-3} A/cm^2 are observed, which are nearly an order of magnitude smaller than those for similarly prepared GaAs junctions.

A. General

The large energy gap (Refs. 120,14) ($\approx$ 2.16 eV) of AlAs makes it potentially attractive for electroluminescent and high-temperature applications. In addition, the excellent lattice match of AlAs and GaAs has proven to be of significant value in the preparation of high-quality layers of $Al_{1-x}Ga_xAs$ alloys on GaAs substrates for spontaneous (Ref. 121) and coherent (Ref. 122) light-emitting junctions. However, until recently, the extremely hygroscopic nature of AlAs has caused its rapid decomposition in normal ambients (Ref. 123), thereby hampering practical device fabrication and evaulation.

Recently, vapor-grown layers of AlAs, prepared epitaxially on GaAs substrates, have been found to be more stable (Ref. 124) than previously reported (Ref. 123), thereby allowing fabrication of p-n junctions in AlAs for the first time. It is the purpose of this paper to discuss the fabrication and evaluation of these junctions, and furthermore, to describe the yellow-green radiation which is emitted from the junctions at room-temperature under forward bias.

Single-crystal epitaxial layers of n-type AlAs, 3 to 4 mils thick, were grown on <100>-oriented n^+ GaAs substrates by a vapor-phase technique described elsewhere (Ref. 35). The epitaxial surfaces following growth were reasonably smooth, and upon exposure to air, developed a thin blue-violet (interference) layer, probably due to the formation of an aluminum-oxide film. Dopants were not intentionally added during growth, although Hall measurements on the AlAs layers indicated n-type conduction with electron concentrations on the order of 3×10^{17}cm^{-3}, presumably due to Si contamination.

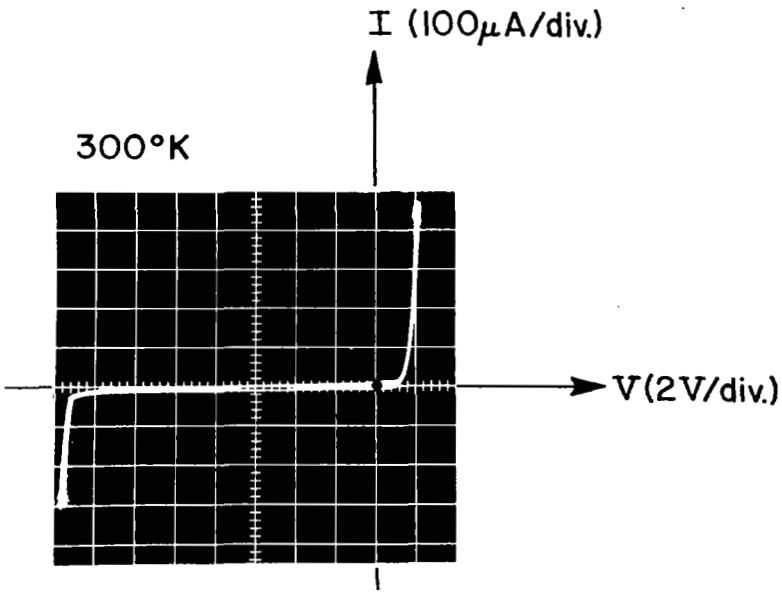

Figure 28. I-V characteristics for Zn-diffused AlAs p-n junction at 300°K. I = 100 μA/div, V = 2 V/div. Note that the origin has been displaced horizontally three divisions from the center of the grid.

P-n junctions were formed in several such layers by the diffusion of Zn at temperatures between 850° and 900°C under 1 atm. of arsenic pressure. Diffusion times on the order of 15 min resulted in p-n junctions 1 to 2 mils deep, which could be directly observed on cleavage planes. After each diffusion, the epitaxial surface indicated p-type when thermally probed.

The room-temperature I-V characteristics of a Zn-diffused AlAs junction are shown in Figure 28. The forward voltage saturation begins close to 2 V, which is appropriate for the high bandgap energy of AlAs. At forward currents higher than those shown in Figure 28, a series resistance of 10 ohms becomes evident, which may be due to the resistance of Ag-Mn (Ref. 125) evaporated contacts to the p-type AlAs. At 77°K, however, the I-V characteristics indicate severe carrier freeze-out, which is found to originate primarily in the bulk p-type layer of the Zn-diffused AlAs. Removal of the GaAs substrates from the epitaxial layers did not alter the electrical or electroluminescent properties of the AlAs p-n junction.

The reverse-bias breakdown voltage of 15 V shown in Figure 28 can be used to estimate the carrier concentration on the more lightly-doped (n-side) of the junction. For an abrupt junction (Ref. 126), where $V_{BR} \alpha (E_g)^{3/2}$, the 15 V breakdown in AlAs corresponds to a GaAs breakdown of about 8 V, or a carrier concentration (Ref. 126) of $3 \times 10^{17} cm^{-3}$. The I-V characteristics

of most AlAs junctions were found to be quite free of leakage currents, with reverse current densities (at 3 V) as small as 4×10^{-8} A/cm^2 at room temperature and 1×10^{-3} A/cm^2 at 600°K. These values are an order of magnitude lower than normally observed for vapor-grown GaAs junctions (Ref. 127), and illustrate the expected high-temperature potential of AlAs.

The capacitance-voltage relation for these junctions was found to be of the form $C = C_o (V + V_B)^{-1/n}$, with a value of $n = 1.97$ and a value of $V_B = 1.6$ V. The value of the built-in potential, V_B, is considerably smaller than the energy gap of AlAs, but is identical to that determined for GaP junctions prepared by liquid-phase epitaxy (Refs. 128,129). A plot of $1/C^2$ vs. V yielded a straight line whose slope indicated a carrier concentration of 1.7×10^{17}cm^{-3}, in reasonable agreement with donor concentrations determined by the reverse breakdown voltage and by Hall measurements prior to diffusion.

In order to provide an independent estimate of the energy gap of AlAs, the p-n junction photovoltage was determined as a function of the energy of the incident light. Although this technique is not as accurate for p-n junctions as it is for surface Schottky diodes, the low-energy edge of the photoresponse, when extrapolated to zero voltage, provides an approximate measure of the semiconductor bandgap. Energy gaps determined in this fashion were 2.15 eV at room-temperature and 2.23 eV at 77°K. These values compare quite well with those previously reported in the literature (Refs. 120,98), and with values of 2.16 and 2.233 eV recently determined by precise optical absorption measurements on AlAs (Ref. 14).

The room-temperature electroluminescent spectra of an AlAs Zn-diffused junction is shown in Figure 29. In general three peaks were observed, which appear qualitatively similar to those previously reported for Zn-diffused GaP junctions (Ref. 130). The most intense peak in Figure 29 is a broad impurity peak centered at 1.66 eV with a half-width of approximately 0.35 eV. Mass spectrographic analysis of the vapor-grown AlAs layers indicates the presence of two impurities, iron and oxygen, which may be responsible for this peak. Both have appropriately deep levels, 0.5 to 0.6 eV from the valence band edge (Ref. 131), in GaAs. In addition, the somewhat similar (red) emission peak of GaP junctions is known to arise from Zn-O transitions (Refs. 128,129,130).

The narrow (0.11 eV) high-energy peak at 5780 Å (2.146 eV) provides a yellow-green emission near the plane of the AlAs p-n junction. Because of high-energy absorption in the p-type layer, the true junction emission energy is expected to be somewhat larger than 2.146 eV. The fact that the observed emission energy is only 14 meV less than the 2.16 eV energy gap suggests that free excitons may be involved in the emission process, as they are for the green emission in GaP at room-temperature (Ref. 128). Recombination via a reported 18 meV Si donor level (Ref. 10) is not considered likely, since recent photoluminescent measurements on layers doped with Si, Te, and Zn indicate impurity ionization energies no less than 55 meV, consistent with the relatively low electron mobilities (300 cm^2/V-sec) observed in n-type AlAs (Ref. 35).

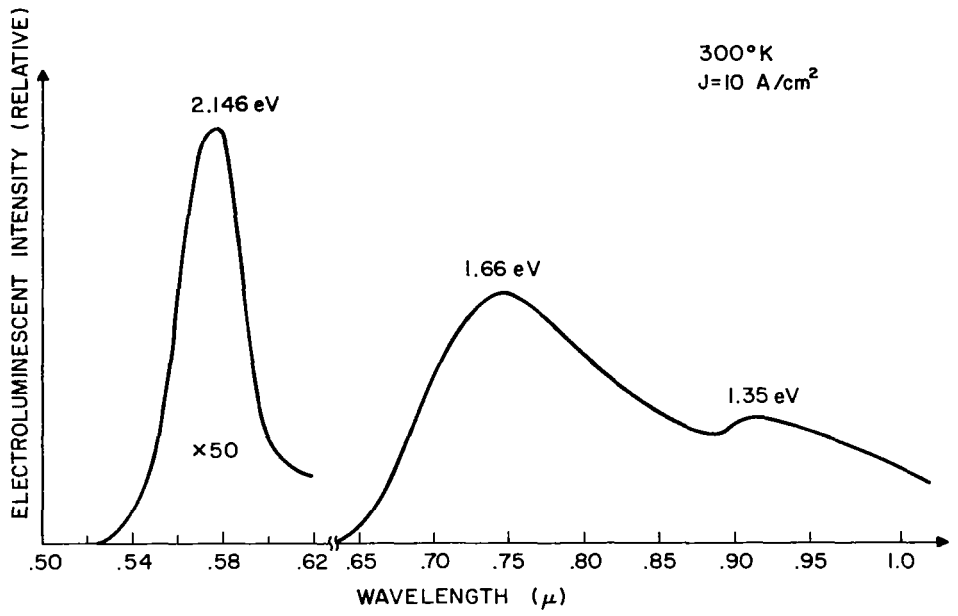

Figure 29. Electroluminescent spectra at 3000°K for AlAs p-n junction. $J = 10$ A/cm^2. Spectra have been corrected for S-1 photomultiplier response. Note that the weaker 2.146 eV peak has been amplified by a factor of 50.

The origin of the low-energy emission at 1.35 eV is unknown, but could arise from either crystal defects or contamination. Mass spectrographic analysis did show the presence of 1 ppm Cu in the AlAs layers prior to diffusion.

Finally, the room-temperature dependence of the emission intensity on applied current was found to be of the form, Intensity α I^m, where $1 < m < 2$ for the 2.146 eV peak and $m \approx 1/3$ for the two infrared impurity peaks. The intensity ratio of the impurity peaks to the 2.146 eV peak therefore varied with current from a value of about 100 at low currents (0.2 A/cm^2) to as little as three at high currents (100 A/cm^2), with a corresponding variation in the observed emission color from orange to yellow-green.

The AlAs junctions described here are electrically well-behaved, and have remained relatively stable under normal laboratory environments for times on the order of weeks. Long-term stability problems have not been considered here, but may be circumvented by various encapsulation techniques. Although the external electroluminescent efficiencies are low ($\approx 10^{-5}$), the AlAs emission spectra appear similar to those of Zn-diffused GaP junctions. If the near-bandgap peak in AlAs can be enhanced and optimized, as the red and

green peaks have been in GaP, the capability of preparing single-crystal AlAs layers on readily-available large-area GaAs substrates would be attractive for electroluminescent applications.

APPENDIX I

VAPOR-PHASE GROWTH OF EPITAXIAL $GaAs_{1-x}Sb_x$ ALLOYS USING ARSINE AND STIBINE

R. B. CLOUGH AND J. J. TIETJEN

Abstract

A technique previously used to prepare alloys of $InAs_{1-x}P_x$ and $GaAs_{1-x}P_x$, using the gaseous hydrides arsine and phosphine, has been extended to grow single crystalline $GaAs_{1-x}Sb_x$ by replacing the phosphine with stibine. Procedures were developed for handling and storing stibine which now make this chemical useful for vapor phase growth. This represents the first time that this series of alloys has been grown from the vapor phase. Layers of p-type GaSb and GaSb-rich alloys have been grown with the carrier concentrations comparable to the lowest ever reported. In addition, a p-type alloy containing 4% GaSb exhibited a mobility of 400 cm^2/V-sec which is equivalent to the highest reported for GaAs.

A. Introduction

Recently, interest has been shown in the preparation and properties of $GaAs_{1-x}Sb_x$ alloys, since it was predicted* that for compositions in the range of $0.1 < x < 0.5$, they might provide improved Gunn devices. However, preparation of these alloys presents fundamental difficulties. In the case of liquid phase growth, the large concentration difference between the liquidus and solidus in the phase diagram, at any given temperature, introduces constitutional supercooling problems. It is likely that, for this reason, virtually no description of the preparation of $GaAs_{1-x}Sb_x$ by this technique has been reported. In the case of vapor phase growth, problems are presented by the low vapor pressure of antimony, and the low melting point of GaSb and many of these alloys. In previous attempts* at the vapor phase growth of these materials, using antimony pentachloride as the source of antimony vapor, alloy compositions were limited to those containing less than about 2% GaSb. This was in part due to the difficulty of avoiding condensation of antimony on introducing it to the growth zone.

A growth technique has recently been described (Ref. 17) for the preparation of III-V compounds in which the hydrides of arsenic and phosphorous (AsH_3 and PH_3) are used as the source of the group V element. With this method, $GaAs_{1-x}P_x$ and $InAs_{1-x}P_x$ have been prepared (Refs. 17,18) across both alloy series with excellent electrical properties. Since the use of stibine (SbH_3) affords the potential for effective introduction of antimony to the growth apparatus, in analogy with the other group V hydrides, this growth method has

*G. F. Day, Varian Associates, private communication.

been explored for the preparation of $GaAs_{1-x}Sb_x$ alloys. In addition to GaSb, these alloys have now been prepared with values of x as high as 0.8. In the case of GaSb, undoped p-type layers were grown with carrier concentrations equivalent to the lowest reported in the literature. Thus it has been demonstrated that, with this growth technique, all of the alloys in this series can be prepared.

B. Experimental Procedure

1. Growth Technique. - The growth apparatus, shown schematically in Figure 30, and procedure are virtually identical to that described (Ref. 17) for the growth of $GaAs_{1-x}P_x$ alloys, with the exception that phosphine is replaced by stibine.* HCl is introduced over the gallium boat to transport the gallium predominantly via its subchloride to the reaction zone, where it reacts with arsenic and antimony on the substrate surface to form an alloy layer.

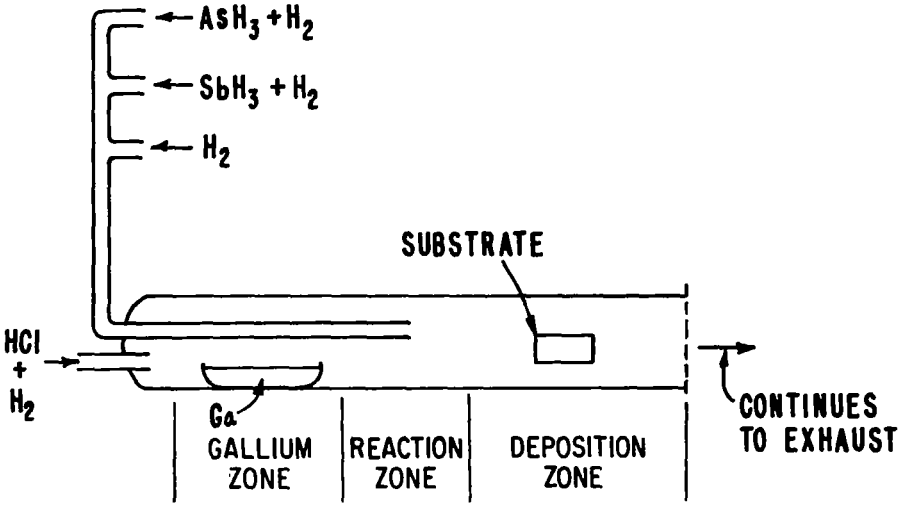

Figure 30. Schematic representation of vapor deposition apparatus.

The fundamental limiting factors to the growth of $GaAs_{1-x}Sb_x$ alloys from the vapor phase are the low melting point of GaSb (712°C) and the low vapor pressure of antimony at this temperature (< 1 mm). Thus, relatively low antimony pressures must be employed, which, however, imply low growth rates. To provide low antimony pressures, very dilute concentrations of arsine and stibine in a hydrogen carrier gas were used. Typical flow rates were about 4 cm^3/min of HCl, from 0.1 to 1 cm^3/min of AsH_3, and from 1 to 10 cm^3/min of SbH_3, with a total hydrogen carrier gas flow rate of about 6000 cm^3/min.

*Purchased from Matheson Co., E. Rutherford, New Jersey.

The high linear velocities attendent with the high total flow rate delays cracking of the stibine until it reaches the reaction zone and prevent condensation of antimony in the system. To improve the growth rates, growth temperatures just below the alloy solidus are maintained to allow for a maximum partial pressure of antimony in the system. Typical temperatures used are gallium zone and reaction zone at 850°C, with the growth zone held at from 650° to 750°C.

Substrates of semi-insulating GaAs oriented 3° off the <100> axis were used in order to make electrical measurements, since the growth rates were too low to result in self-supporting epitaxial layers. As pointed out below, growth on these substrates has a deleterious effect on the electrical properties of the epitaxial layers.

2. Use of Stibine. - Since little was known of the properties and handling procedures for stibine, experiments were performed to determine these. The vapor pressure was measured from -195°C to +27°C and found to agree with that obtained by Berka et al. (Ref. 132). We found it to be more stable than anticipated, especially if stored in the dark. Although it was reported (Ref. 133) that stibine has a half-life of from 2 to 4 hours at room temperature, we found that there was no measurable decomposition at 0°C for a period of 12 hours. Thus, the gas can easily be kept above its boiling point (-18°C) for use during growth. We found it to be stable for a period of several months at -78°C (solid CO_2 temperature), so that it may be stored at this temperature prior to use.

Based on this stability data, a simple technique to use the stibine was established using the apparatus shown in Figure 31. The stibine is stored at

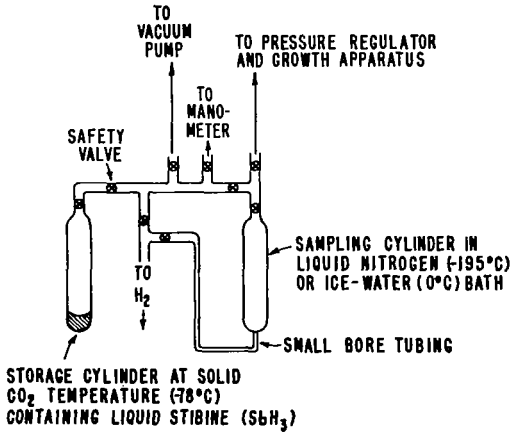
TO VACUUM PUMP
TO PRESSURE REGULATOR AND GROWTH APPARATUS
TO MANO-METER
SAFETY VALVE
SAMPLING CYLINDER IN LIQUID NITROGEN (-195°C) OR ICE-WATER (0°C) BATH
TO H_2
SMALL BORE TUBING
STORAGE CYLINDER AT SOLID CO_2 TEMPERATURE (-78°C) CONTAINING LIQUID STIBINE (SbH_3)
● INDICATES VALVE

Figure 31. Schematic representation of stibine storage and sampling apparatus.

-78°C (solid CO_2 temperature) in the liquid state. For use during growth, an aliquot portion is first distilled from the storage cylinder to a reserve cylinder at -195°C (liquid nitrogen temperature). The reserve cylinder is then warmed to 0°C and the distillation rate established by measuring the stibine pressure at this temperature. Typically, the distillation rates for our apparatus were about 0.01 mole/min (they are very sensitive to slight temperature changes of the storage cylinder and, therefore, must be carefully monitored). The stibine at 0°C is then pressurized with hydrogen for use during growth. To increase the amount of mixing, the hydrogen is introduced at high velocity. By preparing each aliquot immediately prior to use, problems due to settling of the mixture were minimized.

C. Results

Using this technique, we have grown alloys of $GaAs_{1-x}Sb_x$ with compositions ranging from 1 to 80 mole % GaSb, as well as GaSb. This is the first time that they had been prepared from the vapor phase over this range of compositions. The preparation of $GaAs_{1-x}Sb_x$ was limited to 2 mole % GaSb. These layers are all monocrystalline and epitaxial.

1. Growth Conditions. - Studies on the effect of flow rates and growth temperature on the composition of the grown layers have shown the following. First, the mole fraction of antimony in the vapor phase is always greater than that in the grown layers. This indicates that there is a greater rate of incorporation of arsenic than antimony in the alloys, even though the vapor pressure of antimony is over four orders of magnitude lower than that of arsenic at the growth temperature. Second, the composition of the grown layers is independent of the growth temperature, varying less than $\pm$ 0.5 mole % over approximately a 200°C range of growth temperature. Thus, the composition of the grown layers is a function only of the composition of the gas phase, so that all of the alloys in the series may be grown by selecting the appropriate flow rates of arsine and stibine.

2. Electrical Properties. - The results of Hall coefficient and resistivity measurements for these alloys are presented in Table XV. The carrier concentrations obtained for the p-type GaSb and GaSb-rich alloys are somewhat lower than those reported for melt-grown GaSb, where only a limited number of undoped p-type crystals have been grown with hole concentrations in the $10^{16}cm^{-3}$ range. One explanation for this is that the acceptor concentration is due to excess gallium on antimony sublattice sites (Ref. 134), and is supported by the fact that the lowest hole concentrations reported (Refs. 135,136) were obtained only with an antimony-rich melt. In the case of vapor-phase growth of GaSb, the lower carrier concentrations obtained may be due to the excess antimony pressure in the growth zone.

Table XV

ELECTRICAL PROPERTIES OF P-TYPE $GaAs_{1-x}Sb_x$ ALLOYS

x	Hole Concentration (cm^{-3})		Hole Mobility (cm^2/V-sec)	
	300°K	77°K	300°K	77°K
0.01	$1.8x10^{15}$	$1.2x10^{15}$	220	400
0.02	$1.3x10^{16}$	$5.1x10^{15}$	190	700
0.04	$3.0x10^{15}$	---	400	---
0.10	$1.2x10^{18}$	$4.5x10^{17}$	55	160
0.21	$2.9x10^{17}$	$1.7x10^{17}$	45	80
0.31	$1.5x10^{18}$	$1.5x10^{18}$	24	30
0.64	$9.0x10^{18}$	$1.2x10^{19}$	20	15
0.70	$3.4x10^{16}$	---	251	---
0.75	$1.0x10^{17}$	---	48	---
0.80	$4.6x10^{16}$	---	21	---
1.00	$1.2x10^{19}$	$1.9x10^{19}$	215	120
1.00	$6.0x10^{16}$	$1.2x10^{16}$	240	270
1.00	$4.7x10^{16}$	---	120	---
1.00	$2.3x10^{17}$	$4.3x10^{16}$	336	405

Due to the thermodynamic reasons stated previously, the growth rates of these alloys were generally low (< 5 μm/hr), so that in order for electrical measurements to be made, semi-insulating GaAs substrates were used. This has the detrimental effect of producing strain in the grown layers due to a mismatch in lattice constant and thermal expansion coefficient between the substrate and grown layer. As a result, the GaSb-rich compounds, which are all p-type, generally exhibit low mobilities compared to melt-grown GaSb, where hole mobilities are typically 700 to 800 cm^2/V-sec. It is expected that compositional grading, or deposition on GaSb substrates, would result in higher mobilities. In this respect, it is noteworthy that the hole mobility of 400 cm^2/V-sec achieved in an alloy containing only 4 mole % GaSb is equivalent to the highest value ever reported for unalloyed GaAs. A few layers, all less than 3 mole % GaSb, were n-type, and these show (Table XVI) electron mobilities which, in general, are slightly lower than commonly observed for melt-grown n-type GaAs. Those p-type alloys having extremely low

mobility show very broad x-ray diffraction peaks with half-widths often an order of magnitude wider than those of the substrate diffraction peak, indicating considerable inhomogeneous strain in the layers or an inhomogeneous composition.

Table XVI

ELECTRICAL PROPERTIES OF N-TYPE $GaAs_{1-x}Sb_x$ ALLOYS

x	Net Carrier Conc. cm^{-3}		Electron Mobility $cm^2/V\text{-}sec$	
	at 300°K	at 77°K	at 300°K	at 77°K
< 0.01	$1.1x10^{16}$	$7.8x10^{15}$	3840	4975
.025	$4.5x10^{16}$	$2.6x10^{16}$	2920	5550
.033	$4.7x10^{16}$	---	5370	--

D. Conclusions

Stibine can be successfully used as a source of antimony in vapor phase crystal growth, and $GaAs_{1-x}Sb_x$ alloys can be prepared from the vapor phase across the entire alloy series. This growth technique shows promise of preparing these alloys with good electrical properties if problems of strain and inhomogeneity can be overcome.

APPENDIX J

THE PREPARATION AND PROPERTIES OF VAPOR DEPOSITED EPITAXIAL $InAs_{1-x}P_x$ USING ARSINE AND PHOSPHINE

J. J. TIETJEN, H. P. MARUSKA, AND R. B. CLOUGH

Abstract

Single crystalline $InAs_{1-x}P_x$ layers have been prepared by a vapor phase growth technique previously used to prepare very high-quality $GaAs_{1-x}P_x$. These $InAs_{1-x}P_x$ alloys exhibit the highest electron mobilities yet reported for this system. Electron mobility data is reported for the alloys at 77°K for the first time. At this temperature, a mobility value of 120,000 cm^2/V-sec was measured for InAs, which is the highest yet reported. Vegard's law is obeyed over the entire composition range. Both n- and p-type doping has been achieved during vapor growth to provide a broad range of electrical resistivities and p-n junctions.

A. Introduction

$InAs_{1-x}P_x$ alloys have an exceptionally broad range of band gaps and electron mobilities. Consequently, they have potential advantage for a number of device applications. These include infrared emitting and detecting devices, utilizing their low energy band gaps, and devices operating at high frequencies, which can take advantage of their high mobilities. Nevertheless, only limited results (Refs. 137-139) have been reported pertaining to improving the preparation and properties of these crystals, and virtually no work has involved the vapor-phase growth of these materials. As a result, the potential of $InAs_{1-x}P_x$ alloys has not been fully realized.

In constrast, with $GaAs_{1-x}P_x$ alloys, a very significant effort has been undertaken to improve and characterize these materials, and in this respect, vapor phase growth methods have played a significant role (Refs. 17,140-143). In particular, one vapor phase growth technique (Ref. 17) has been developed which permits the preparation of $GaAs_{1-x}P_x$ alloys with high purity, homogeneity, and crystalline perfection. In addition, this method facilitates controlled n- and p-type doping over a wide resistivity range, and the preparation of multilayer structures incorporating layers of different resistivity and/or composition. This, in turn, has led to the fabrication of a variety of outstanding electro-optic (Refs. 23,37) and microwave (Refs. 20,21) devices. With this growth method, Ga is transported as its subchloride via a reaction with HCl gas, and AsH_3 and PH_3 serve as the sources of the group V elements.

As a logical extension of this growth technique, a simple substitution of In for the Ga has permitted the preparation of $InAs_{1-x}P_x$ single crystals having the highest electron mobilities ever reported, which supplements the earlier work on $GaAs_{1-x}P_x$. In addition, both n- and p-type doping has been achieved, and multilayer structures have been prepared.

B. Experimental

1. Apparatus and Materials. - The apparatus, shown schematically in Figure 32, is essentially identical to that described previously (Ref. 17)

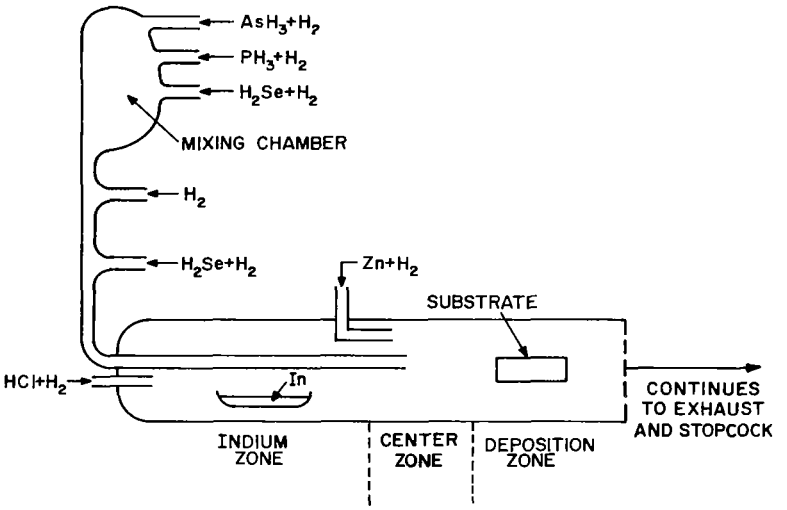

Figure 32. Schematic representation of vapor deposition apparatus.

with the exception that the source Ga is replaced by In. It consists principally of a straight tube through which the pertinent vapors pass. A large bors stopcock separates the growth region from a forechamber which may be independently purged to facilitate insertion and withdrawal of the specimens without comtaminating the system. HCl gas, AsH_3, PH_3, and H_2Se, which serves as the n-type dopant source, are all monitored into the apparatus by precision valves and flowmeters. P-type doping is achieved by vaporizing metallic Zn in a heated side-arm and transporting the vapors into the deposition zone with H_2 carrier gas.

With the exception of the use of <100>-oriented InAs single crystalline substrates,* the materials employed in this study are as described previously (Ref. 17). The InAs substrates were mechanically polished to a flat, mirror-smooth finish, and then chemically polished in a solution of 2% by volume of bromine in methanol. Typical substrate dimensions were about 2 cm^2 in area and 0.5 mm thick.

*Purchased from Monsanto Company, St. Louis, Missouri.

2. Procedure. - The growth procedure also closely follows that described previously (Ref. 17). Freshly etched substrates are inserted in the growth chamber and heated in hydrogen at a rate of about 20°C/min. When the substrate temperature reaches 600°C, the AsH_3 flow is started in order to provide an arsenic atmosphere to stabilize the substrate surface. When the final operating temperatures are reached, the HCl flow over the In is started and the epitaxial deposition of InAs occurs. The flow of PH_3 is then initiated and slowly increased to produce a final gas phase mixture of AsH_3 and PH_3 appropriate to the desired alloy composition. The dependence of the alloy composition on the concentration of PH_3 in the AsH_3-PH_3 mixture is presented in Figure 33. By slowly increasing the PH_3 flow, a region is introduced which is graded in composition from InAs at the substrate to the selected alloy composition. This graded region, which has been as thick as 50 μm for phosphorous-rich alloys, is included to minimize strain arising from differences between the lattice constants of the substrate and the final alloy layer.

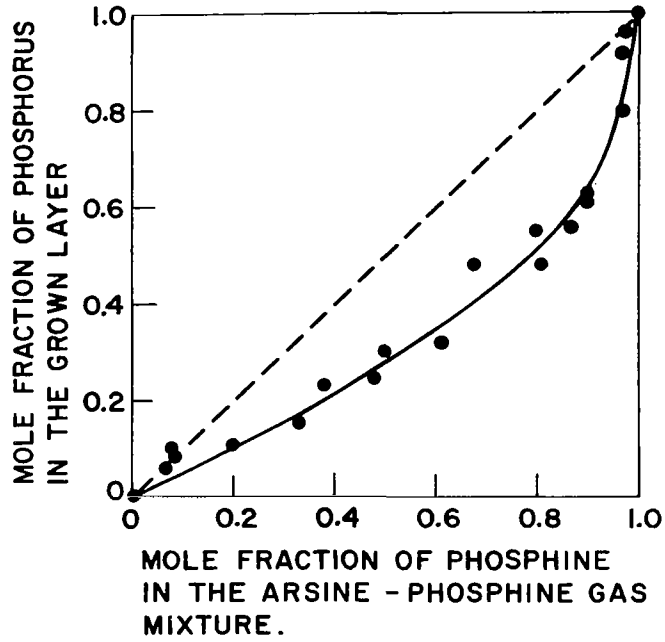

Figure 33. The dependence of the alloy composition on the concentration of PH_3 in the AsH_3-PH_3 gas mixture.

The sum of the flow rates of pure AsH_3 and PH_3 are in the range of 20 to 60 cc/min. The HCl flow rate is about 5 cc/min, and between 1 and 2 l/min of hydrogen is used as a carrier. With these flow rates, with a substrate temperature in the range ot 675° to 725°C, a center zone temperature of 950° to 975°C, and an indium zone temperature of between 850° and 950°C, growth rates in the range 1/4 to 1/2 μm/min are obtained under steady-state conditions. Typical thicknesses for the constant composition region of these deposits have been between 50 and 150 μm.

C. Results and Discussion

1. Crystallinity and Growth Morphology. - X-ray analysis by the Debye-Scherrer technique indicates that these layers are single phase, cubic, solid solutions, and show no detectable range of composition. In addition, Laue back-reflection analysis reveals that the layers are epitaxial. The lattice constant is presented as a function of alloy composition in Figure 34, which

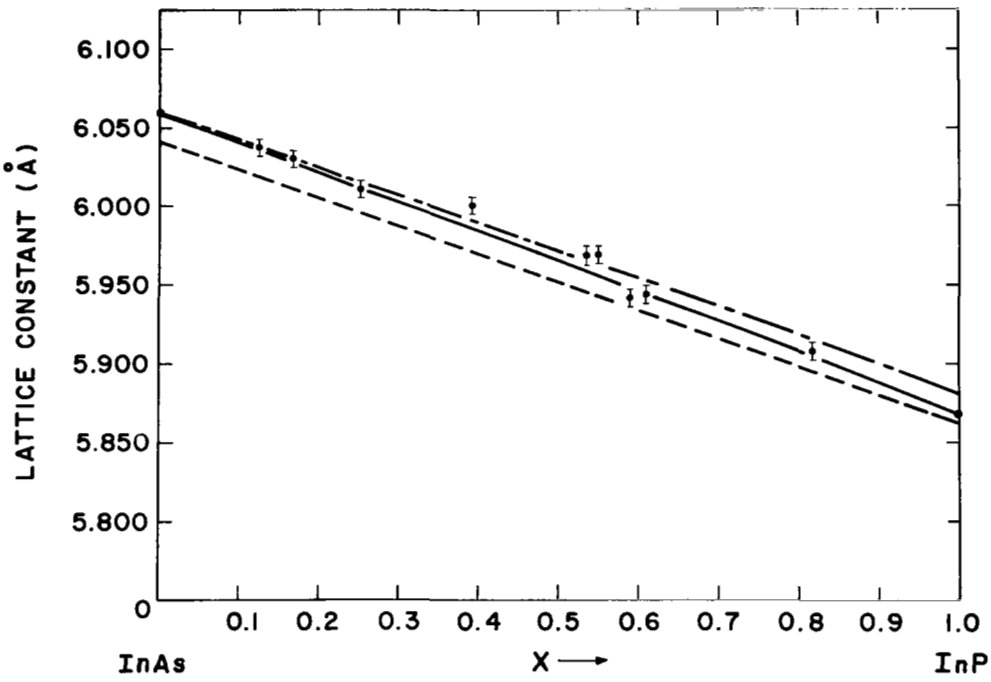

Figure 34. The dependence of the lattice constant on alloy composition in the system $InAs_{1-x}P_x$. The dependence observed by Folberth (Ref. 137) and Koster and Ulrich (Ref. 144) is also included: ---Folberth; ___ _ ___Koster and Ulrich; _____this Appendix.

demonstrates that Vegard's law of solid solutions is obeyed in this system. This result is in general agreement with those of Folberth (Ref. 137), and Koster and Ulrich (Ref. 144). The compositions were determined by chemical analysis* with an accuracy of ± 0.5%.

Although no detailed evaluation of the crystalline perfection of these layers was carried out, examination by optical microscopy revealed that macroscopic surface imperfections, such as hillocks, were prevalent only in phosphorous-rich alloys. For alloys containing less than 50% InP, surfaces are obtained which show virtually no gross structure, and to the unaided eye appear to be mirror-smooth.

*B. L. Goydish, RCA Laboratories, private communication.

2. Electrical Properties. - The epitaxial layers were examined by Hall coefficient and resistivity measurements using a technique (Ref. 17) which permits these measurements to be made on layers as thin as 50 μm. Typical electron carrier concentrations for undoped alloys are in the range of $5x10^{15}$ to $1x10^{16}/cm^3$. The electron mobilities are presented as a function of alloy composition in Figures 35 and 36 for room-temperature and 77°K, respectively. The data of Weiss (Ref. 138), and the results of a theoretical analysis of Ehrenreich (Ref. 145) based on the absence of alloy scattering in this system, and assuming perfect purity, are included for comparison. In general, the mobility values at room temperature are very high, with several values exceeding the best previously reported. In addition, these data corroborate Ehrenreich's contention that alloy scattering is negligible in this alloy system, at room temperature. The relatively low values obtained for alloy compositions approaching InP are attributed to strain arising from lattice and thermal-expansion differences between the InAs substrate and the alloy layer. It is anticipated that further compositional grading can alleviate this problem.

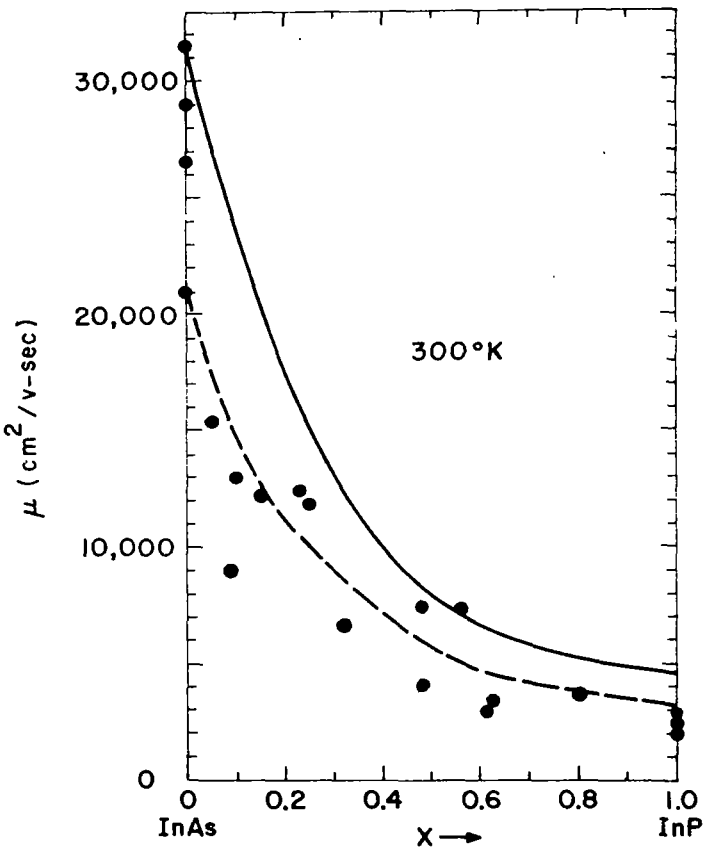

Figure 35. The dependence of the electron mobility on alloy composition in the system $InAs_{1-x}P_x$ at room temperature. The experimental results of Weiss (Ref. 138) and a theoretical analysis of Ehrenreich (Ref. 145) are also included. _ _ _Weiss; _____Ehrenreich.

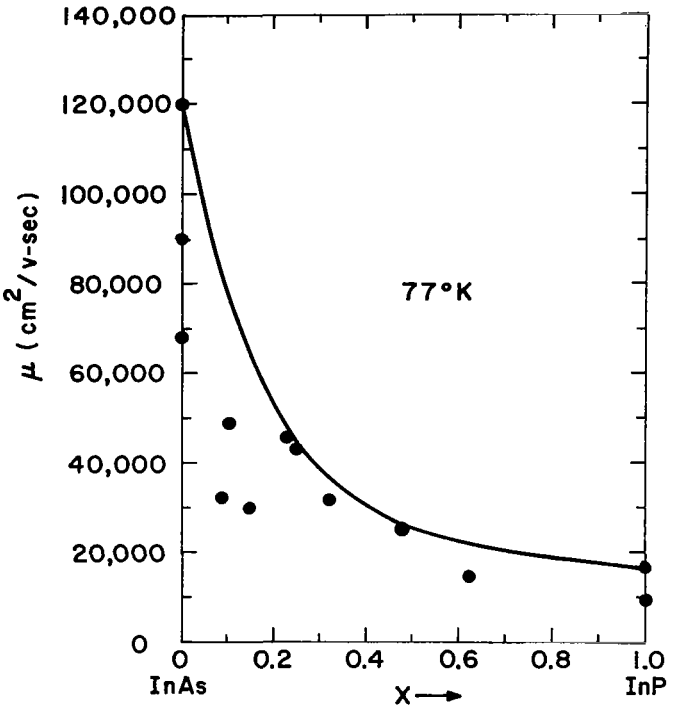

Figure 36. The dependence of the electron mobility on alloy composition in the system $InAs_{1-x}P_x$ at 77°K.

The data presented in Figure 36 are the first data ever reported for 77°K for this alloy system. These high values indicate that the crystals are nearly uncompensated. It is particularly noteworthy that the value of 120,000 cm^2/V-sec for InAs is the highest ever reported for 77°K (Ref. 146).

3. Doping. - Doping of InAs has been investigated using H_2Se gas as a source of Se for n-type doping, and zinc for p-type doping. Electron concentrations as high as $3x10^{19}/cm^3$ were achieved and in general these crystals exhibit mobilities comparable to the best reported in the literature for untreated samples (Refs. 147,148). For example, at carrier concentrations of $1x10^{18}$ and $3x10^{19}cm^{-3}$ the mobility values at room temperature are 10,000 and 1,500 cm^2/V-sec, respectively. Thus, doping to these high donor concentrations does not degrade the material. With respect to hole concentrations, values in the range of $5x10^{17}$ to $7x10^{18}/cm^3$ can be readily obtained, with mobilities of between 150 and 90 cm^2/V-sec for this doping range.

Both n- and p-type doping were also demonstrated for some $InAs_{1-x}P_x$ alloys, and for InP, as characterized by point-contact breakdown and thermal probe measurements. In addition, multilayer structures involving both n- and p-type regions were prepared for selected alloy compositions.

D. Conclusions

The ability to prepare high-quality material by this growth method, which was previously demonstrated in the preparation of $GaAs_{1-x}P_x$ alloys, has now been extended to the preparation of $InAs_{1-x}P_x$ alloys. Electron mobilities have been obtained for these $InAs_{1-x}P_x$ alloys which are higher than ever previously reported. Both n- and p-type doping can be achieved over a broad resistivity range, and these doped layers can be incorporated in multilayer structures. Vegard's law of solid solutions was found to be obeyed in this alloy system.

REFERENCES

1. J. I. Pankove, J. E. Berkeyheiser, H. P. Maruska, and J. Wittke, Solid State Comm. 8, 1051-1053 (1970).

2. R. J. Archer, Electrochem. Soc. Meeting, paper 66 (May 1970).

3. B. W. Hakki, Electrochem. Soc. Meeting, paper 74 (May 1970).

4. M. R. Lorenz and A. Onton, 10th International Conference on Phys. Semiconductors, paper Wab-7 (Aug. 1970).

5. C. J. Nuese, D. Richman, and R. B. Clough, Metall. Trans. 2, 789 (1971).

6. C. Hilsum and P. Porteous, Proc. 9th International Conf. on the Physics of Semiconductors 2, 1214 (1968).

7. H. Rodot, J. Horak, G. Rouy, and J. Bourneix, C. R. Acad. Sc. Paris 269B, 381 (1968).

8. R. E. Enstrom, D. Richman, M. S. Abrahams, J. R. Appert, D. G. Fisher, A. H. Sommer, and B. Williams, Proceedings of Third International Conference on GaAs, Aachen, Germany (1970).

9. C. E. E. Stewart, Conference on Crystal Growth and Epitaxy from the Vapor Phase, Zurich, Switzerland (1970).

10. J. Whitaker, Solid-State Electronics 8, 649 (1965).

11. W. M. Yim, J. Appl. Phys. (June 1971).

12. H. Maruska and J. J. Tietjen, Appl. Phys. Letters 15, 327 (1969).

13. H. Kressel, F. H. Nicoll, M. Ettenberg, W. M. Yim, and A. G. Sigai, Solid State Comm. 8, 1407-1409 (1970).

14. M. R. Lorenz, R. Chicotka, and G. D. Pettit, Solid-State Comm. 8, 693 (1970).

15. R. J. Archer, Meeting of the Electrochemical Society, Los Angeles, California (May 1970).

16. A. Onton and R. J. Chicotka, J. Appl. Physics 41 10, 4205 (1970).

17. J. J. Tietjen and J. A. Amick, J. Electrochem. Soc. 113, 724-728 (1966).

18. J. J. Tietjen, H. P. Maruska, and R. B. Clough, J. Electrochem. Soc. 116, 492-494 (1969).

19. R. B. Clough and J. J. Tietjen, Trans. Met. Soc. of AIME 245, 583-585 (1969).

20. J. J. Tietjen, G. Kupsky, and H. Gossenberger, Solid-State Electronics 9, 1049-1053 (1966).

21. R. E. Enstrom and C. C. Peterson, Trans. Met. Soc. of AIME 239, 413-418 (1967).

22. C. J. Nuese, J. J. Tietjen, J. J. Gannon, and H. F. Gossenberger, J. Electrochem. Soc. 116, 248-253 (1969).

23. J. J. Tietjen, J. I. Pankove, I. J. Hegyi, and H. Nelson, Trans. Met. Soc. of AIME 239, 385-387 (1967).

24. R. E. Enstrom, H. Kressel, and L. Krassner, "Semiconductors and Semimetals," 7B, R. K. Willardson and A. C. Beer, editors, Academic Press, New York, 1971.

25. J. P. Dismukes, R. H. Dean, and C. J. Nuese, Final Report, Contract No. NAS 12-2091, December 1969; also C. J. Nuese and R. H. Dean, Quarterly Technical Report No. 4, August 1970.

26. D. Richman and J. J. Tietjen, Trans. Met. Soc. of AIME 239, 418-420 (1967).

27. R. E. Simon, A. H. Sommer, J. J. Tietjen, and B. F. Williams, Appl. Phys. Ltrs. 13, 355-356 (1968).

28. R. E. Simon, A. H. Sommer, J. J. Tietjen, and B. F. Williams, Appl. Phys. Ltrs. 15, 43 (1969).

29. D. Richman, J. Electrochem. Soc. 115, 945-947 (1968).

30. W. M. Yim, J. Appl. Phys. 40, 2617-2623 (1969).

31. J. P. Dismukes, W. M. Yim, J. J. Tietjen, and R. E. Novak, RCA Review 31 (1970).

32. R. E. Enstrom and J. R. Appert, Int. Symp. on GaAs, Inst. of Physics and the Physical Society, 213-221 (1968).

33. J. J. Tietjen and L. R. Weisberg, Appl. Phys. Ltrs. 7, 261-263 (1965).

34. J. I. Pankove, H. P. Maruska, and J. E. Berkeyheiser, Appl. Phys. Ltrs. 17, 197 (1970).

35. M. Ettenberg, A. G. Sigai, S. Gilbert, and A. Dreeben, J. Electrochem. Soc. 118 (1971).

36. C. J. Nuese, A. G. Sigai, M. Ettenberg, J. J. Gannon, and S. L. Gilbert, Appl. Phys. Letters 17, 90 (1970).

37. C. J. Nuese, J. J. Tietjen, J. J. Gannon, and H. F. Gossenberger, Trans. Met. Soc. of AIME 242, 400-405 (1968).

38. H. P. Maruska and J. I. Pankove, Solid-State Electronics 10, 917-925 (1967).

39. C. J. Nuese, H. Schade, and D. Herrick, Trans. AIME 1, 587 (1970).

40. H. Schade, C. J. Nuese, and D. Herrick, J. Appl. Phys. 41, 9 (1970).

41. J. I. Pankove, H. Nelson, J. J. Tietjen, I. J. Hegyi, and H. P. Maruska, RCA Review 28, 560-568 (1969).

42. J. J. Tietjen and S. Ochs, Proc. IEEE (Correspondence) 53, 180 (1965).

43. L. E. Norton, R. E. Enstrom, and I. J. Hegyi, IEEE Trans. Elect. Dev., 142-143 (1968).

44. B. E. Berson, R. E. Enstrom, and J. F. Reynolds, NEREM Record 10, 94-95 (1968).

45. T. E. Walsh, B. S. Perlman, and R. E. Enstrom, IEEE J. of Solid State Circuits SC-4, 375 (1969).

46. J. F. Reynolds, B. E. Berson, and R. E. Enstrom, Proc. IEEE 57, 1692-1693 (1969).

47. R. E. Enstrom, J. F. Reynolds, and B. E. Berson, Electronics Letters 5, 714-715 (1969).

48. S. Y. Narayan, R. E. Enstrom, and A. R. Gobat, Electronics Letters 6, 17-18 (1970).

49. B. E. Berson, R. E. Enstrom, and J. F. Reynolds, RCA Review 31, 20 (1970).

50. B. E. Berson and S. Y. Narayan, Proc. IEEE (Letters) 55, 6, 1078 (1967).

51. B. E. Berson and S. Y. Narayan, IEEE Trans. El. Devices ED 14, 610-611 (1967).

52. S. Y. Narayan, B. E. Berson, and J. F. Reynolds, NEREM Record, November 1967.

53. A. E. Hahn and A. Matzelle, IEEE Trans. El. Devices ED 14, 403-404 (1967).

54. S. Y. Narayan and A. R. Gobat, Electronics Letters 4, 504-505 (1968).

55. F. P. Califano, Electronics Letters 4, 411-412 (1968).

56. M. C. Steele, F. P. Califano, and R. D. Larrabee, Electronics Letters 5, 81 (1969).

57. R. E. Enstrom and B. F. Williams, Conference on Photoelectric and Secondary Electron Emission, Auguts 27-28, 1969, University of Minnesota, Minneapolis, Minnesota.

58. W. C. Johnson et al., J. Phys. Chem. 36, 2651 (1932).

59. M. R. Lorenz and B. B. Binkowski, J. Electrochem. Soc. 109, 24 (1962).

60. A. Addamiano, ibid 108, 1072 (1961).

61. H. G. Grimmeiss et al., Z. Naturforschung 15a, 799 (1960).

62. J. R. Knight et al., Solid-State Electronics 8, 178 (1965).

63. W. G. Oldham, J. Appl. Phys. 36, 2887 (1965).

64. R. B. Clough and J. J. Tietjen, Trans. TMS-AIME 245, 583 (1969).

65. R. A. Smith, "Semiconductors," Cambridge University Press, 193 (1959).

66. C. Hilsum and A. C. Rose-Innes, "Semiconducting III-V Compounds," Pergamon Press, 167 (1961).

67. E. Kauer and A. Rabenau, Z. Naturforschung 12a, 942 (1957).

68. R. A. Smith, Semiconductors, Cambridge Press New York, N. Y. (1961).

69. W. G. Spitzer and C. A. Mead, Phys. Rev. 133A, 872 (1964).

70. C. A. Mead and W. G. Spitzer, Phys. Rev. Letters 11, 358 (1963).

71. P. J. Dean and D. G. Thomas, Phys. Rev. 150, 690 (1966).

72. M. R. Lorenz, G. D. Pettit, and R. C. Taylor, Phys. Rev. 171, 876 (1968).

73. E. W. Williams, A. M. White, A. Ashford, C. Hilsum, P. Porteous, and D. R. Wight, Brit. J. Appl. Physics 3D, L55 (1970).

74. A. M. White, E. W. Williams, P. Porteous, and C. Hilsum, Brit. J. Appl. Physics 3D, 1322 (1970).

75. B. W. Hakki, A. Jayaraman, and C. K. Kim, Tenth International Conf. on the Physics of Semiconductors, Cambridge, Mass., Paper ThAb-6 (August 1970).

76. R. Zallen and W. Paul, Phys. Rev. 134, A1628 (1964).

77. M. L. Cohen and T. K. Bergstresser, Phys. Rev. 141, 789 (1966).

78. W. P. Dumke, M. R. Lorenz, and G. D. Pettit, Phys. Rev. B1, 4668 (1970).

79. C. J. Nuese and J. J. Gannon, J. Electrochem. Soc. 115, 327 (1968).

80. F. Z. Oswald, Z. Naturforsch. 10a, 927 (1955).

81. C. J. Nuese, A. G. Sigai, M. Ettenberg, J. J. Gannon, and S. L. Gilbert, Appl. Phys. Letters 17, 90 (1970).

82. M. Gershenzon, R. A. Logan, and D. F. Nelson, Phys. Rev. 149, 580 (1966).

83. S. Mayburg and J. Black, J. Appl. Phys. 34, 1521 (1963).

84. K. K. Shih and G. D. Pettit, J. Appl. Phys. 39, 5025 (1968).

85. J. J. Uebbing and R. L. Bell, Proc. IEEE 56, 1624 (1968).

86. B. F. Williams, Appl. Phys. Letters 14, 273 (1969).

87. W. Klein, J. Appl. Phys. 40, 4384-4389 (1969).

88. H. Sonnenberg, Appl. Phys. Letters 16, 245-246 (1970).

89. M. S. Abrahams, L. R. Weisberg, and J. J. Tietjen, J. Appl. Phys. 40, 3754-3758 (1969A).

90. M. S. Abrahams, L. R. Weisberg, C. J. Buiocchi, and J. Blanc, J. Materials Science 4, 223-234 (1969B).

91. M. S. Abrahams, C. J. Buiocchi, and B. F. Williams, Appl. Phys. Letters 18, 220 (1971).

92. M. S. Abrahams and C. J. Buiocchi, J. Appl. Phys. 36, 2855-2863 (1965).

93. P. R. Thornton, Scanning Electron Microscopy, Chapman and Hall Ltd., London, pp. 278-288 (1968).

94. L. W. James, J. L. Moll, and W. E. Spicer, Gallium Arsenide, Institute of Physics and the Physical Society, London, pp. 230-237 (1969).

95. E. F. Hockings, I. Kudman, T. E. Seidel, C. M. Schmelz, and E. F. Steigmeier, J. Appl. Phys. 37, 2879-2887 (1966).

96. J. C. Woolley, C. M. Gillett, and J. A. Evans, Proc. Phys. Soc. (London) 77, 700-704 (1961).

97. D. G. Fisher, R. E. Enstrom, and B. F. Williams, Appl. Phys. Lett. 18, (1971).

98. V. W. Kischio, Z. Anorgan. Allg. Chem. 328, 187 (1964).

99. H. M. Manasevit, Proceedings 135th National Electrochemical Soeicty Meeting (May 1969).

100. D. E. Bolger and B. E. Barry, Nature 199, 1287 (1963).

101. J. Whitaker, Solid-State Electronics 8, 649 (1965).

102. H. Kressel, F. Z. Hawrylo, and N. Almeleh, J. Appl. Phys. 40, 2248 (1969).

103. M. Ettenberg and R. J. Paff, J. Appl. Phys. 41, 3926 (1970).

104. Chow. Janef Thermochemical Tables, 1964.

105. T. Kikuchi, T. Kurosawa, and T. Yagihashi, Trans. Jap. Inst. of Metals 122, 5 (1964).

106. M. Hoch and K. S. Hinge, J. of Chem. Phys. 35, 451 (1961).

107. R. Hultgren, R. L. Orr, P. D. Anderson, and K. K. Kelley, Selected Values of Thermo. Prop. of Metals and Alloys, John Wiley & Sons, 1963.

108. D. R. Stull and G. C. Sinke, Adv. in Chem. Series 18 (1956).

109. M. Ettenberg and S. L. Gilbert, National Meeting Electrochem. Soc., Los Angeles, May 1970.

110. F. H. Nicoll, Ref. Scientific Instruments 40, No. 8, 1108 (Aug. 1969).

111. M. R. Lorenz, R. Chicotka, G. D. Pettit, and P. J. Dean, Solid-State Comm. 8, 9, 693-697 (1970).

112. H. Kressel and F. Z. Hawrylo, J. Appl. Phys. 41, No. 4 (1970).

113. D. G. Thomas, M. Gershenzon, and F. A. Trumbore, Phys. Rev. 153, A269 (1964).

114. E. D. Pierron, D. L. Parker, and J. B. McNeely, ACTA Cryst. 21, 290 (1966).

115. R. O. Simmons and R. W. Balluffi, Phys. Rev. 19, 600 (1960).

116. M. V. Cohen, Rev. Sci. Instruments 6, 68, 1935; 7, 155, 1936.

117. Yu. T. Pashintsev and N. N. Sirota, Dokrady AKAD Nauk Belorus S.S.R. 3, 2, 38 (1959).

118. E. D. Pierron, D. L. Parker, and J. B. NcNeely, J. Appl. Phys. 12, 38, 4669 (1967).

119. W. D. Sylwestrowicz, Phil. Mag. 7, 83, 1825 (1962).

120. M. R. Lorenz, 1970 IEEE International Convention, New York, paper 2A.3 (1970).

121. H. Rupprecht, J. M. Woodal, and G. D. Pettit, Appl. Phys. Letters 11, 81 (1967).

122. H. Nelson and H. Kressel, Appl. Phys. Letters 15, 7 (1969).

123. H. M. Manasevit, 135th National Electrochemical Society Meeting (May 1966).

124. M. Ettenberg and S. Gilbert, 137th National Electrochemical Society Mtg., 1970.